Stockholm University

Master Thesis

Degree Project in
Geochemistry 60 hp

Nitrous Oxide in Himmerfjärden: Seasonal Variability in Production Rates and Fluxes

Camilla Olsson

Stockholm 2015

Department of Geological Sciences
Stockholm University
SE-106 91 Stockholm
Sweden

Contents

Abstract 4

1 Introduction 5

2 Background 5

2.1 Factors controlling N_2O production 5

2.2 Nitrification 7

2.2.1 General background of the nitrification process 7

2.2.2 Nitrification and ^{15}N-tracer experiments 8

2.3 Denitrification 9

2.3.1 General background of the denitrification process 9

2.3.2 Denitrification and the ^{15}N-tracer experiment 11

2.4 Exchange of DIN and O_2 between the sediment and water column 12

2.5 Effects of Macrobenthos 13

2.6 The Sewage treatment plant (STP) facility at Himmerfjärden 13

3 Objectives and hypotheses 14

4 Materials and methods 15

4.1 Study site 15

4.2 Sample collection 16

4.3 Water column 16

4.3.1 Converting peak areas of N_2O into concentrations (nM) 17

4.3.2 Bunsen solubility for N_2O in the water column 17

4.3.3 N_2O saturation values in the water column 18

4.4 Sediment 18

4.4.1 Calculations of N_2O and DIN fluxes 18

4.4.2 N_2O and O_2 microelectrode profiles 19

4.4.3 PROFILE (Version 1.0) 19

4.4.4 Oxygen consumption 20

4.4.5 DIN concentration in pore water extraction through slicing 20

4.5 Samples taken from the Sewage treatment plant facility at Himmerfjärden 20

4.6 Elemental Analyzer-DeltaV Advantage mass spectrometer 21

4.6.1 $^{15}NH_4^+$ tracer experiment for potential N_2O production during nitrification 22

4.6.2 Calculations for production rates of N_2O from the nitrification 23

4.6.3 Denitrification rates 24
4.6.4 Calculations for denitrification rates 25
4.7 Statistics 26
5 Results 27
5.1 N_2O-, temperature-, salinity-, O_2- and DIN profiles from the water column 27
5.1.1 N_2O-, temperature-, salinity- and O_2 profiles in the water column 27
5.1.2 DIN profiles in the water column 30
5.2 Benthic fluxes of O_2, N_2O and DIN 32
5.2.1 Sediment- and bottom water characteristics 32
5.2.2 Raw data of O_2 uptake from measurements with Firesting O_2 optodes 33
5.2.3 Benthic Fluxes of O_2 35
5.2.4 Raw data of the benthic fluxes of N_2O 36
5.2.5 Benthic flux of N_2O 38
5.2.6 Seasonal benthic flux of DIN 38
5.3 DIN concentrations in sediment 39
5.4 N_2O and O_2 concentration profiles from PROFILE (Version 1.0) 42
5.4.1 Microelectrode profiles of N_2O in November 42
5.4.2 Microelectrode profiles for O_2 44
5.4.3 The ratio between the calculated and the measured flux of O_2 47
5.5 N_2O concentrations from the outgoing sewage water at the STP in Himmerfjärden 47
5.6 Evaluation of the Elemental Analyzer-DeltaV Advantage mass spectrometer 48
5.7 Potential N_2O production through the nitrification process 49
5.7.1 $^{45-46}N$-N_2O production in the water column from $^{15}NH_4^+$ tracer experiments 49
5.8 Potential denitrification rates in the sediment 51
5.8.1 $^{29}N_2/^{30}N_2$ ratios during ^{15}N-NO_3^- tracer experiments for core incubation 51
5.8.2 Verifying D_n independence of water column concentrations of $^{15}NO_3^-$, and a linear increase of D_w^{tot} with increasing $^{15}NO_3^-$ concentrations 53
6 Discussion 56
6.1 N_2O-, temperature-, salinity-, O_2- and DIN profiles 56
6.1.1 Correlation between N_2O and temperature-, salinity-, O_2- and DIN profiles in the water column 56
6.2 Benthic DIN-, O_2- and N_2O fluxes and O_2 penetration depth 56
6.2.1 Benthic fluxes of DIN and sediment concentrations 56
6.2.2 O_2 uptake- and penetration depth 58
6.2.3 Benthic N_2O fluxes and microelectrode profiles 58

6.3 Evaluation of the analytical results 60
6.3.1 Analysis of the ^{15}N-N_2O 60
6.3.2 Evaluation of the $^{15}NH_4^+$ incubation method 61
6.3.3 Analysis of the ^{15}N-N_2 62
6.3.4 Evaluation of the $^{15}NO_3^-$ tracer method 62
7 Conclusion 64
8 Acknowledgments 65
9 References 66
10 Appendices 69
10.1 Statistical analysis for N_2O in the water column 69
10.2 Statistical Results for N_2O Production during Nitrification 70
10.2.1 K-values for the production of $^{45\text{-}46}$Production in both spiked- and blank samples 70
10.2.2 Statistical results for N_2O production at H3 in November 71
10.2.3 Statistical results for N_2O production at H6 in November 76

Abstract

Seasonal variations of denitrification in the sediments and nitrification in the water columns were measured by a ^{15}N isotope pairing technique, in November, January and March, at two stations in the Himmerfjärden estuary (Sweden). One station was situated further up and close to a sewage treatment plant (STP), whereas the other one was located further down and less affected by the STP. The study focused on distinguishing nitrification and denitrification as the main source of the oversaturation of N_2O that has been seen in a previous study (Unpub. Olsson, 2013), and also to determine if the main source of the oversaturation either comes from the water column or the sediment. Benthic fluxes of N_2O, O_2, DIN (NH_4^+, NO_3^-/NO_2^-) and denitrification were measured simultaneously in incubation cores together with nitrification rates in the water column and complementary microprofiles of N_2O and O_2 in the sediment. The station closest to the STP contained the highest N_2O levels in the water and ranged between a saturation of 760 % in October to 110 % in January. This station also contained the highest efflux of N_2O from the sediment (2.1 µmol $m^{-2}d^{-1}$), whereas the flux was statistically equal during the other seasons and ranged between -0.1 to 1.1 µmol $m^{-2}d^{-1}$. The station further away was always in equilibrium with the atmosphere and hence not a source of N_2O. Seasonal changes in the O_2-penetration depth, sediment O_2 uptake rates, DIN flux or the water column concentrations of DIN did not have an effect on the benthic N_2O fluxes. Samples from outgoing sewage water from the STP showed extremely high emission of N_2O. A saturation of 275 481 % of N_2O could be seen in March and April, which is a factor of 2650 higher than atmospheric values. This extremely high emission of N_2O completely rule out other producers in the natural environment. The high emissions during March and April from the STP, the location of the N_2O maxima in the water column and the fact that the station with less influence from the STP was not a source of N_2O, points to the STP as the cause behind the elevated N_2O values, rather than due to seasonal changes. Continuous measurements are needed, preferably throughout the year so the change in emissions can be well documented and correlated with changes in the Himmerfjärden estuary, to strengthen the fact that the STP as the most dominant source. $^{15}NH_4^+$ incubations experiment for potential nitrification rates showed no production of N_2O, questions whether N_2O actually was detected arose since only a pure N_2O standard could be detected. The $^{15}NO_3^-$ incubation experiment for potential denitrification rates did not fulfill crucial assumption and could hence not be discussed, which was both caused by an analysis error and the experimental setup. A change of the $^{15}NO_3^-$ addition spectra, pre-incubation time and a combined endpoint- and time-series experiment could enhance the quality of the results. Hence, denitrification nor nitrification can be ruled out or stated as a source of the oversaturation of N_2O in the waters at Himmerfjärden.

1 Introduction

Ozone-depleted substances (ODSs) were considered one of the major environmental issues during the 20th century (Ravishankara, et al., 2009). It is believed that N_2O is the most important ODS, not only for today's emissions but also through the whole 21th century (Ravishankara, et al., 2009). Regulation of the emissions would not only speed up the recovery of the ozone layer, but also reduce the anthropogenic impact on the climate (Ravishankara, et al., 2009). The emissions of N_2O are today unregulated by the Montreal Protocol (Ravishankara, et al, 2009). Another aspect is the efficiency of absorbing sunlight, N_2O being more efficient than carbon dioxide (CO_2) by a factor of 300 and is at the moment increasing at a rate of 0.3 % per year in the atmosphere (Sutka et al., 2006, Murray, et al., 2015, and references there in). With this being said, the anthropogenic activity has over the last decades doubled the annual input of dissolved inorganic nitrogen (DIN) into the environment, which stimulates the natural microbial activity and hence the emissions of N_2O to the atmosphere (Sutka, et al., 2006, Rönner, 1982, Townsend-Small et al., 2014). A future global increase of the DIN concentration has been projected, causing a significant increase of the N_2O flux (Murray, et al., 2015, and references there in), with subsequent effects on the ozone layer (Ravishankara, et al., 2009). Estuaries are an environment known to act as a N_2O source to the atmosphere but the numbers of investigations are few and the spatial and the temporal coverage of this trace gas emission is lacking and any global estimate is therefore associated with large uncertainties (Bunge, 2006. Murray, et al., 2015, and references there in).

To be able to decrease future emissions, the knowledge of responsible microbial processes for the N_2O production are of high relevance. One step on the way is to determine the relative importance of nitrification and denitrification and numbers of factors controlling these processes (Sutka et al., 2006). Defining this would be an important step in projecting future N_2O emissions and its effect on future climate.

2 Background

2.1 Factors controlling N_2O production

According to existing literature, the amount of DIN (NH_4^+, NO_3^-,NO_2^-) could be the most important factor in controlling the production rates of N_2O (Murray, et al., 2015, and references there in). Abundant NH_4^+ fuels the nitrification process, both in the sediment and in the water column, whereas NO_3^- and NO_2^- fuels the denitrification in the sediment (Klotz, 2011, Murray et al., 2015, and references there in). High concentrations of DIN has been associated with high bacterial production of N_2O, causing a higher flux of N_2O to the atmosphere (Murray, et al., 2015, and references there in). Experiments involving addition of DIN have increased the benthic N_2O flux, even if the magnitude

of the effect has varied depending on the type of environment (e.g. Marches, mangrove sediment, estuaries, open water etc.) (Murray, et al., 2015, and references there in). High DIN concentrations have in many cases lead to a high N_2O:N_2 ratio from denitrification in estuaries, which is thought to be an effect of higher microbial activity and lower rates of bacteria consumption of N_2O (Murray, et al., 2015, and references there in). Other studies have reported negative N_2O fluxes during high DIN, especially when NH_4^+ dominates the pool (Murray, et al., 2015, and references there in). Other parameters controlling the N_2O:N_2 ratio are the concentration of H_2S and pH. Higher ratios has been seen in environments with higher pH-, H_2S- and DIN levels (Murray, et al., 2015, and references there in).

Several studies found a positive correlation between levels of NO_3^- and the exchange of N_2O between water and air, whereas the correlation between NH_4^+ and N_2O water-air fluxes is weaker (Murray, et al., 2015, and references there in). This could be due to sparse sampling in combination with a short turn-over time of NH_4^+ in the water column (Murray, et al., 2015, and references there in).

Other studies indicated that nitrification in estuarine environments produce less N_2O than denitrification. At the same time, denitrification also acts as a sink of N_2O during anoxic conditions with associated negative benthic fluxes of N_2O. When the O_2 levels are low, denitrification starts to use N_2O as an electron acceptor instead of producing it (Rönner, 1982, Murray, et al., 2015, and references there in). Anoxic conditions favor denitrification in both sediment and water, while oxic environments favor nitrification or combined nitrification-denitrification pathways. Highest production rates have been measured when the O_2 levels are low and the DIN is high, which is typical for eutrophic stagnant water or further up in estuaries (Murray, et al., 2015, and references there in).

The penetration depth for O_2 is only a couple of millimeters, which creates a narrow zone where nitrification can take place in the sediment and denitrification is the main producer of N_2O (Murray, et al., 2015). However, the amount produced in the nitrification zone has a higher possibility to escape by diffusion before it is consumed (Murray, et al., 2015, and references there in). In some estuary sediment, plants transfer O_2 by their root system to the rhizosphere and suppress the denitrification, which could lower the N_2O production (Murray, et al., 2015, and references there in). But if the same situation would occur in an environment with high levels of available NH_4^+, it would stimulate the coupled nitrification-denitrification process and lead to higher N_2O emissions (Murray, et al., 2015, and references there in). This means that sediment structure is an additional parameter controlling the fate of the produced N_2O.

Studies have shown that N_2O changes with season with generally high N_2O fluxes during summers, probably due to warmer temperatures and high microbial activity (Murray, et al., 2015, and references there in).

2.2 Nitrification

2.2.1 General background of the nitrification process

The energy yield from a certain reaction determines the sequence of oxidants that the microorganisms would prefer to use in its metabolism (Schulz et al., 2006). A comparison between nitrification and denitrification shows a higher energy yield using O_2 instead of NO_2^- as the terminal acceptor. This becomes evident looking at equation 1 and 2 (Schulz et al., 2006).

O_2 respiration and nitrification:

$$(CH_2O)_{106}(NH_3)_{16}(H_3PO_4) + 138\ O_2 \rightarrow 106C + O_2 + 16\ HNO_3 + H_3PO_3 + 122\ H_2O \qquad \text{Eq.1}$$

$$\Delta G^0 = -3190\ \text{kJ mol}^{-1}$$

Denitrification:

$$(CH_2O)_{106}(NH_3)_{16}(H_3PO_4) + 94.4\ HNO_3 \rightarrow 106\ C + O_2 + 55.2\ N_2 + H_3PO_3 + 177.2\ H_2O \qquad \text{Eq.2}$$

$$\Delta G^0 = -3030\ \text{kJ mol}^{-1}$$

The process involves a stepwise reduction with both ammonia- and nitrite oxidizers, which are two different groups of bacteria that physiologically depends on each other (Schulz et al., 2006). NH_4^+ is transformed by ammonia oxidizing bacteria (AOB) in two steps (fig. 1). Equation 3 describes the first step involves the oxidation of NH_4^+ to NH_2OH, which is catalyzed by ammonia monooxygenase (AMO) (Bing-Jie, et al., 2011).

$$NH_4^+ + O_2 + H^+ + 2e^- \rightarrow NH_2OH + H_2O \qquad \text{Eq.3}$$

One oxygen atom from O_2 is reduced with two electrons and incorporated in the NH_2OH molecule. To reduce the second oxygen atom and transform it into H_2O, additional inputs of reductants are needed. Further oxidation of NH_2OH to NO_2^- provides this, which is catalyzed by hydroxylamine oxidoreductase (HAO) (Bing-Jie, et al, 2011). This is described in equation 4.

$$NH_2OH + H_2O \rightarrow NO_2^- + 5\,H^+ + 4e^- \qquad \text{Eq.4}$$

Four electrons are released from this reaction where two are returned to AMO to sustain the oxidation of NH_4^+. N_2O can be produced in two different routes, either as 1) a byproduct of an incomplete oxidation of NH_2OH to NO_2^- (fig. 1A), or 2) under limiting O_2 levels and in the presence of NO_3^- or NO_2^- these substances can act as an electron acceptor instead of O_2 in the nitrifier denitrification process (fig. 1B). The reduction of NO_2^- in the nitrifier denitrification process is

catalyzed by nitrite reductase (NIR) and nitric oxide reductase (NOR) (Bing-Jie, et al, 2011). All the described reactions above are visualized in figure 1 A and B.

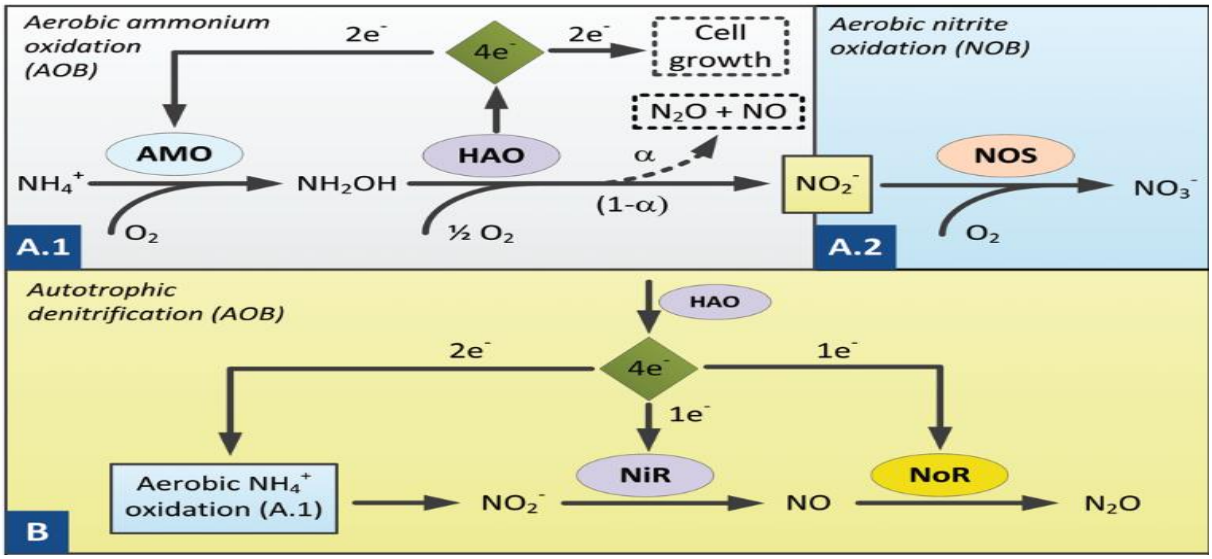

Figur. The biochemical processes during N_2O production: A) NH_4^+ oxidation under oxic conditions by AOB followed by NO_2^- oxidation by NOB; B) NH_4^+ oxidation under anoxic conditions by AOB, driven by denitrification. Bing-Jie, et al., 2011

Changes in N_2O emissions depending on substrates have been examined (NH_4^+ or NH_2OH). Using different inhibitors, it was observed that the emissions were higher when NH_2OH was used as a substrate (four electrons can be used to produce N_2O in the NH_2OH oxidation whereas only two in the oxidation of NH_4^+(Sutka, et al, 2006, Bing-Jie, et al, 2011). Therefore it has been considered that the nitrifier denitrification pathway is the dominating one (Sutka, et al, 2006, Bing-Jie, et al, 2011).

When N_2O levels are high in well mixed oxygenated waters, it often has been correlated with an increase of NO_3^- and a decrease of O_2, which supports nitrification as the process producing N_2O (Bange, 2006). Moving from the oxic- to the anoxic interface has been consistent with a sharp drop of the N_2O concentration, which remain close to zero in anoxic deep waters (Bange, 2006). Though some investigations have shown that nitrification can occur at O_2 levels as low as 10 % saturation (Rönner, 1983). The nitrification is also inhibited of light and is therefore not active in the top water column (Rönner, 1983).

2.2.2 Nitrification and ^{15}N-tracer experiments

One of the advantages in using the stable isotope, ^{15}N, as a tracer is the high sensitive and no need for steady state assumptions (Klotz, 2011). High sensitivity is needed to a relative high natural abundance of ^{15}N (Holtappels, 2011). A tracer is added but without exceeding the ambient pool by more than 10 %. To determine a suitable addition of the tracer in a certain environment,

measurements of the ambient concentrations should be made before the experiment (Klotz, 2011). The amount of the labeled substrate in the production after the incubation is the transformation rate (Klotz, 2011). Since the mass spectrometer is used to analyze the samples, an incubation time of only a few hours to 24 hours is needed since it is a highly sensitive instrument. The transformation between $^{15}NH_4^+$ to ^{15}N-N_2O can be detected even if other processes are going on in the sample (Holtappels, 2011)

Since the nitrification is an O_2 sensitive process, it is important to maintain the *in situ* concentrations, especially in waters with low O_2 (Klotz, 2011). The length of the incubation time is important and should be kept as short as possible since the substrate pool can be diluted by regeneration of NH_4^+ (Klotz, 2011). This can happen even during short incubations and a long incubation time could make it impossible to account for the dilution effect in the rate calculations (Klotz, 2011). A drawback with this method is if the natural abundance of DIN is extremely low, it could be difficult to add such a small amount of the tracer. The problem has been solved by the use of even more sensitive mass spectrometers (Holtappels, 2011).

2.3 Denitrification

2.3.1 General background of the denitrification process

Denitrification starts when the O_2 level is low or totally absent (Schulz et al., 2006). This process is maintained by facultative aerobic bacteria that reduces NO_3^- to N_2 in several steps through nitrate- and nitrite reductase (Schulz et al., 2006). Denitrification has been believed to be the only N-removing process in O_2 limited zones, this paradigm has however been challenged by the discovery of another process; anammox (Holtappels, 2009). This process oxidizes NH^+_4 anaerobically to NO^-_2 and further N_2 (Holtappels, 2009).

Equations 5 to 8 are the reduction of NO^-_3 to N_2 in four steps with NO_2^-, NO and N_2O as intermediates (Bing-Jie, et al, 2011).

$$NO_3^- + 2\,H + + 2e^- \rightarrow NO_2^- + H_2O \qquad \text{Eq.5}$$

$$NO_2^- + 2H^+ + e^- \rightarrow NO + H_2O \qquad \text{Eq.6}$$

$$2NO + 2H^+ + 2\,e^- \rightarrow N_2O + H_2O \qquad \text{Eq.7}$$

$$N_2O + 2H^+ + 2e^- \rightarrow N_2 + H_2O \qquad \text{Eq.8}$$

Four different enzymes are involved in the transformations (fig. 2) and whether N_2O is produced or not depends on the kinetics for the different reactions and the threshold values for O_2 inhibition, which is different for the reactions (Bing-Jie, et al., 2011).

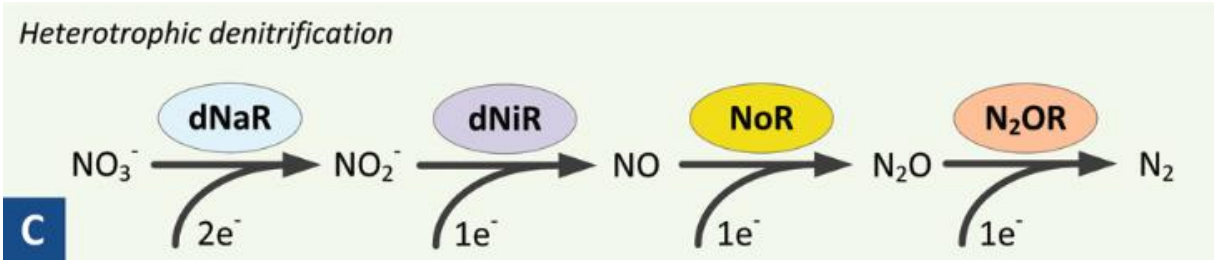

Figure 2. The heterotrophic denitrification process, which involves four different enzymes; dNaR (dissimilatory nitrate reductase), dNiR (dissimilatory nitrite reductase), NoR (nitric oxide reductase) and N_2OR (nitrous oxide reductase). Bing-Jie, et al, 2011

Controlling parameters are O_2, H_2S, DIN levels and pH (Schulz et al., 2006, Murray, et al., 2015, and references there in). The availability of NO_3^- is one of the most important factor, which is mainly supplied from the nitrification or the water layer closest to the sediment by means of bioturbation, bioirrigation and diffusion (Schulz et al., 2006). Other factors controlling denitrification are temperature, availability of organic matter and the SO_4^{2-} reduction rates. The latter, since the product from the SO_4^{2-} reduction, H_2S, already at low concentrations inhibits nitrification, which is essential for the denitrification (Schulz et al., 2006). Other studies made in estuaries with the classical salinity gradient, have indicated that denitrification and the NO_3^- reduction becomes more important as SO_4^{2-} concentrations decreases during higher freshwater inputs (Schulz et al., 2006).

Both the nitrification within the sediment and the diffusion of NO_3^- from the overlying water are potential sources for denitrification (Christensen, et al., 1990). The flux of NH_4^+ into the sediment is another parameter since it stimulates the coupled nitrification-denitrification. The vertical distribution of respective process determines the degree of coupling (Christensen, et al., 1990). If nitrification occur close to the sediment surface, a major part of the produced NO_3^- will diffuse upwards and not to the denitrification zone due to too long diffusion distance (Christensen, et al., 1990). However, diffusion of NO_3^- from the water column could still be the primary source for denitrification (Christensen, et al., 1990). If diffusion of NO_3^- from the water column is the primary source, the thickness of the oxic layer above the denitrification zone and the concentration of NO_3^- in the water are the controlling factors (Christensen, et al., 1990). The denitrification should be proportional to the NO_3^- concentration and inversely proportional to the thickness of the oxic layer (Christensen, et al., 1990). Modelling studies have shown a 1st order kinetic relationship between denitrification and the NO_3^- concentration in the water column, which is determined by the gradient in the upper oxic layer (Rysgaard, et al., 1995).

Denitrification occurs directly under the oxic zone and the shape of the NO_3^- profile in the sediment is dependent on both nitrification- and denitrification rates (Schulz et al., 2006). Lower denitrification rates results in a deeper NO_3^- penetration depth since it is not consumed (Schulz et al.,

2006). High denitrification rates would result in a NO_3^- maximum further up with a resulting decrease in the sediment up- and downward flux and a sediment NO_3^- uptake from the overlying water (Schulz et al., 2006).

2.3.2 Denitrification and the ^{15}N-tracer experiment

In this work, an isotope pairing technique (IPT) has been chosen to quantify both the coupled nitrification-denitrification (D_n) in the sediment, and the denitrification caused by a NO_3^- supply from the water column (D_w^{tot}). Adding the $^{15}NO_3^-$ tracer, both single-labeled ($^{14}N^{15}N$) and doubled-labeled ($^{15}N^{15}N$) pairs are produced and a *potential* denitrification rate can be calculated (Nielsen, 1992). The 15 IPT is established with three assumptions:

1) The added $^{15}NO^-_3$ is mixed uniformly with the endogenous $^{14}NO_3^-$, both in the water column and in the sediment. With the present knowledge, it is not possible to measure the nitrification-denitrification coupled process close around roots of aquatic macrophytes since these microsites are isolated from the added $^{15}NO_3^-$ (Nielsen, 1992, Steingruber, et al., 2001). Sediment heterogeneity and bioturbation can affect the ratio between nitrification and the influx of $^{15}NO_3^-$ into different spots in the sediment. This in turn would lead to a higher production of $^{28}N_2$ and $^{30}N_2$ (Nielsen, 1992, Steingruber, et al., 2001). This means that the total denitrification activity would be underestimated, which is dependent on the amount of added tracer. This is why different amounts were added in this experiment; more tracer will be trapped when higher tracer amount are added and measured directly as $^{29}N_2$. By doing this, the significance of the possible miscalculation of the produced $^{28}N_2$ decreases in comparison with environments containing low amounts of $^{15}NO_3^-$ (Nielsen, 1992). The ratio between $^{29}N_2$ and $^{30}N_2$ tests whether the mix between the two isotope species are uniform or not (Nielsen, 1992, Lohse, et al., 1996). A ratio below two indicates that all of the $^{14}NO_3^-$ molecules are paired with a $^{15}NO_3^-$ molecule. This ratio generally decreases with increasing $^{15}NO_3^-$ addition (Lohse, et al., 1996). Another way to see whether the assumption is fulfilled or not, is to see if the coupled nitrification-denitrification is independent of the ^{15}N-concentration. The fulfillment of this assumption also gives indications of an even mix of the isotopes in the zone of denitrification (Jensen, et al., 1996).

2) D_w^{tot} increases linearly with the NO_3^- concentration, indicating no disturbance of the 1st order kinetic relationship between denitrification and the NO_3^- concentration in the water column, and hence neither the natural denitrification rates (Jensen, et al., 1996, Rysgaard, et al., 1996). This can also be tested by adding different amounts of the tracer. However, it has become evident that this assumption is not valid in environments with too high NO_3^- concentrations. Saturation affects can occur with high NO_3^- concentrations due to a limited supply of electron donors. This also causes a deeper NO_3^- penetration depth in the sediment, which will cause a non-linear response between

denitrification rates and the NO_3^- concentrations in the overlying water (Steingruber, et.al, 2001). This assumption is essential for calculating the *in situ* denitrification with $^{14}NO_3^-$ (D_w) (Steingruber, et al., 2001). However, if the assumption is not met, the calculated *in situ* denitrification rates do not represents true rates.

3) A stable concentration gradient of NO_3^- across the sediment- and water interface is established after the addition of $^{15}NO_3^-$ (Steingruber, et.al, 2001). A too short pre-incubation time would result in an overestimation of the production rates of $^{29}N_2$ and $^{30}N_2$, since $^{15}NO_3^-$ would not be available for denitrification in the beginning, and hence cause an underestimation of the initial denitrification rates (Steingruber, et.al, 2001). If the $^{15}NO_3^-$ is well mixed in the water column, the amount of time it takes for establishing a stable gradient is dependent on the O_2 penetration depth. The O_2 penetration depth determines the diffusion length the NO_3^- molecules needs to move before entering the denitrification zone in the sediment (Steingruber, et al., 2001). The level of biological activity and the season are other parameters; a shorter pre-incubation time for establishing a steady-state gradient is needed for summer months and environments with high biological activity (Steingruber, et al., 2001).

2.4 Exchange of DIN and O_2 between the sediment and water column

The physiological environment between the water column and sediment is distinctly different, which largely influence the biological and the chemical processes in respective environment (Holtappels, 2011). The transport of solutes in fine-grained sediments with high permeability is determined by the molecular diffusion, which in contrast to the convection and the turbulent mixing in the water column, is really slow (Holtappels, 2011). Sediments at continental shelves and coastal areas, receive a large input of particulate matter and often a high organic matter load, whereas the water column in comparison contains low organic matter amounts (Holtappels, 2011).The water column is often oxygenated whereas an active sediment becomes depleted from O_2 after a couple of millimeters.

One of the breakdown products from the organic matter mineralization is NH_4^+, which diffuses towards the sediment surface (Holtappels, 2011). Reaching the interface between the oxic and the anoxic zone means entering a zone where nitrification takes place. From this zone NO_3^- or NO_2^- either diffuses upwards towards the water column or downwards into the denitrification zone, where it becomes reduced to N_2 (Holtappels, 2011). The direction of the mineralized N is heavily dependent on the O_2 concentration in the bottom water and also the input of organic matter (Holtappels, 2011). It has been shown that the sedimentary denitrification is high when both the carbon inputs and the NO_2^- concentrations in bottom waters are high (Holtappels, 2011). If the sediment contains high organic matter amounts, then a high O_2 concentration would stimulate the coupled nitrification-denitrification process and increase the rates (Holtappels, 2011).

2.5 Effects of Macrobenthos

One of the dominant factors influencing the mass transport in marine sediments are bottom-living animals, which move particles and fluids during their way through the sediment (Aller, 1982). This largely affects the chemistry, not only in the sediment but also in the overlying water (Aller, 1982). The classically assumed vertical zonation in the sediment with specified electron acceptors for each level are strongly influenced by the benthic fauna (Aller, 1982). The benthic fauna can be differentiated by their size; macrofauna are animals in a dimension above 1 millimeter and meiofauna those with dimensions beteen 0.4- to 1 mm (Bonaglia, et al., 2014B).
Reactions and diffusion pathways for solutes change due to burrow and fecal pellets formations, and through the transfer of material between the zones. This altogether creates biogeochemical microenvironments rather than vertical stratified distributions (Aller, 1982). Type of species, number and size of the macrobenthos are some factors that determine their effects on the biogeochemistry in the sediment (Aller, 1982). Sediments with high bioirrigation- and bioturbidity have in general a deeper penetration of O_2, which would stimulate the coupled nitrification-denitrification process and increase the fluxes of N_2O (Murray, et al., 2015).

2.6 The Sewage treatment plant (STP) facility at Himmerfjärden

The department of System Ecology at Stockholm University has been researching the eutrophication in Himmerfjärden. The nutrient concentrations have hence been monitored since 1976, and the area is one of the best investigated in Sweden. Water, at a rate of 1600 L s^{-1}, is pumped from the STP through two wooden tubes 1600 m into Himmerfjärden at a depth of 25 m during 2014/2015 (the depth was 10 m under 2013). The cleaned water is pumped above the chemocline during autumn-, spring- and winter time, whereas during summer the water is spread along the thermocline at approximately 15 m depth. The first step in the biological purification is the nitrification process, which uses the NH_4^+ in the water and produces NO_3^-. The ultimate step is when NO_3^- is transformed to N_2 by denitrifier bacteria in the denitrification process. The process is of course more complex and involves several additional steps. For a more detailed description, the reader is referred to Syvabs webpage (http://www.syvab.se/himmerfjardsverket/vattnets-vag).

In October 2013, the biggest shutdown, since the STP started in the 1970s, occurred for the biological purification. It was reported to Syvab in the middle of November and the decreased quality of the purification could be seen in the week after. Soon after, the microbes died and could not be filtered away from the outgoing water and the base value for the Biochemical Oxygen Demand (BOD), could not be kept. After a month, the nitrification was totally shutdown and huge amounts of NH_4^+ were released (http://www.syvab.se/information/dokument/syvabs-miljorapporter). It takes time to re-start the process, especially during low temperatures, and the

purification step involving nitrification did not reach stability until July 2014, this of course led to an increased release of DIN during the first part of 2014. The biological purification continued at maximum rates and without breaks for the usual maintenance and service during the second part of 2014. This decreased the emissions and the total release of N during 2014 were under the allowed levels (http://www.syvab.se/information/dokument/syvabs-miljorapporter).

The amount of sewage plant discharge has increased with 15 % in comparison with the same time frame the previous year, which is higher than the permitted values and a trend of increasing levels of the N release has been noted (http://www.syvab.se/information/dokument/kvartalsrapporter). Further information about these events can be read in environmental- and quarterly reports from 2013, 2014 and 2015 (http://www.syvab.se/information/dokument).

3 Objectives and hypotheses

The main objective for this study is to discriminate the processes producing N_2O in Himmerfjärden, which could explain the N_2O oversaturation that has been seen in a previous study (Unpub. Olsson, 2013), and also investigate in how different parameters affect the N_2O production. To accomplish this, a seasonal study is made at two different locations in Himmerfjärden; one closer to the STP and hence higher up in the estuary, and one further away and less exposed to the STP emissions. A ^{15}N-labeling technique is used in both water column and sediment to detect whether nitrification or denitrification has a significant contribution to the N_2O production. This is complemented by microelectrode profiles of both O_2 and N_2O, core incubations to measure fluxes of DIN, O_2 and N_2O from the sediment and O_2-, salinity-, temperature-, DIN- and N_2O concentration profiles in the water column. Samples are taken from the outgoing sewage water at the STP and analyzed for N_2O concentrations. The following hypotheses will be tested:

1. There is a seasonal variation of N_2O in the water column with higher concentrations during the warmer months, which is an effect for a chainreaction caused by well oxygenated waters, a deeper O_2 penetration depth and a higher benthic- and microbial activity.
2. H6 has a high NO_3^- level in the water column and a low O_2 penetration depth in the sediments, which enhances the relevance of the NO_3^- supply from the overlying water for denitrification rates, whereas the deeper O_2 penetration depth at H3 stimulates the coupled nitrification-denitrification rates. The latter more important and hence causing a higher denitrification rate at H3.
3. N_2O is mainly produced in the water columns, due to well oxygenated waters in the middle- and top part of the column at both stations. This stimulates nitrification in combination with

high DIN supplied from the STP. Sediments are not a main producer of N_2O at H6 since there is not enough O_2 and too much H_2S, which inhibits nitrification and denitrification. Sediment at H3 is in comparison to H6 a bigger producer of N_2O, but not as big as the well oxygenated water column at H3.

4 Materials and methods

4.1 Study site

The Baltic Sea has over the last 50 years been exposed to increasing inorganic- and organic nutrient loads, which has caused eutrophication and a spread of bottom water anoxia (Bonaglia, et al, 2014A, Thang, et al., 2012). There are few investigations on key regulators (O_2 levels, macrofauna, organic matter content in the sediment, or different human loads from human activity) of benthic N cycling (Bonaglia, et al., 2014A), which make it difficult to do accurate predictions of the future climate.

Himmerfjärden is located in the southern archipelago of Stockholm, Sweden. The estuary is characterized by a salinity gradient from around 5.5 permil in the inner part to 6.5 permil at the opening to the Baltic Sea. Himmerfjärden is also influenced by a STP, which was built in the 1970s with the main effluent in the form of DIN and dissolved inorganic phosphorous (DIP) (Bonaglia, et al., 2014). The inner parts undergoes thermohaline stratification during summer and autumn, which causes a seasonal hypoxia in bottom waters (Bonaglia, et al., 2014). The input of external water is mainly coming from Lake Mälaren, surface run-off and discharge from the STP (Bonaglia, et al., 2014). These external inputs have led to eutrophication in the estuary and the STP has a direct effect on the plankton productivity (Thang, et al., 2012).

For the purpose of this study, stations H6 and H3 were selected. H6 is situated closest to the STP and is characterized by anoxic conditions in the bottom water with black, soft and laminated sediment with a high sedimentation rate (Thang et al., 2013). The sediment at H3 is characterized by an oxygenated bottom layer through the year with sediment that consists of a brown, oxidized top layer with a lot of benthic activity. The bigger picture on the left side in figure 1 shows the location of the Himmerfjärden estuary, whereas at the right is a close up picture of the location of the stations and the STP within the estuary.

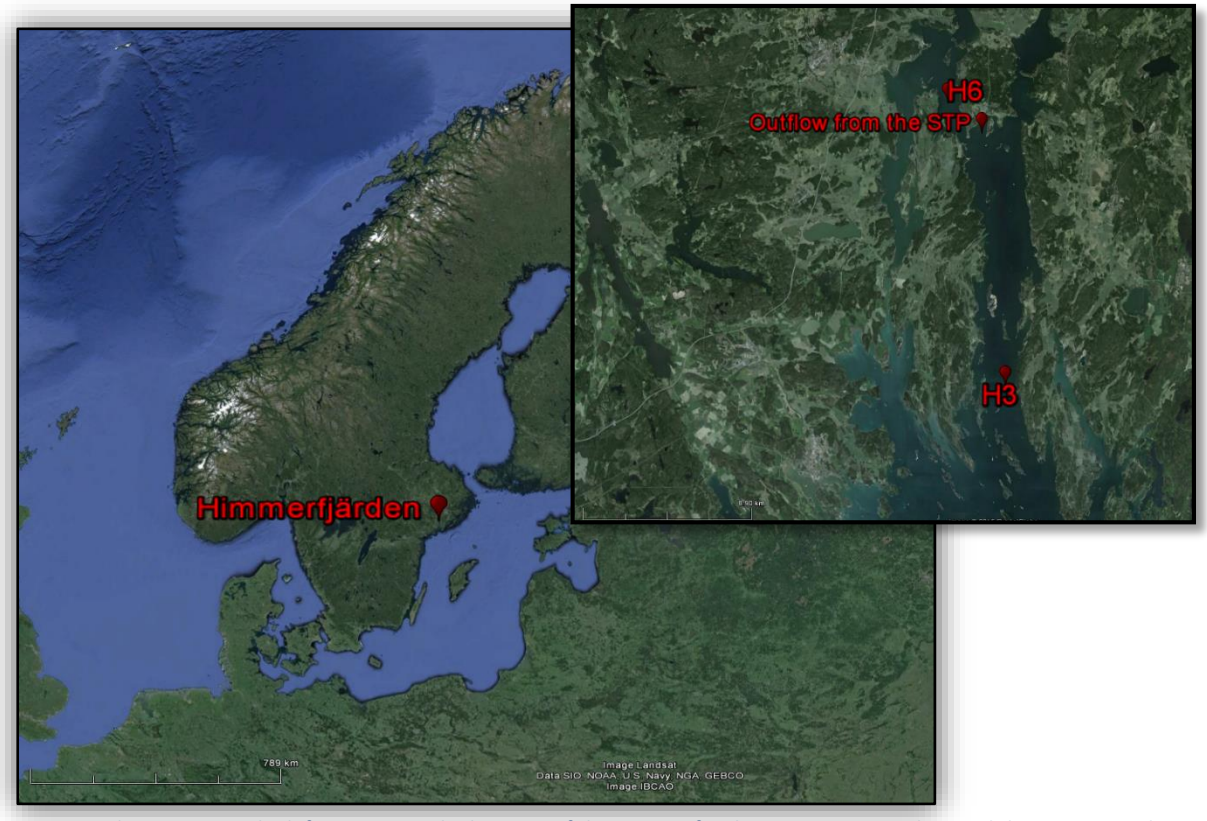

Figure 3. The picture on the left represents the location of the Himmerfjärden estuary in Sweden, and the picture on the left a close up picture of the estuary and the location of the stations and the STP. Source: Google Earth (15.07.16)

4.2 Sample collection

Water and sediment samples were collected in October, November, January and March to achieve a seasonal study at H6 and H3 in 2014/2015 with the research vessel R/L Limanda. A CTD system always began the measurements, recording the salinity-, oxygen- and temperature data. The samples for N_2O concentrations, DIN and nitrification rates in the water column were taken using a 5L Niskin bottle at every 5th meter. All water samples were taken using a tight tubing device to avoid O_2 contamination.

The sediment samples were collected by a multicorer from K.U.M Umwelt-und Meerestechnik Kiel, equipped with 40 centimeter long Plexiglas cores (i.d. 9.6 cm). Four casts were done at each site and the first eight cores were subsampled immediately on the boat for denitrification rates (Plexiglas tubes; L: 25 cm, i.d. 3.6 cm; n=3). Cores for DIN- and N_2O fluxes were immediately subsampled as well (Plexiglas tubes; L: 25 cm, i.d. 6.0 cm; cm; n=4) and one core for sediment concentrations of DIN and two cores for microelectrode measurements.

4.3 Water column

Three replicates were collected for N_2O concentrations at every depth with 12 ml exetainer and 100 µl of 50% (w/w) saturated $ZnCl_2$ to prevent a continued microbial activity. Samples for DIN were sampled at every depth as well, which were filtered and stored frozen within four hours from the

time point of the sampling. All water samples were placed upside down until the analysis, in which a headspace was done by bubbling the samples with helium while they were upside down. 4 ml of the sample was simultaneously taken using a syringe. To acquire an accurate headspace volume, the exetainers were weighted both before and after headspacing and placed upside down again until the analysis. The exetainers were shaken on a shaker table for one hour at 200 rpm to reach equilibrium between the water and the gas phase. The analysis started a couple of hours after the shaking. TO analyze N_2O concentrations in the water column and benthic fluxes, a gas chromatograph (SRI 8610C) with an ECD (electron capture detector) detector was used.

4.3.1 Converting peak areas of N_2O into concentrations (nM)

The calibration curve, produced from different concentrations of N_2O standard gas, enables the transformation between a peak areas in the gas chromatograph into concentrations of N_2O. This is seen in equation 9.

$$y = kx + m \qquad Eq.9$$

Where *y* is the peak area from the gas chromatograph, *k* the coefficient line, *x* the unknown concentration and *m* is put to zero. Rearranging equation 1, the next step to convert the peak area into a concentration of N_2O is seen in equation 10.

$$x = \frac{y}{k} \qquad Eq.10$$

The concentration is now in ppb and to convert this to moles, the ideal gas law is used and can be seen in equation 11.

$$n = \frac{RT}{pV} \qquad Eq.11$$

Where *p* is the pressure in kPa, *T* is the temperature in kelvin, *R* the gas constant in J $K^{-1}mol^{-1}$, *V* the volume (liters) and *n* the number of moles. The volume is achieved through multiplying the calculated ppb of the N_2O with 10^{-9} and multiply it with the volume (L) in the headspace. The moles are transformed to nmol and by dividing this with the amount of water in the exetainer, the nmol/l is calculated in the samples.

4.3.2 Bunsen solubility for N_2O in the water column

The Bunsen solubility coefficient (β) makes it possible to accurately measure gases in freshwaters and seawaters in equilibrium with the atmosphere. The equations for N_2O solubility were taken from *Weiss and Price, 1980.* These data have been corrected for standard conditions, one mole of N_2O occupies ~0, 7% less volume than one mole of ideal gas. The equilibrium concentration of the substrate is calculated as in equation 12.

$$C^* = x'F \qquad Eq.12$$

Where *x'* is the dry mole fraction in air and *F* is expressed as moles l^{-1} atm^{-1}. The calculation of F is seen in equation 13.

$$\ln F = A^1 + A^2\left(\frac{100}{T}\right) + A^3 \ln\left(\frac{T}{100}\right) + A^4\left(\frac{T}{100}\right)2 + S\left[B^1 + B^2\left(\frac{T}{100}\right) + B^3\left(\frac{T}{100}\right)2\right] \quad \text{Eq.13}$$

The parameters (A^1, A^2, A^3, A^4, B^1, B^2, B^3) have been derived experimentally and can be found in the article from Weiss and Price, 1980.

4.3.3 N_2O saturation values in the water column

Saturation values were calculated as the ratio between the dissolved gas in water, C_w, and the concentration of the dry mole fraction in air, C_a. This is expressed in equation 14 and 15 and is taken from *Bange, et al, 1998*.

$$Sat = \frac{Cw}{Ca} * 100 \quad \text{Eq.14}$$

$$C_a = \frac{\beta}{x} \text{ and } C_w = \frac{\beta}{x'} \quad \text{Eq.15}$$

Where *x* is the concentration of the gas in the air and *x'* is the measured concentration in the headspace of the sample and *β* is the Bunsen solubility described in section 4.3.2.

4.4 Sediment

The cores for sediment fluxes were immediately subsampled onboard to boat to avoid gas accumulation in the sediment and hence great bubbles and destruction of the sediment surface. In the laboratory, the cores were immediately stored and overflowed with cold bottom water in a cold room with the same temperature as the bottom water. The cores were given five to six hours to settle down before the incubation started. One sample from each core was taken in the beginning for both N_2O and DIN fluxes with stopper put on top of the cores. The DIN samples were immediately filtered and frozen. The procedure was the same when ending the fluxes and the incubations lasted between 10 and 12 hours. The samples for the N_2O fluxes were later analyzed in a GC (SRI 8610C).

4.4.1 Calculations of N_2O and DIN fluxes

The conversion from peaks area to concentrations are described in section 4.3.1. The only difference is that the nM is transformed to nmol/ml in this calculation. Equation 16 describes the N_2O flux.

$$^{F}N_2O = \frac{\left(\frac{nmol}{ml}\right) in\ exetainer * V_W}{(A*t)} \quad \text{Eq.16}$$

Where the *nmol/ml* is calculated from the exetainer, V_W is the water volume of the core in ml, *A* is the area in m^2 and *t* is the time interval. This value is then multiplied by 24 to obtain a flux in nmol $m^{-2}d^{-1}$.

4.4.2 N_2O and O_2 microelectrode profiles

Three to six microprofiles of O_2 and N_2O were measured in order to determine the penetration depth. A 5 % solution of Acetylene was prepared for the N_2O measurements in case non-detectable N_2O levels were present. Acetylene inhibits N_2O reductase, which means that if acetylene is used only *potential* N_2O concentrations are measured in the sediments.

Profiles were obtained by using a manual micromanipulator (Unisense) and microsensors with a tip of 50 µm in diameter (OX-50; Unisense) for the O_2, and 500 µm in diameter (N_2O-500) for N_2O. Both O_2 and the N_2O microsensor were calibrated by using a 2-point calibration method according to Unisense recommendations. Detection range for the N_2O microelectrodes was 500 to 0.1 µM concentrations in water.

4.4.3 PROFILE (Version 1.0)

For interpretation of measured concentration profiles of O_2 and N_2O in the sediments, the software program PROFILE (Version 1.0) was used. This was conducted to do a more precise prediction of zones with both consumption and production of the different species. Steady state conditions are assumed and pore water movements (i.e. burial, compaction, groundwater flow, wave action) neglected, the equation used in the program is expressed in equation 17.

$$\frac{d}{dx}(\Phi (D_S + D_B) + \phi\alpha (C_0 - C_0) + R = 0 \qquad \text{Eq.17}$$

Where C is the pore water concentration, C_0 is the bottom water concentration, x is the depth, ϕ is the porosity, D_S is the molecular diffusivity (corrected for tortuosity), D_B is the biodiffusivity, α is the irrigation coefficient and R is the net rate production (or consumption if R is negative) per volume of sediment (Berg, 1998). The PROFILE program creates series of least squares, which fit the obtained concentration profiles from multiple solutions of the equation above. From these series, one particular fit is selected through a statistical F-testing (Berg, 1998).

The result from the program is based on a *control volume approach*, which implies that the sediment column and the diffusivity boundary layer (DBL) (not included in this analysis) is divided into N horizontal layers. Grid points are located in the center of these layers where values of ϕ, D_S, D_B and α are known with the assumption that these grid points are unchanged through the whole control volume. In these calculations, irrigation and bioturbidity are neglected.

The processing of data involves two steps; 1) find the lowest number of equally spaced zones and the production rate that best explains the data and 2) to determine if adjacent zones can be submerged without reducing the quality of the fit. To choose the best fit the null hypothesis is as follows; "*Given a number of zones (K), the addition of one or more zones does not significantly improve the prediction of the measured concentration profiles*" (Berg, 1998).

The benthic activity is not measured in this project but is still an important factor to consider when talking about the geochemistry in the sediment. To have some indications on the influence of the benthic activity, calculated O_2 fluxes from the program is compared to the measured O_2 flux. Since the program does not include bioirrigation and bioturbidity and only accounts for the diffusion process, a difference could indicate on a benthic activity even if the quality of the data needs to be considered carefully.

4.4.4 Oxygen consumption

The O_2 consumption was measured at the same time as the core incubations. It was made by a *PC based fiber optic oxygen meter FireSting OXYGEN* from the company *PyroScience*, which measured the concentration in *µmol/l*. Similar to the core incubations the measurements were stopped after 10, 5 hours and calculated in the same way; the final concentration was subtracted with the start concentration and multiplied with the volume (liters) of water in the core, and divided by the incubation time in hours and multiplied by 24 to get the flux per day. The flux was then multiplied with the surface area (transformed from cm^2 to m^2 by multiplying with factor 10,000) and expressed as µmol $m^{-2}d^{-1}$.

4.4.5 DIN concentration in pore water extraction through slicing

To get a higher resolution of the spatial distribution of NH_4^+ NO_3^- and NO_2^- in the sediment, the top two centimeters were sliced every 0.25 cm and then every centimeter until a depth of ten centimeter. The samples were put into 50 ml Falcon tubes and centrifuged at a rate of 3000 rpm for ten minutes. The samples were then filtered and stored in the freezer until the analysis. The samples were thawed a couple hours before the analysis in the fridge and analyzed with a continuous segmented flow analyzer (QuAAtro SEAL) with a XY-2 sampler, at the department analytical chemistry and environmental science.

4.5 Samples taken from the Sewage treatment plant facility at Himmerfjärden

Samples were taken from the outgoing sewage water at the STP once a week between 11th of February to the 16th of April. The first five sample opportunities were taken from a large tank where treated water regularly enters during a time period of 24 hours. The samples were taken in the morning and represents the average N_2O concentration over a day. All samples were killed by 50 % (w/w) $ZnCl_2$ in 12 ml exetainers and transported to Stockholm University for later analysis on the gas chromatograph. During the other sample opportunities, samples were directly taken of the outgoing sewage water, which enters Himmerfjärden. The samples were killed in the same procedure as explained above.

4.6 Elemental Analyzer-DeltaV Advantage mass spectrometer

The abundances of $^{29}N_2$ and $^{30}N_2$ were determined by a gas chromatography-isotope ratio mass spectrometer (GCMS). The samples are injected into a continuous flow of Helium at a rate of (26-27 ml min^{-1}) and transported through a water trap (filled with ice and NaCl to lower the temperature) and separated in a packed GC column (Poropak Q, 6ft, 1/8 in, 80/100 mesh). The samples enter the mass spectrometer by an open split (1/10) interface (Conflo IV, Thermo Scientific) and analyzed by Delta V Advantage (Thermo Scientific). The vacuum at the inlet of the mass spectrometer extracts the sample from the continuous flow of helium from the column. The parameters controlling the amount of sample entering the mass spectrometer are the flow rates of helium and the size of the column. The samples for N_2 are then passed through a reduction copper oven at 650°C to reduce all remaining O_2 and N_2O to N_2. The description of the mass spectrometer can also be read in the paper of Holtappels et al, 2011.

The N_2O analysis is a modified version of the N_2 analysis, using the N_2 line with a configuration for CO_2 since it has a similar mass as N_2O. A good separation between CO_2 and N_2O is important since they have similar masses and would interfere with the N_2O peak. The reduction oven is not included in the setup for the N_2O analysis.

Important things to diminish are the CO (mass 28), H_2O and NO (mass 30) contaminations for the N_2 analysis and NO_2 (mass 46) for the N_2O analysis. The source of CO mainly comes from the air and contaminate the samples if vacuum is established in the syringe. A fast transfer of the syringe to the inlet is necessary and to always check the syringe in between the injections. This can be done by injecting air into water; seeing bubbles implies that the syringe is working properly. Removing water and O_2 is important since it can be ionized and split into reactive oxygen species, which can react with N_2 and produce NO.

30 µL of a pure N_2O standard and air samples for N_2 standard, were injected between every 5th samples. Figure 4 illustrates the GSMS-preparation line.

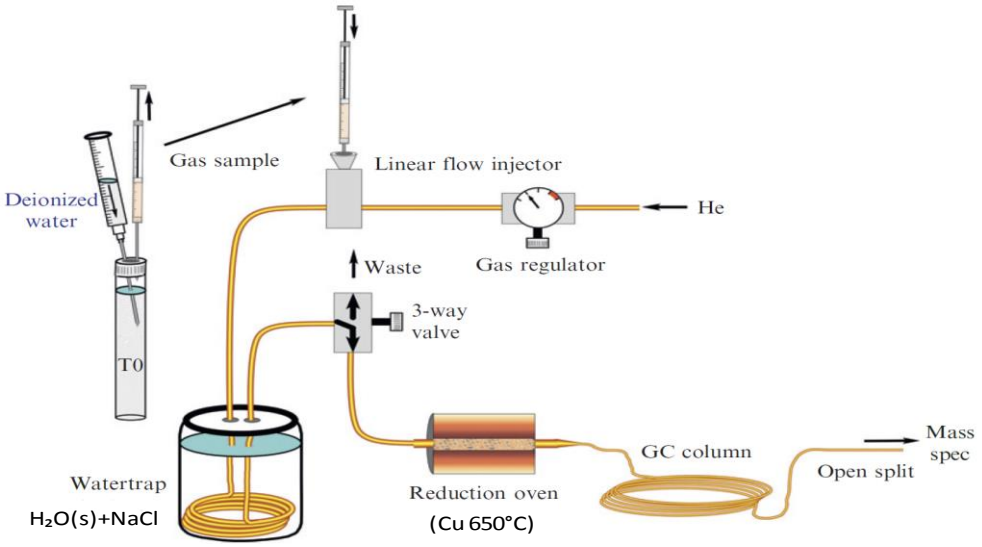

Figure 4. A sketch of the GSMS-preparation line. The sample is injected in a continuous flow system into a helium stream of 26-27 ml min^{-1}. The water trap removes water and the copper oven reduces O_2 before the sample is separated in the GC column (Porapak Q, 6 ft, 1/8 in) and goes into the mass spectrometer by an open split.

4.6.1 $^{15}NH_4^+$tracer experiment for potential N_2O production during nitrification

Samples for nitrification were collected in clean 500 ml glass bottles at five depths. The depths were chosen after looking at the CTD profile depending on the turbidity and light signal, since light inhibits the nitrification (Rönner, 1982). It was also important to take samples from different waters layers as well, which could be determined by looking at the CTD profiles. Six exetainers were filled with untreated water through large syringes from each glass bottle, which represented the blanks. Afterwards 1 ml of 50 mM of $^{15}NH^+_4$ was added and carefully mixed without shaking the bottle too much to avoid O_2 contamination. When the mixing was done, nine exetainers were filled; three time points with three replicates at each time to create a time series. One hour after the addition, time point zero (T_0) was taken by stopping the reaction with 100 µl 50 % (w/w) of $ZnCl_2$. Time point 1 (T_1) was taken after 24 hours and time point 2 (T_2) after 48 hours. They were stored in the cold during the whole experiment and put upside down until they were analyzed.

The method described above was changed in March sampling since the results from November did not show any nitrification rates. In March two depths were chosen after looking at the results from the gas chromatograph of the N_2O concentration in the water column from the previous sampling. Depths with an elevated abundance of N_2O were preferred. Two 2 L glass bottles were filled with seawater and surrounded by aluminum foil to avoid sun light. These were later subsampled into four 500 ml glass bottles in a cold room. One bottle contained no tracer, one had a tracer concentration of 2 µM, one with 10 µM and finally one with a 2 µM of tracer with an addition

of acetylene to an-end concentration of 5 % of the total water volume in the bottle. Acetylene was added to inhibit the N_2O reductase caused by denitrification, which would allow only nitrification to produce N_2O.

4.6.2 Calculations for production rates of N_2O from the nitrification

The calculations explained in this section have been modified to suit calculations for N_2O from the method description of Holtappels, et al., 2011. These equations are used for the analysis of N_2 as well, but with the masses $^{28}N_2$, $^{29}N_2$ and $^{30}N_2$.

From the mass spectrometer measurements, the integrated peaks for ^{44}N-N_2O, ^{45}N-N_2O and ^{46}N-N_2O are derived. The peaks represent both the natural levels of N_2O and the amounts produced during the experiment. This is represented in equation 18 to 20:

$$^{44}A_M = {}^{44}A_N + {}^{44}A_B \qquad \text{Eq.18}$$

$$^{45}A_M = {}^{45}A_N + {}^{45}A_B \qquad \text{Eq.19}$$

$$^{46}A_M = {}^{46}A_N + {}^{46}A_B \qquad \text{Eq.20}$$

Where *A* represents the peak area, index *M* the measured peak area, which is the sum of the background peak area (index *B*) and the produced isotope (index *N*) (Holtappels, et al, 2011). It is assumed that the relative isotope composition of the background in the samples are the same as the relative isotope composition of the pure N_2O standard, the latter is further assumed to have the same isotopic composition as the N_2O in the atmosphere. A difference between these are assumed to be caused by the isotope fractionation during the production of N_2O. But, since the change of the isotopic composition is several orders of magnitude higher than natural fractionation effects, it can be neglected and the ratios between $\frac{^{45}A_B}{^{44}A_B}$ and $\frac{^{46}A_B}{^{44}A_B}$ can be determined from the pure N_2O standard $\left(\frac{^{45}A_{Std}}{^{44}A_{Std}} \text{and} \frac{^{46}A_{Std}}{^{44}A_{Std}}\right)$.

In this experiment there were two blanks per time point without any tracer but otherwise treated in the same way as the spiked samples. It is then possible to distinguish between normal background levels and the excess amounts produced from the labeled ^{15}N experiment. The ratio between the peak area of $\frac{^{45}A_{Std}}{^{44}A_{Std}}, \frac{^{46}A_{Std}}{^{44}A_{Std}}$ and $\frac{^{45}A_{Sample}}{^{44}A_{Sample}}, \frac{^{46}A_{Sample}}{^{44}A_{Sample}}$ is subtracted from each other. This *excess ratio* is expressed in equation 21.

$$^{45}A_N \approx \frac{^{45}A_{Sample}}{^{44}A_{Sample}} - \frac{^{45}A_{Std}}{^{44}A_{Std}} \qquad \text{Eq.21}$$

Since the ratio between the injected moles of N_2 and peak area is known in the standard, the peak area from the injection can be transformed into moles. This expression can be seen in equation 22.

$$^{45}M_N = {}^{45}A_N \left(\frac{^{tot}M_{Std}}{^{tot}A_{Std}}\right) \qquad \text{Eq.22}$$

M is the moles injected into the mass spectrometer and $^{45}A_N$ is the excess ratio. The total area of the standard is calculated according to equation 23.

$$^{tot}A_{Std} = {}^{44}A_{Std} + {}^{45}A_{Std} + {}^{46}A_{Std} \qquad \text{Eq.23}$$

To calculate $^{tot}M_{std}$, the molar volume of air (in standard conditions) and the fraction of N_2O in the atmosphere is used. This is displayed in equation 24.

$$^{tot}M_{Std} = 3.20 * 10^{-9} \left(\frac{V_{Std}}{24.055}\right) \qquad \text{Eq.24}$$

From this, the initial concentration in the exetainer for each respective N_2O isotope can be calculated according to equation 25.

$$^{45}C_N = (^{45}M_N) \left(\frac{V_H + (V_W / F_{\left(\frac{g}{h}\right)})}{V_I V_W}\right) \qquad \text{Eq.25}$$

Where V_I is the volume of the injection, V_H the headspace volume, V_W the water volume and $F_{g/w}$ the fractionation factor of N_2O between the gas and the water phase.

4.6.3 Denitrification rates

The cores were immediately transferred back to the lab and stored in a bucket of cold bottom water in a cold room with the same temperature as the bottom water. The cores were covered with bottom water for one hour before small magnets were put on at a stir rate of 60 rpm. The mixing and homogenizing of the water was established with a bubbling stone (in station H3 since the water already was close to 100 % saturated by O_2) for six hours before the pre-incubation started. Four samples were randomly collected in the bucket before and after the addition of the tracer to check background concentrations of NO_3^- but also to establish a ratio between the unlabeled and labeled NO_3^- (Bonaglia et al, 2014A). The NO_3^- samples were filtered and frozen immediately after sampling.

The tracer, $Na^{15}NO_3^-$(99% atom, 10 mmol L^{-1} stock solution), was added in each core to reach a final concentration of 25-, 50-, 100- and 150 µM of $^{15}NO_3^-$, which required a pre-calculation of the water volume for each core. The pre-incubation time is dependent on the O_2 penetration depth; deeper penetration depth increases the time for NO_3^- to reach the denitrification zone, therefore a longer pre-incubation time is needed. It is extremely important to have a correct pre-incubation time since a linear production of ^{15}N-N_2 is essential for the experiment (Bonaglia et al, 2014). When the incubation began, the cores were capped with rubber stoppers without any air bubbles. The incubation started immediately after the lag time and samples for N_2 and N_2O were taken from each

concentration after mixing the upper seven centimeters of the sediment with the overlying water and mixed with 50 % (w/w) $ZnCl_2$. The incubation lasted for twelve hours and samples for N_2 and N_2O were taken from every core and triplicates were made for each concentration.

4.6.4 Calculations for denitrification rates

The samples were analyzed using a MSGC and the calculations for converting peak areas to concentrations can be seen in section 4.6.2. A helium headspace is introduced into the exetainer and after one hour of vigorously shaking the samples, more than 98% of the N_2 is found in the gas phase (Steingruber, S.M., 2001). Since the setup for these experiments results in endpoint incubations, the production rates of $^{29}N_2$ and $^{30}N_2$ (r^{29}, r^{30}) are calculated as described in equation 26.

$$r^{29} = \left([^{29}N_2]_f - \frac{[^{29}N_2]i}{A*t}\right) * (Vw + \phi Vs) \quad \text{Eq.26}$$

Where $[^{29}N_2]_f$ and $[^{29}N_2]_i$ represents the final and the initial concentration of $^{29}N_2$, *A* is the area, *t* is the time interval, V_w is the incubated water volume (liters), V_s is the volume of the sediment (liters) and ϕ is the sediment porosity. The initial concentration is measured by sacrificing a reference core in the beginning and measuring the water-sediment slurry. The same is calculated for r^{30}. After calculating the production rates the next step is to calculate the denitrification rates of $^{15}NO_3^-$ (D_{15}), which is the sum of the ^{15}N in the produced labeled N_2. This is displayed in equation 27.

$$D_{15} = r^{29} + 2 * r^{30} \quad \text{Eq.27}$$

Since the tracer is mixed with unlabeled NO_3^-, the denitrification rate of $^{14}NO_3^-$ (D_{14}) can be calculated according to equation 28.

$$D_{14} = D_{15} * \frac{r29}{2*r30} \quad \text{Eq.28}$$

The total denitrification rate is expressed in equation 29.

$$D^{tot} = D_{15} + D_{14} \quad \text{Eq.29}$$

Through equation 29, denitrification rates caused by the influx of $^{15}NO_3^-$ from the water column and into the sediment can be calculated according to equation 30 (D^{tot}_W).

$$D_w^{tot} = \frac{D_{15}}{\varepsilon} \quad \text{Eq.30}$$

Where *ε* is the enrichment factor for the isotopic NO_3^- during the incubation, which is expressed in equation 31.

$$\varepsilon = \frac{[NO_3^-]a - [NO_3^-]b}{[NO_3^-]a} \quad \text{Eq.31}$$

Where the brackets represents the concentration after and before the addition of the tracer. Denitrification in the sediment can occur either by a NO_3^- supply from the water column (D_W) or by NO_3^- produced in the sediment through nitrification (D_n). These processes can be measured and distinguished by IPT. Therefore, the last step is to calculate the coupled nitrification-denitrification within the sediment (D_n). This is expressed in equation 32.

$$D_n = D^{tot} - D_w^{tot} \qquad \text{Eq.32}$$

If it is assumed that D_w^{tot} increases linearly with higher NO_3^- concentrations, an extrapolation can be made to calculate the denitrification rate in tracer-free conditions. This is expressed in equation 33:

$$D_w = D_w^{tot} * (1 - \varepsilon) \qquad \text{Eq.33}$$

Figure 5 represents the transformation pathways during this experiment. For a deeper reading of the equations and steps, the reader is referred to the paper of Nielsen, 1991 and Steingruber, et al., 2001.

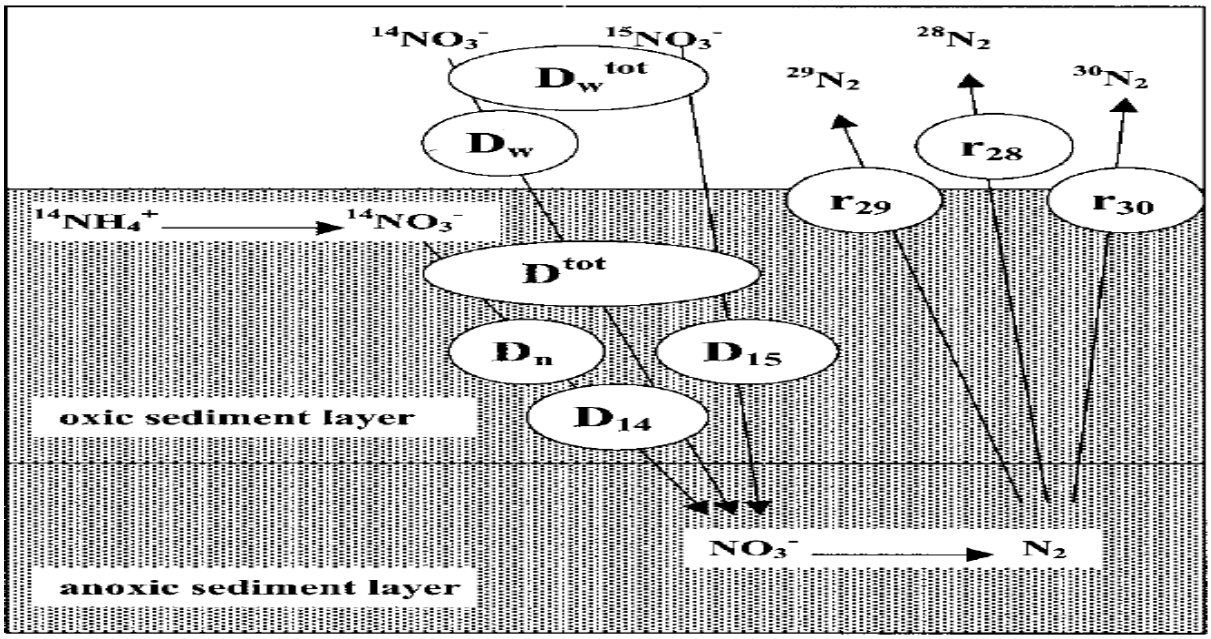

Figure 5. A representation of the transformation rates during a $^{15}NO_3^-$ tracer experiment. D_w^{tot} is denitrification supported by diffusion of $^{15}NO_3^-$ from the water column, D_w is denitrification rates under tracer-free conditions, D_n is the coupled nitrification-denitrification, D^{15} and D^{14} are the specific denitrification rates for ^{14}N and ^{15}N, D^{tot} is the sum of D_{14} and D_{15}, and the production rates of the mass of 28, 29 and 30 are represented by $^{29}N_2$, $^{29}N_2$ and $^{30}N_2$ respectively. (Steingruber, et al., 2001)

When $^{28}N_2$, $^{29}N_2$ and $^{30}N_2$ was analyzed, a reduction oven was placed after the water trap where the remaining O_2 in the sample is reduced at the surface of the cupper granules at a temperature of 650°C. Remaining O_2 molecules can split into reactive oxygen species, which can recombine with N to form NO (mass 30). The consequences would be a higher detection limit for $^{30}N_2$ in the samples. 30 µl of air standard was injected between every 5th samples.

4.7 Statistics

The software program JMP®11 was used for all the statistical analysis. Looking at the distribution, variance, number of groups and the sampling size, either the non-parametric Kruskal-Wallis , Mann-Whitney test, the parametric ANOVA test or a pooled- or a non-pooled t-test was conducted to see whether there was a significant difference between the groups or not. When the sampling size was

small, a non-parametric test was more favorable to choose since it consisted fewer assumptions. For a better and easier evaluation of the data, an *Unequal Variance* test (Levenes test with the null hypothesis; equal variance) was conducted. If the test resulted in rejection of the null hypothesis the Kruskal-Wallis test was conducted. If Levenes test not rejected H_0, the ANOVA test was applied instead.

To see *where* the significant differences between each group, the nonparametric multiple comparison *Wilcoxon Each Pair* test was used after a Kruskal-Wallis test, which is a test that compare all pairs in all possible combinations. If the ANOVA test was conducted, the parametric multi-comparison Tukey-HSD test followed.

5 Results

5.1 N_2O-, temperature-, salinity-, O_2- and DIN profiles from the water column

5.1.1 N_2O-, temperature-, salinity- and O_2 profiles in the water column

Figures 6 and 7 illustrate the concentrations of N_2O through the seasons together with temperature-, salinity- and O_2 data for H3 in figure 6 (A, C) and figure 7 (E, G), and for H6 in figure 6 (B, D) and figure 7 (F, H).

The N_2O profiles at H3 did not change statistically between the seasons ($p<0.05$), and have a uniform distribution throughout the water column. H6 had elevated values at all depths in both October and March (fig. 6B and fig. 7H). The peak of N_2O in October (50.7 nM) occurs right under the chemocline at a depth of 20 m (fig. 6B), which was also the case in March but at 10 m (37.8 nM) (fig. 7F). The maxima in January was at 25 m (12.4 nM) and the maxima in November at 30 m (10.3 nM) (fig. 7C and fig. 7D respectively).

Surface waters were well mixed at both stations throughout the year. The extent of this well mixed layer changed depending on season and was different depending on station; more distinct chemocline during October and a less deep well mixed zone (fig. 7A and B), and a weaker signal in November with a deeper well-mixed zone (fig. 7C and D). January and March had the weakest chemocline signal with H6 in January as an exception, where the chemocline was a bit more distinct (fig. 7F).

Since the data was normally distributed for the N_2O concentrations in the water column, an ANOVA test was applied to determine if the groups had equal mean values. Since H_0 (H_0: $\mu_1=\mu_2\ldots\mu_k$) was rejected, an *All Pairs Tukey-Kramer test* was conducted to determine which mean values were different. The N_2O concentrations were equal in October and March for H6 and somewhat elevated in January, but statistical different from the others. H3 had a statistical similar

N_2O level throughout the year. The results from the statistical analysis can be read in appendices 10.1.

N_2O-, temperature-, salinity- and O_2 water profiles in October and November

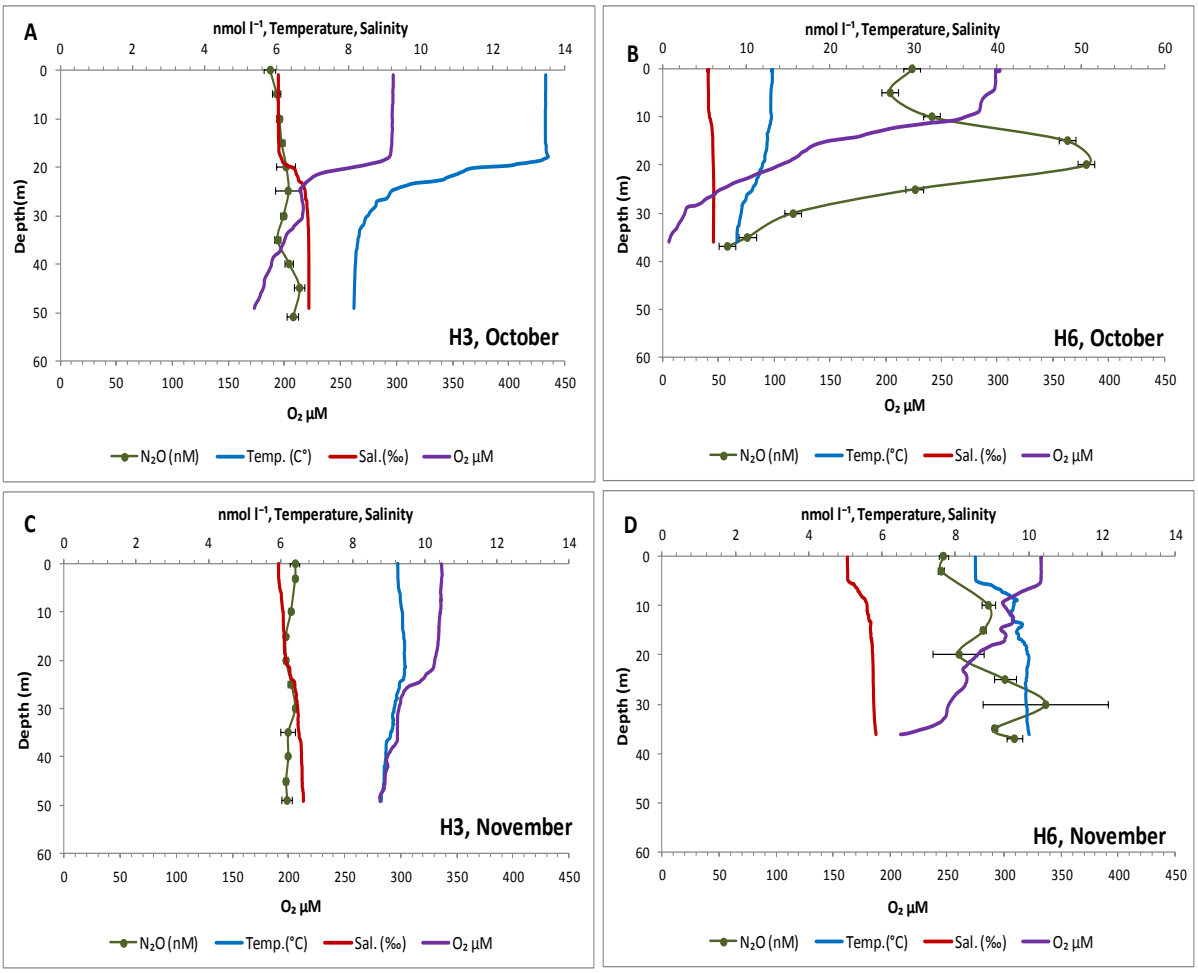

Figure 6. CTD and concentration profiles of N_2O for both H3 (A, C) and H6 (B, D). The upper x-axis represents the [N_2O] in nM, the temperature (C°) and the salinity (‰) whilst the lower X-axis represents saturation values of O_2. Note the change in the upper x-axis in diagram B.

N_2O-, temperature-, salinity- and O_2 water profiles in January and March

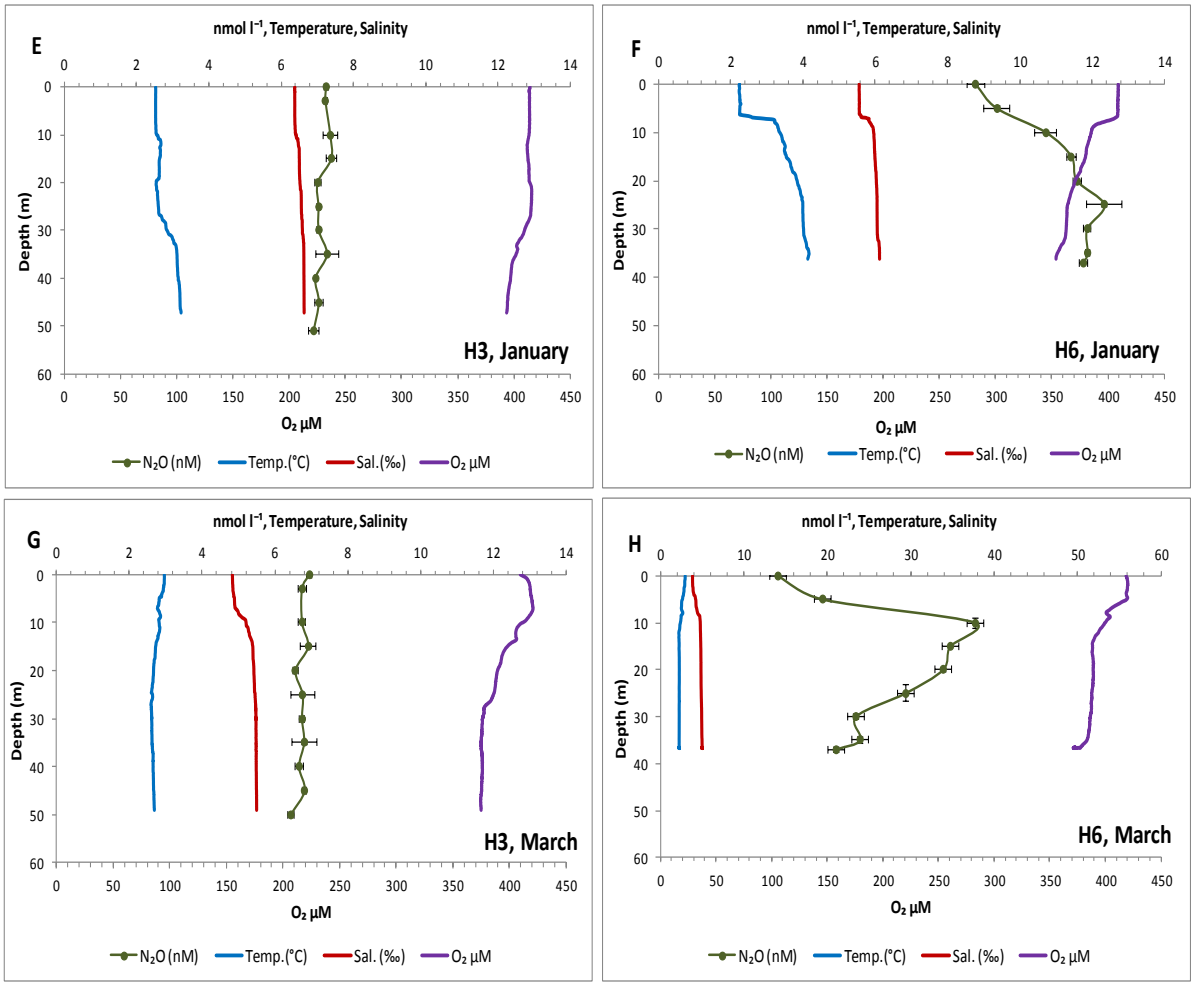

Figure 7. CTD and concentration profiles of N_2O for both H3 (E, G) and H6 (F, H). The upper x-axis represents the [N_2O] in nM, the temperature (C°) and the salinity (‰) whilst the lower X-axis represents saturation values of O_2. Note the change in the upper x-axis in diagram H.

5.1.2 DIN profiles in the water column

Figures 8 and 9 shows the NH_4^+ (red line) and NO_3^-/NO_2^-(green line) concentrations throughout the year with N_2O (blue line) saturation values in the water column at H3 and H6. The results from H3 can be seen in figure 8 (A, C) and figure 9 (E, G), while H6 can be seen in figure 8 (B, D) and figure 9 (F, H).

The concentrations of NO_3^-/NO_2^- in October increased with depth and had a maxima at 45 (6.2 µM) - and 30 m (9.0 µM) for H3 and H6 respectively, followed by a decrease towards the sediment (fig. 8A and B). The N_2O concentration was slightly undersaturated throughout the water column at H3, with an 85 % saturation at the surface and 97 % in bottom waters (fig. 8A). H6 had a supersaturation of 458 % at the surface, 761 % at 25 m and 115 % in bottom waters (fig. 8B).

The NO_3^-/NO_2^- profile in November at H3 showed three peaks at 10-(5.9 µM), 30-(5.0 µM) and 45 m (5.0 µM) (fig. 8C). In comparison with October, the NO_3^-/NO_2^- level was slightly higher at H6 but with a steep decrease between 5-(10.7 µM) and 20 m (4.8 µM), followed by a steep increase between 20- and 25 m (10.3 µM) and a bottom maxima at 38 m (11.5µM) (fig. 8D). The N_2O concentration was slightly undersaturated throughout the water column at H3, with a 94 % saturation at the surface and decreasing levels with depth with minimum values at the bottom (90 %) (fig. 8C). H6 had the lowest saturation values at the surface in November (109 %), with increasing levels towards the bottom where maximum values were reached (146 %) (Fig. 8D).

The month with the highest NO_3^-/NO_2^- levels for both stations, were January (fig. 9E and F). The peaks were right above or near the chemocline at a depth of 15-(11.8 µM) and 5 m (24.3 µM) for H3 and H6 respectively, even if the chemocline signal for H3 was somewhat weak. The concentration slightly decreased towards the bottom, but the minima for H3 occurred at 25 m (6.0 µM) whereas H6 had a minima at 37 m (10.5 µM). The N_2O profile was rather stable around a 103- to 109 % saturation throughout the water column at H3 (fig. 9E). H6 had the lowest saturation at the surface in January (123 %) with increasing levels towards the bottom with a peak at 25 m (173 %) (fig. 9F).

The highest NO_3^-/NO_2^- levels in March, were at the surface (4.3 µM) with two smaller peaks at 30-(3.1 µM) and 49 m (3.5 µM) at H3 (fig. 9G). H6 had an irregular increase until 25 m (11.8 µM), where it started to decrease until the last 5 m (6.5 µM), which then increased again towards the bottom (10.1 µM) (fig. 9H). The N_2O saturation ranged between 98- to 104 % throughout the water column at H3 (fig. 9G). H6 had the lowest saturation of N_2O at the surface (213 %), a saturation of 551 % at 10 m and a saturation of 302 % in bottom waters (fig. 9H).

In October two smaller peaks of NH_4^+ were detected at- and right above the chemocline for H3 (1.6- and 1.8 µM) (fig. 8A). The maxima for both stations occurred close to the sediment (3.7- and 4.7 µM for H3 and H6 respectively) (fig. 8A and B).

The NH_4^+ profile at H3 in November was uniform throughout the column with a minima at 15 m (2.3µM) and a slight decrease between 45m (5.0 µM) and 49 m (2.9 µM) (fig. 8C). The NH_4^+ profile at H6 had a maxima at 38 m (4.3 µM) and a minima at 15 m (0.6 µM) (fig. 8D).

NH_4^+ was totally absent in the upper 10 m at H3 in January, with two smaller peaks at 15-(2.4 µM) and 30 m (1.5 µM) (fig. 9E). H6 was totally depleted of NH_4^+, except at the surface (0.5 µM) (fig. 9F). H3 was also totally depleted of NH_4^+ in March with the surface as the only exception (0.85 µM) (Fig. 9G). The concentration of NH_4^+ was low at H6 as well with three smaller peaks at 0-(0.9 µM), 25- (0.6 µM) and 38 m (0.6 µM) (Fig. 9H).

DIN and N_2O profiles in October and November

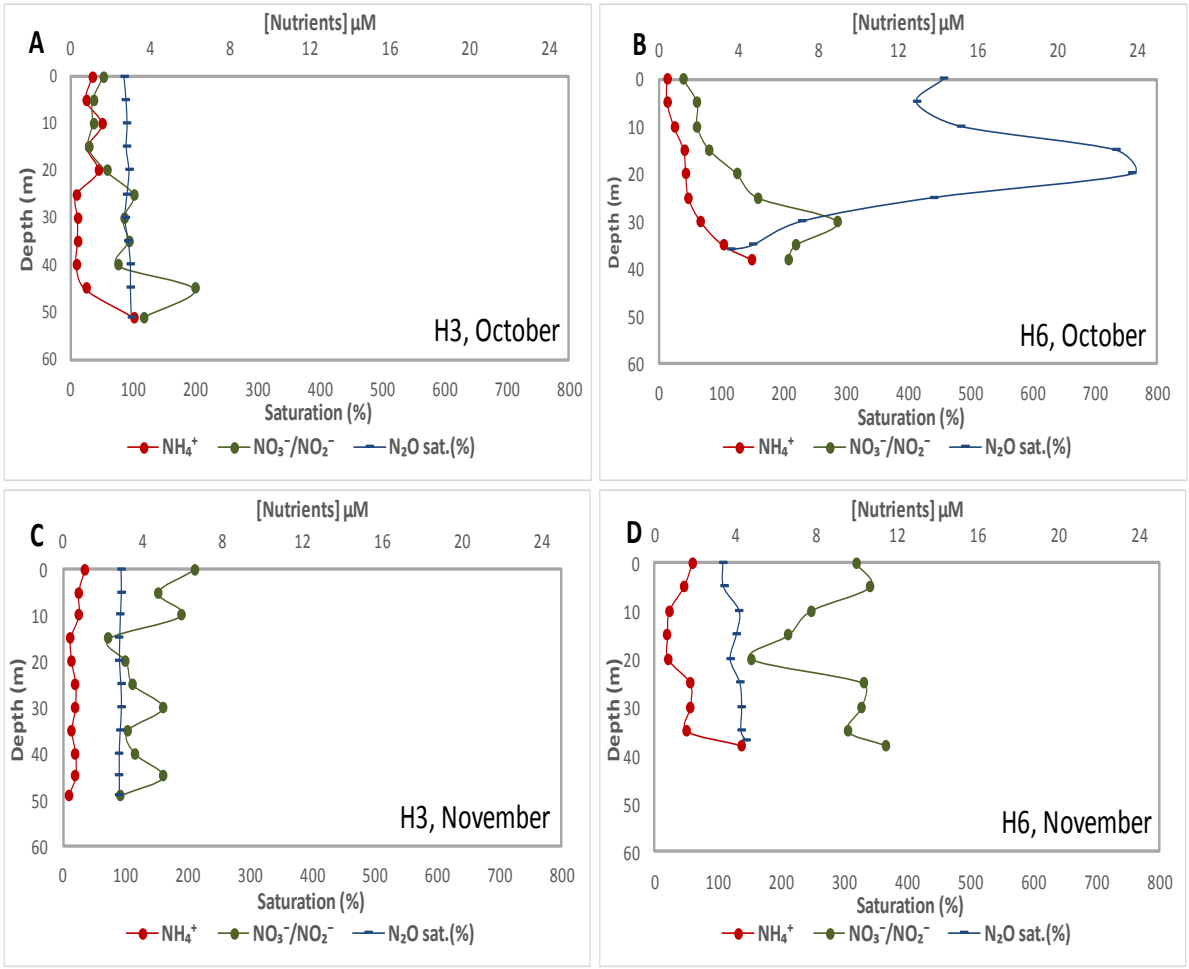

Figure 8. DIN profiles from both H3 (A, C) and H6 (B, D) throughout the year. The upper x-axis represents the DIN concentrations in µmol l^{-1} and the lower x-axis represents saturation values (%) for N_2O.

DIN and N_2O profiles in January and March

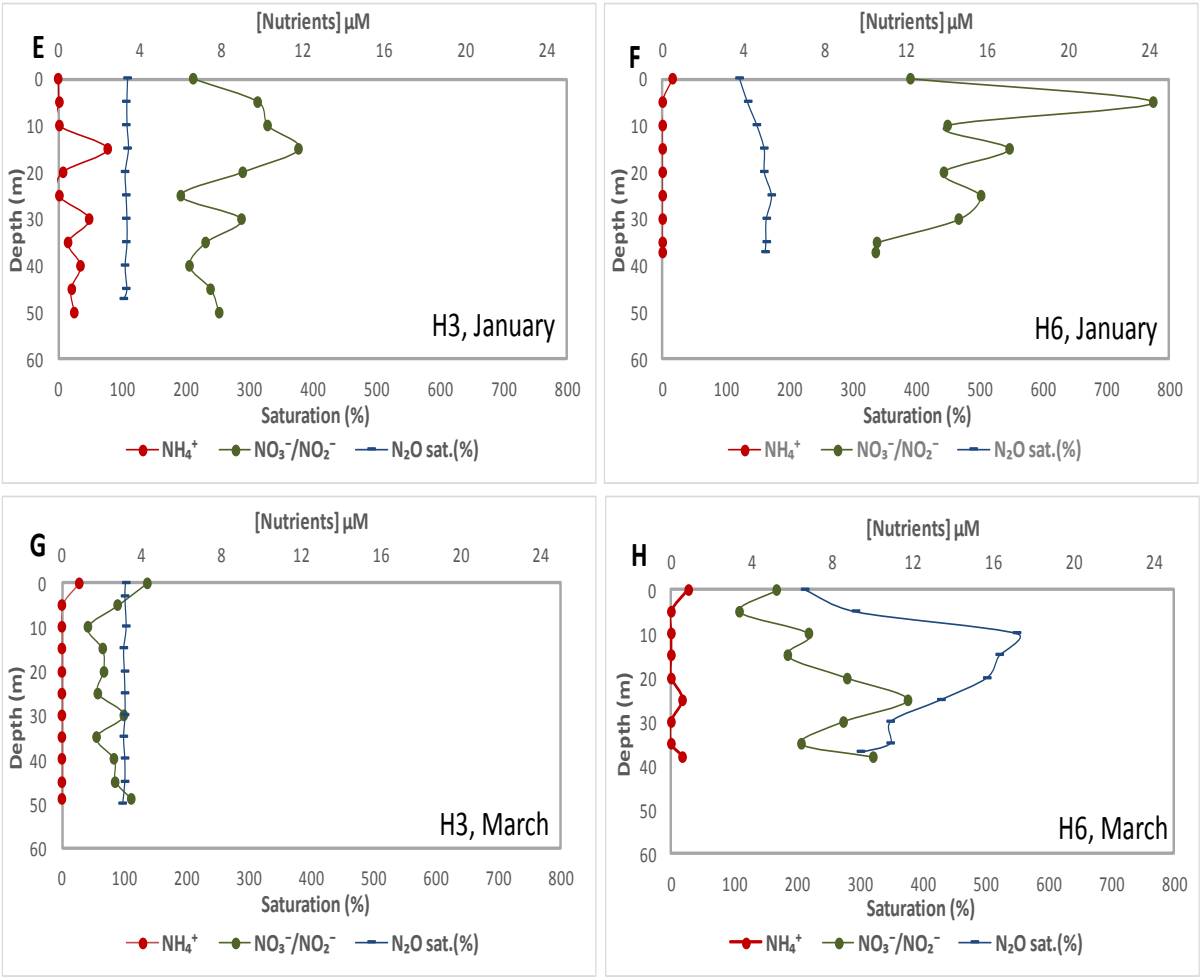

Figure 9. DIN profiles from both H3 (E, G) and H6 (F, H) throughout the year. The upper x-axis represents the DIN concentrations in µmol l^{-1} and the lower x-axis represents saturation values (%) for N_2O.

5.2 Benthic fluxes of O_2, N_2O and DIN

5.2.1 Sediment- and bottom water characteristics

Bottom waters reached minimum values in October for both stations (5.8 µM, corresponding to 1.2 % saturation at H6 and 173 µM, corresponding to 50 % saturation at H3) and maximum values in January for H3 (394 µM, corresponding to 97 % saturation), and March for H6 (373 µM, corresponding to 89 % saturation).

The sediment at H3 was characterized by a brown oxidized top layer that extended several centimeters in the sediment. This was consistent throughout the seasons and a presence of macrobenthos could be seen during all seasons with the highest activity in March. The sediment at H6 in October and November was black and covered by *Beggiatoa* mats at the top, indicating a

reduced environment. In January the sediment top was covered by a narrow, brown oxidized layer, which was extended to approximately one centimeter in March. The smell and the black sediment, gave indications of high levels of dissolved sulfide, which has been confirmed from other studies at H6 (Thang, et al., 2012). Benthic activity could not be seen in any of the seasons at H6.

H3 had a maximum temperature of 8.1°C in October and a minimum in March of 2.7 °C. H6 had a temperature range between 10.0- and 2.2 °C, with the maxima in November and minima in March. The salinity was lowest in March for both stations (5. 5 ‰ at H3 and 5.0 ‰ at H6) and highest in October (6.9 ‰ at H3 and 6.1 ‰ at H6).

5.2.2 Raw data of O_2 uptake from measurements with Firesting O_2 optodes

The Firesting O_2 meter, which uses an oxygen-sensitive red flash indicator technique and contactless sensors, was put on the cores in the beginning of the incubation to continuous record the O_2 levels over the whole time period. Figure 10 shows the consumption of O_2 over time for respective station during the incubations. The lack of results at H3 in January were due to problems with the optodes during measurements.

Raw data of the sediment O_2 uptake at H6 and H3

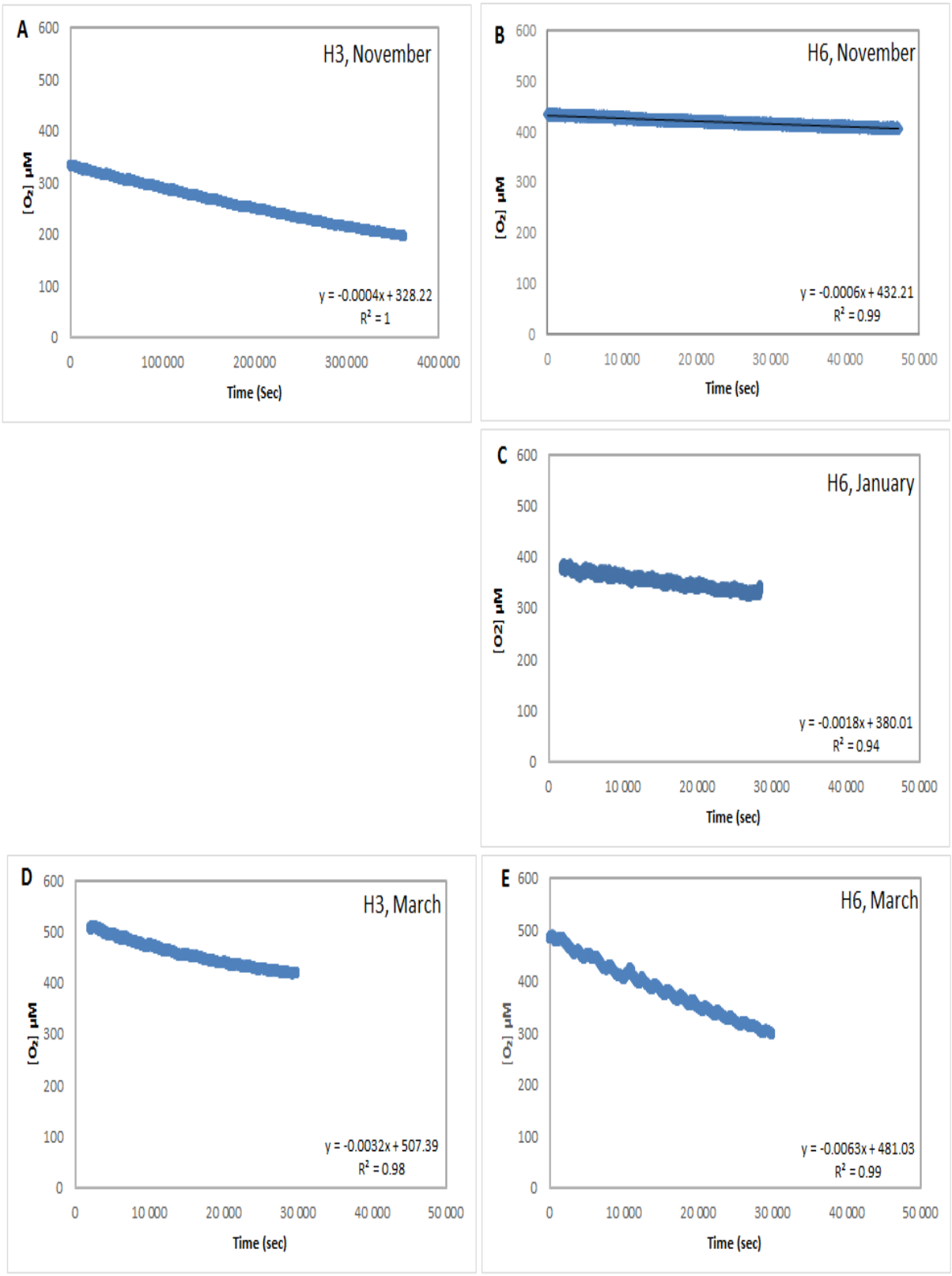

Figure 10. The O_2 uptake in µM over time (sec). Results were lacking from H3 in January due to problems with the measuring device. The results from November and March at H3 were represented in diagram A and D respectively and the results for H6 were represented in B, C and E for November, January and March respectively. Note the different x-axis in figure A.

5.2.3 Benthic Fluxes of O_2

Figure 11 displays the seasonal flux of O_2. Blue- and red bars represents the flux from H3 and H6 respectively. An ANOVA test was conducted together with the multi-comparison Tukey-HSD test. This is represented by letters in figure 11, where connected letters are fluxes which were statistical equal ($p<0.05$).

The O_2 uptakes in November were -3.0- and -3.6 mmol $m^{-2}d^{-1}$ for H3 and H6 respectively. The only result in January was at H6, which had a flux of -14.4 mmol $m^{-2}d^{-1}$. March had fluxes of -50.4- and -38.1 mmol $m^{-2}d^{-1}$ at H3 and H6 respectively. The fluxes in November and January were statistically similar for both stations whereas the fluxes in March at both stations were significant different.

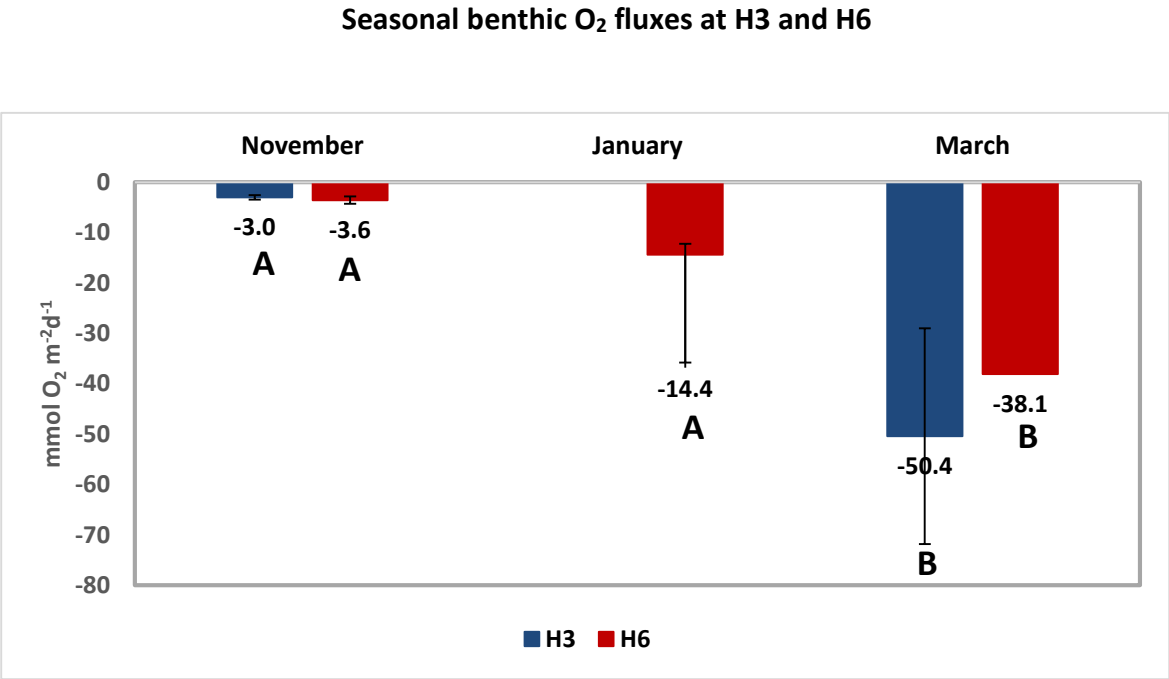

Figure 11. The O_2 uptake through the seasons expressed in mmol $m^{-2}d^{-1}$. Bars represent means followed by the standard deviation. The lack of bar at H6 in March was due to only one sampling point. Letters not connected with each other indicate a significant difference ($p<0.05$).

5.2.4 Raw data of the benthic fluxes of N_2O

When the cores were subsampled into smaller cores, the sediments often became disturbed in the process and filled the overlying water with floating particles. After letting the particles settle down for a couple of hours and then overflowing the cores with bottom water and using a bubbling stone to equilibrate the O_2 concentration, the incubation started when the samples were taken and rubber stoppers placed on top of the cores. The change over time in can be seen in figure 12 for the different cores. There were four replicates of the flux for each station and month, which are represented by different colors. The only exception was at H6 in March, which only had two replicates of the flux (H). Note the change of y-axis in diagram B.

Raw data of the benthic N_2O flux at H3 and H6

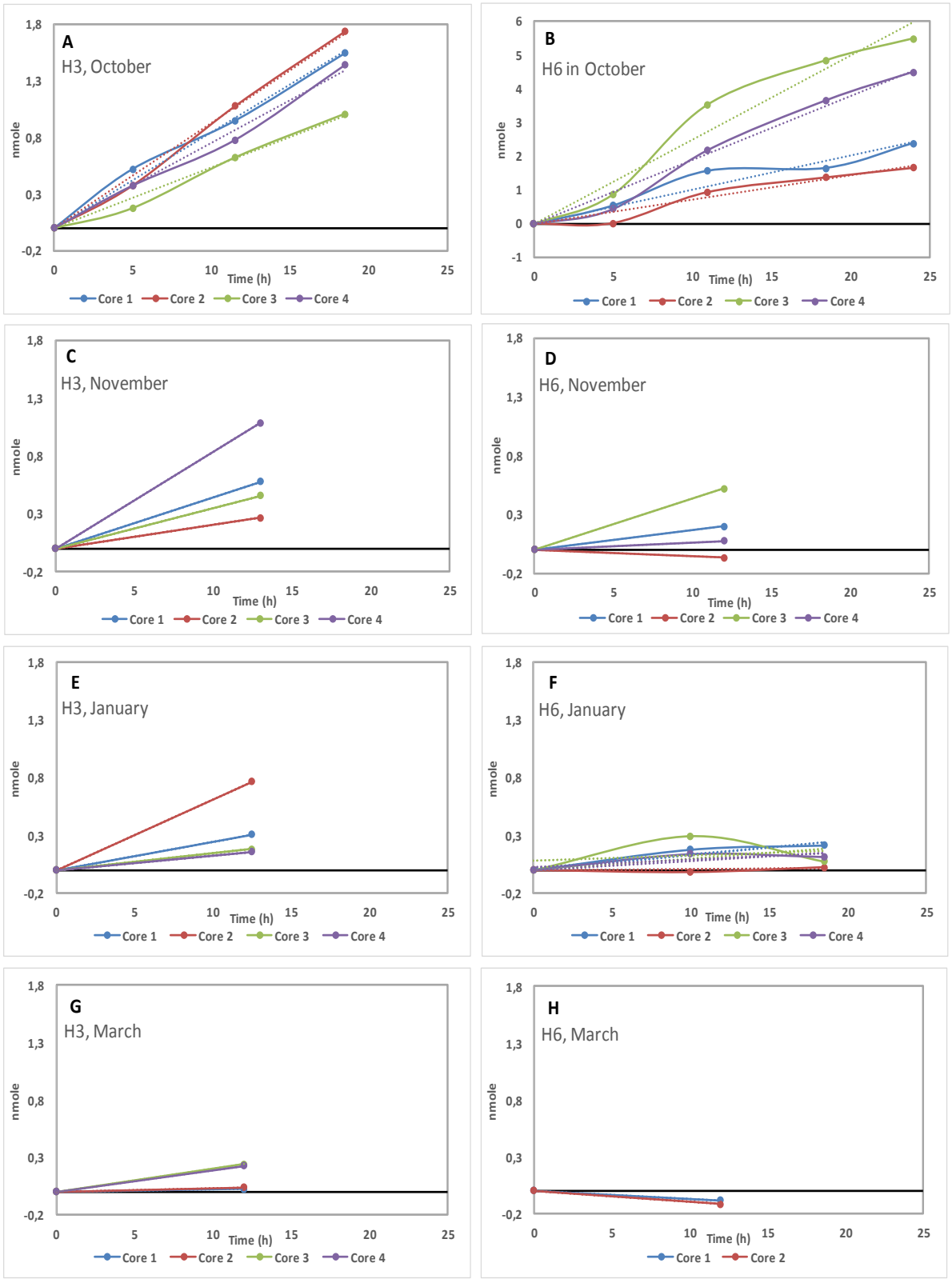

Figure 12. The nmol change of N_2O over time for H3 (A, C, E, G) and H6 (B, D, F, H) during core incubations. There were four replicates of the flux for each station and month, which is represented by different colors. The only exception was at H6 in March, which only had two replicates of the flux (H). Note the change of y-axis in diagram B.

5.2.5 Benthic flux of N_2O

Figure 13 displays the seasonal N_2O flux with complementary statistical data. An ANOVA test was applied together with a multi-comparison Tukey-HSD test. This is represented as letters in the figure, where connected letters indicate an equal flux ($p<0.05$). Blue- and red bars are the fluxes for H3 respective H6 and the complementary error bars the standard deviation.

The fluxes in October were the highest for both H3 and H6 (1.2 and 2.1 µmol $m^{-2}d^{-1}$). The fluxes decreased in November for both stations with a flux of 0.4- and 0.1 µmol $m^{-2}d^{-1}$ for H3 and H6 respectively. In January, the flux at H3 decreased even more (0.2 µmol $m^{-2}d^{-1}$) whereas the flux at H6 remained at the same level as in November (0.1 µmol $m^{-2}d^{-1}$). March had the lowest seasonal flux for both stations, where H6 even had an influx of N_2O into the sediment (-0.1 µmol $m^{-2}d^{-1}$). All fluxes were statistically similar except for the flux in October at H6, which was significant different.

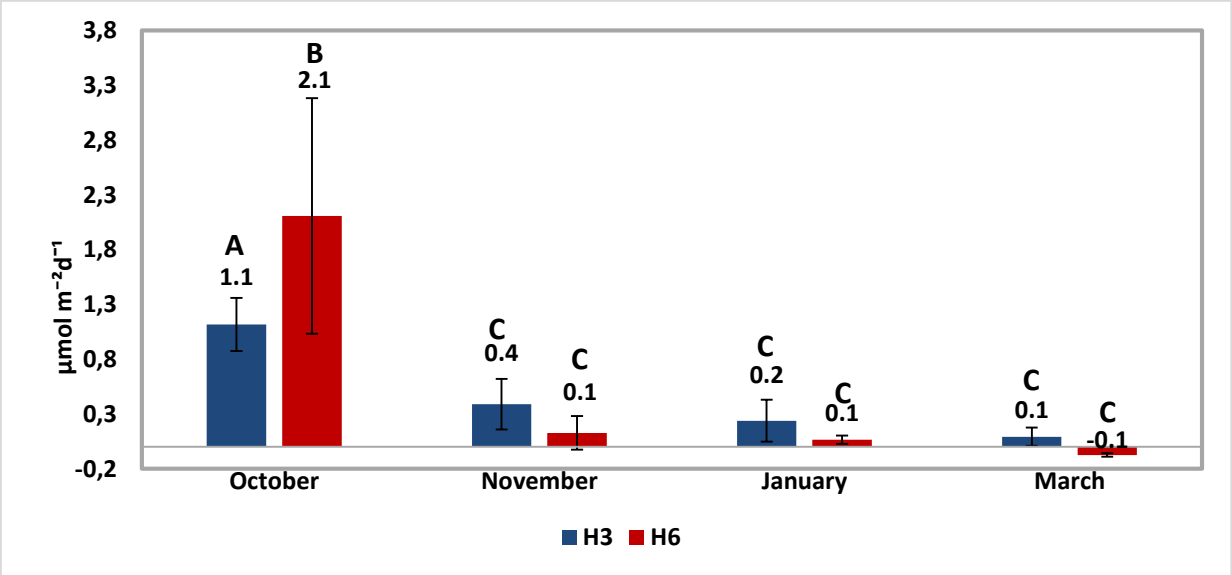

Figure 13. The N_2O flux through the seasons expressed in µmol $m^{-2}d^{-1}$. Blue- and red bars represents H3 and H6 respectively and represent mean values and the error bars the standard deviation. An ANOVA test was applied with the Tukey-HSD multi-comparison test. Bars with connected letters indicate an equal flux ($p<0.05$).

5.2.6 Benthic flux of DIN

Figure 14 displays the seasonal flux of NH_4^+ and NO_3^-/NO_2^- at the two stations, where blue- and red bars represents H3 and H6 respectively. Since the Levenes test did not reject H_0 for the NH_4^+ analysis, an ANOVA test was applied with the comparison for all pairs Tukey-Kramer method. The Wilcoxon multi-comparison test was used in the analysis of the NO_3^-/NO_2^- since H_0 was rejected for both the Levenes- and Wilcoxon test. The results from the statistics were from a seasonal comparison of NH_4^+ and NO_3^-/NO_2^- separately, the letter combinations are hence read separately for the two nutrient species. Connected letters means that there is not a significant difference ($p<0.05$).

The fluxes of NH_4^+ were 28.5-, 338.2 and 57.9 µmol $m^{-2}d^{-1}$ at H3 in November, January and March respectively, and at H6 1788.2-, -0.7- and 462.7 µmol $m^{-2}d^{-1}$. The NO_3^-/NO_2^- fluxes at H3 were -23.6-, 180.5 and -123.9 µmol $m^{-2}d^{-1}$ in November, January and March respectively, and at H6 1058.9-, -37.6- and 257.2 µmol $m^{-2}d^{-1}$.

The fluxes of NH_4^+ were significantly similar for all seasons and stations except in November at H6, which was significantly different. The NO_3^-/NO_2^- fluxes were significantly similar at H3 through the seasons, whereas H6 in November was significantly different. The NO_3^-/NO_2^- flux in March at H6, was significantly equal to the November fluxes.

Seasonal benthic flux of DIN at H3 and H6

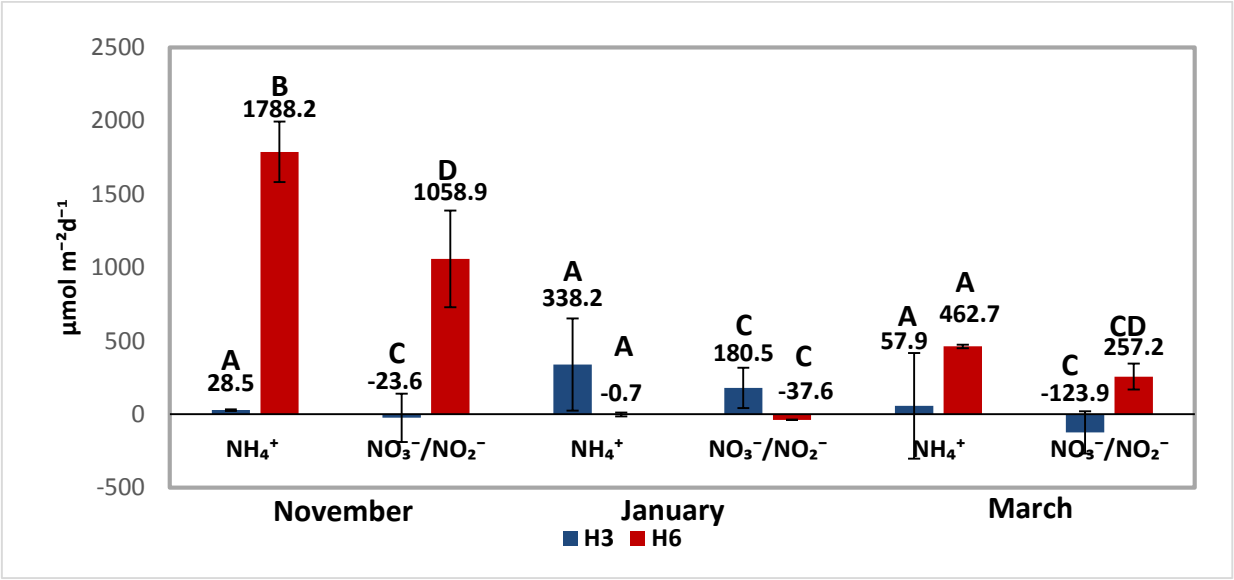

Figure 14. DIN fluxes November, January and March are expressed in µmol $m^{-2}d^{-1}$. Blue- and red bars represents H3 and H6 respectively and represent mean values and the error bars the standard deviation An ANOVA test was applied with the Tukey-HSD multi-comparison test. Bars with connected letters indicate an equal flux and are read separately for each nutrient ($p<0.05$).

5.3 DIN concentrations in sediment

Figure 15 displays the seasonal DIN concentrations in the sediment at the two stations. Note the lack of data for NO_2^- at H6 in November (fig. 15A), NH_4^+ at H3 in January (fig. 15C), NH_4^+ at H6 in January (fig. 15D) and NO_3^- at H3 in March (fig. 15D), H6 in November and January. The results are lacking due to miscalculations of the concentration spectra, which resulted in a sample treatment not favorable for a good analysis for these particular DIN species and are hence not trustworthy results.

The NO_3^-/NO_2^- profile at H3 in November (fig. 15A) had a concentration of 7.5 µM in the overlying water followed by an overall high concentration in the top two cm of the sediments, with a peak at 2 cm (30.4µM). Two peaks further down were detected at 4- (8.7 µM) and 5 cm (5.0

µM). H6 in November (fig. 15B) had the highest level in the overlying water (12.8 µM) and two smaller peaks at 3- and 8 cm (5.8- and 6.9 µM). The NO_3^-/NO_2^- profile at H3 in January (fig. 15C) reached maximum values in the top 0.75 cm, with a peak in the sediment at the surface (17.6 µM). The overlying water had a concentration of 9.0 µM. The concentration was uniform (around 1.5 µM) from 0.75 cm and down towards the bottom. H6 in January (fig. 15D) had its highest NO_3^-/NO_2^- level in the overlying water (9.1 µM) with two sediment peaks at 0.25 cm (6 µM) and 8 cm (3.6 µM). The NO_3^-/NO_2^- profile at H3 in March (fig. 15E) had maximum values at the bottom (18.1 µM) and the lowest in the overlying waters (1.0 µM). The concentration increased from the surface down to 2 cm, where the levels started to increase at a higher rate with depth. H6 in March (fig. 15F) had the highest levels in the overlying waters (8.2 µM) with decreasing values until 1.0 cm depth in the sediment (2.6 µM), where the decrease was interrupted by a small peak at 1. 25 cm (5.3 µM). The profile between 2- and 11 cm was rather uniform (values between 2.5 to 3.1) except for a small peak a 5 cm (5.5 µM).

The concentration of NH_4^+ was low at the top two centimeter in November at H3 (fig. 15A), slowly increased with depth and reached a maximum at the bottom (263 µM). The NH_4^+ profile at H6 in November (fig. 15B) had a concentration of 57.3 µM in the overlying water, with a sediment peak at 10 cm (882 µM). The lowest concentration was at 1.5 cm (25.8 µM). The profile had a similar pattern as H3, with an increasing concentration with depth, except for a small decrease between 10- and 11 cm (882 to 727 µM).

The NH_4^+ profile in January at H3 (fig. 15C) showed low values at the top two cm and a concentration of 1.3 µM in the overlying water. The first 0.5 cm had a concentration close to zero but increased more rapidly after 2 cm and down to 6 cm (303 µM). The measuring points were few at H6 in January (fig. 15D), but the concentration increased between 0.25 cm (84.6 µM) and 1.25 cm (369.1 µM). The overlying water had a concentration of 57.3 µM.

The NH_4^+ concentration in March at H3 (fig. 15E) was totally absent in the overlying water and down to 0.75 cm of the sediment. The concentration slowly increased until 2 cm (128 µM), where is started to increase more rapidly until a bottom maxima was reached (1080 µM). The concentration in the overlying water at H6 in March (fig. 15F) was 809.3 µM. The concentration of NH_4^+ at the top 0.25 cm was 883.8 µM and increased down to 10 cm (4033.1 µM). The concentration decreased between 10- and 11 cm (4033.1- to 2845.1 µM).

DIN profiles in sediment at stations H3 and H6 through the seasons

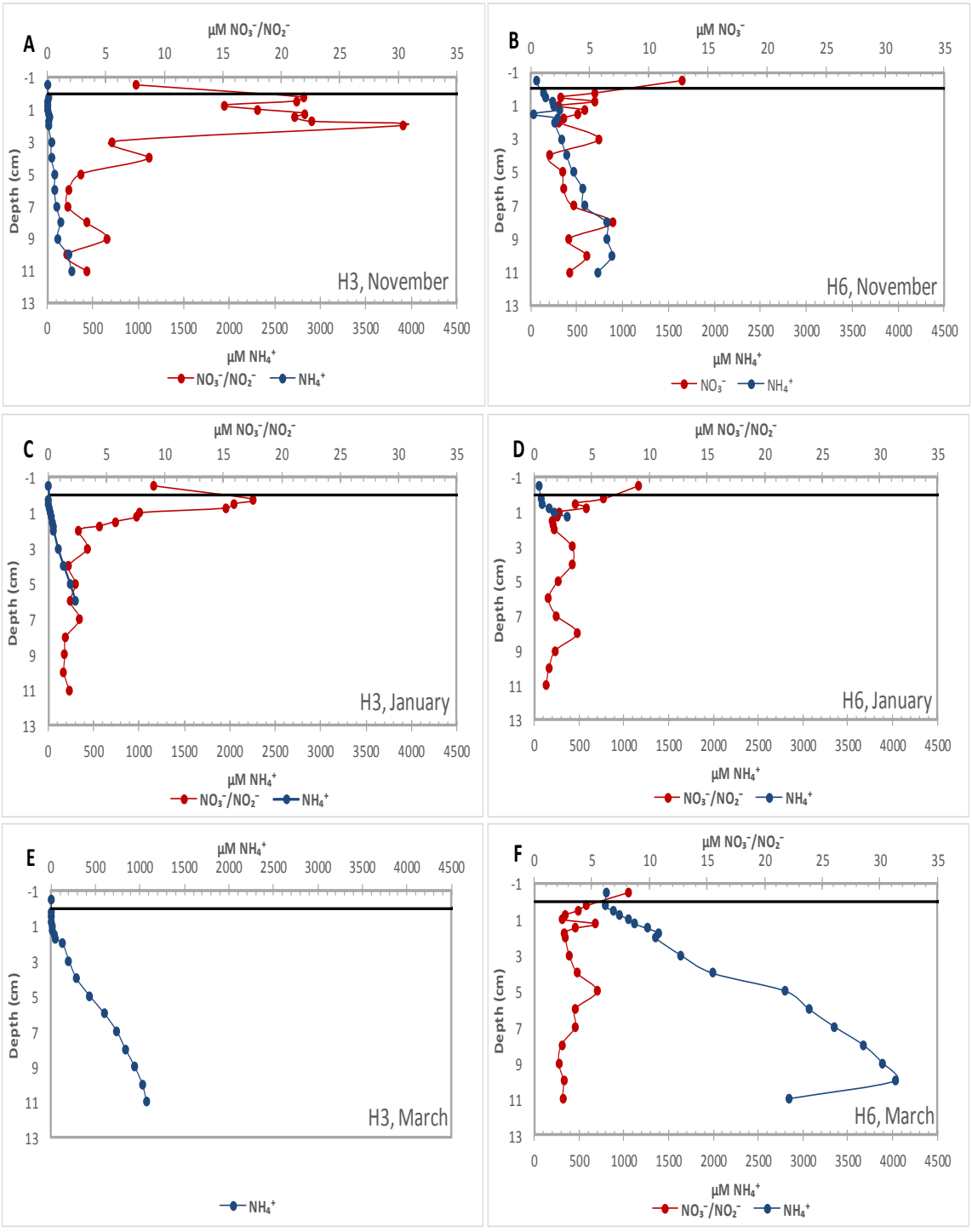

Figure 15. The DIN concentrations from different seasons on station H3 (A, C, D) and H6 (B, D, F). The upper x-axis represents the NO_3^-/ NO_2^- concentration (µM) and the NH_4^+ concentration (µM) can be seen on the lower x-axis. The black horizontal line represents the sediment surface. The missing values for NO_2^- at H6 in November (fig. 15B), NH_4^+ at H3 in January (fig. 15C), NH_4^+ at H6 in January (fig. 15D) and NO_3/NO_2^- at H3 in March (fig. 15D), were due to wrong sample treatment and therefore not likely true results.

5.4 N_2O and O_2 concentration profiles from PROFILE (Version 1.0)

All the following profiles were calculated from 12 zones, the program reduced the numbers of zones in the sediment through F-testing without reducing the quality of the fit. The R^2 values describe this fit. Tables 1 and 2 display the fluxes, concentrations and the production-, or consumption in every zone.

5.4.1 Microelectrode profiles of N_2O in November

Figure 16 shows the consumption or production of N_2O at different zones along a sediment profile at H3 (fig. 16A) and H6 (fig. 16B) in November. Since measurements did not detect N_2O, acetylene was added in the water column with an end concentration of 5% of the total water volume. The microprofiles were measured after 2 hours to make sure that acetylene had reached the sediment. The N_2O (µM) profiles at H3 and H6 are hence potential sediment N_2O concentrations. The green line is the profile made from the program (nmol cm^{-3}), which is shown together with a complementary concentration profile of N_2O (µM) (red line), measured from the microelectrode to control the precision of the calculations.

The N_2O concentration in the overlying water at H3 (fig. 16A) was around 0.21 µM. The concentration decreased from the sediment surface (0.37 µM) to 0.17 cm (1.53 µM). From the maximum point, the levels steadily decreased until all N_2O was gone at a depth of 0.76 cm. At H6 (fig. 16B), the concentration in the overlying water was around 0.17 µM. The concentration increased from the sediment surface (0.17 µM) to 0.17 cm (2.20 µM). From the maximum point, the levels steadily decreased until 0.5 cm (1.53 µM) but without reaching zero values.

Calculated production- and consumption rates for N_2O in the sediments at H3 and H6.

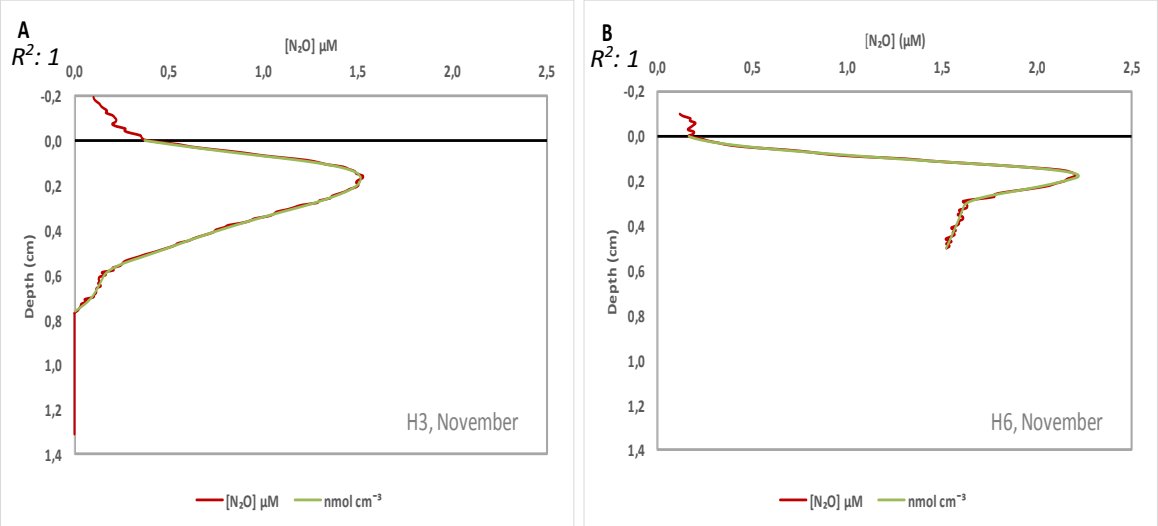

Figure 16. The calculated production and consumption at different zones along the N_2O profile in the sediment at H3 (fig. 16A) and H6 (fig. 16B). The red line represents the measured profile and the green line the calculated profile from the program. The R^2 values are seen in the upper left corner for each diagram, which is a description of the quality of data.

Table 1 illustrates the calculated production- and consumption rates (µmol $m^{-2}d^{-1}$) for the different zones in the produced profile in figure 16. H3 and H6 had a profile with 8 and 6 zones respectively. Both H3 and H6 had a consumption of N_2O at the surface (-51-, and -14, 7 µmol $m^{-2}d^{-1}$ respectively). Both stations had a consumption at the two first zones (-62.2-, -14.7 µmol $m^{-2}d^{-1}$ at H3 and at H6 (-65.7-, -32.0 µmol $m^{-2}d^{-1}$). The maxima for both stations occurred at zone 3 and 4 (138.2-, 95.0 µmol $m^{-2}d^{-1}$ and 138.0-, 17.3 µmol $m^{-2}d^{-1}$) at H3 and at H6 respectively. This was followed by a consumption at zone 5 to 8 for H3 (-13.0-, -38.0-, -51, 8 and -2.2 µmol $m^{-2}d^{-1}$) and zone 5 for H6 (-38.0 µmol $m^{-2}d^{-1}$). Zone 6 at H6 had a production of N_2O at a rate of 0.6 µmol $m^{-2}d^{-1}$.

Table 1. Calculated production and consumption rates for each zone in the sediment and related N_2O fluxes. The number of zones have been determined by the program, which reduced the numbers of zones in the sediment through F-testing without reducing the quality of the fit. All fluxes are in the unit of µmol [$m^{-2}d^{-1}$]

Calculated production- and consumption rates at different zones and fluxes for N_2O			
H3		**H6**	
Calculated flux at top (µmol m^{-2} d^{-1}): -51.0		Calculated flux at top (µmol m^{-2} d^{-1}): -14.7	
Depth integration of production in each zone:		Depth integration of production in each zone:	
Zones	**Production (µmol m^{-2} d^{-1})**	**Zones**	**Production (µmol m^{-2} d^{-1})**
1	-62.2	1	-65.7
2	-14.7	2	-32.0
3	138.2	3	138.2
4	95.0	4	17.3
5	-13.0	5	-38.0
6	-38.0	6	0.6
7	-51.8		
8	-2.2		

5.4.2 Microelectrode profiles for O_2

Figure 17 shows the seasonal penetration depth of O_2 at the two stations. The blue line is the profile made from the program (nmol cm^{-3}), which is shown together with a complementary concentration profile of N_2O (µM) (blue line), measured from the microelectrode to control the precision of the calculations.

At H3 in November (fig. 17A), the average concentration in the overlying water was 307 µM. From the sediment top, the O_2 decreases from 291.6 µM to zero values at 0.63 cm. The O_2 penetration depth was hence 6.3 mm. At H6 in November (fig. 17B), the average concentration in the overlying water was 174 µM. From the sediment top, the O_2 decreases from 146.9 µM to zero values at 0.12 cm. The O_2 penetration depth was hence 1.2 mm.

At H3 in January (fig. 17C), the average concentration in the overlying water was 102 µM. From the sediment top, the O_2 decreases from 92.7 µM to zero values at 0.62 cm. The O_2 penetration depth was hence 6.2 mm. At H6 in January (fig. 17D), the average concentration in the overlying water was 333.8 µM. From the sediment top, the O_2 decreases from 322.3 µM to zero values at 0.21 cm. The O_2 penetration depth was hence 2.1 mm.

At H3 in March (E), the average concentration in the overlying water was 308 µM. From the sediment top, the O_2 decreases from 289 µM to 27 µM at 0.81 cm. The O_2 penetration depth was hence 8.1 mm. At H6 in March (F), the average concentration in the overlying water was

293.9 µM. From the sediment top, the O_2 decreases from 288.3 µM to zero values at 0.21 cm. The O_2 penetration depth was hence 0.21 mm.

Calculated production- and consumption rates for O_2 in the sediments at H3 and H6.

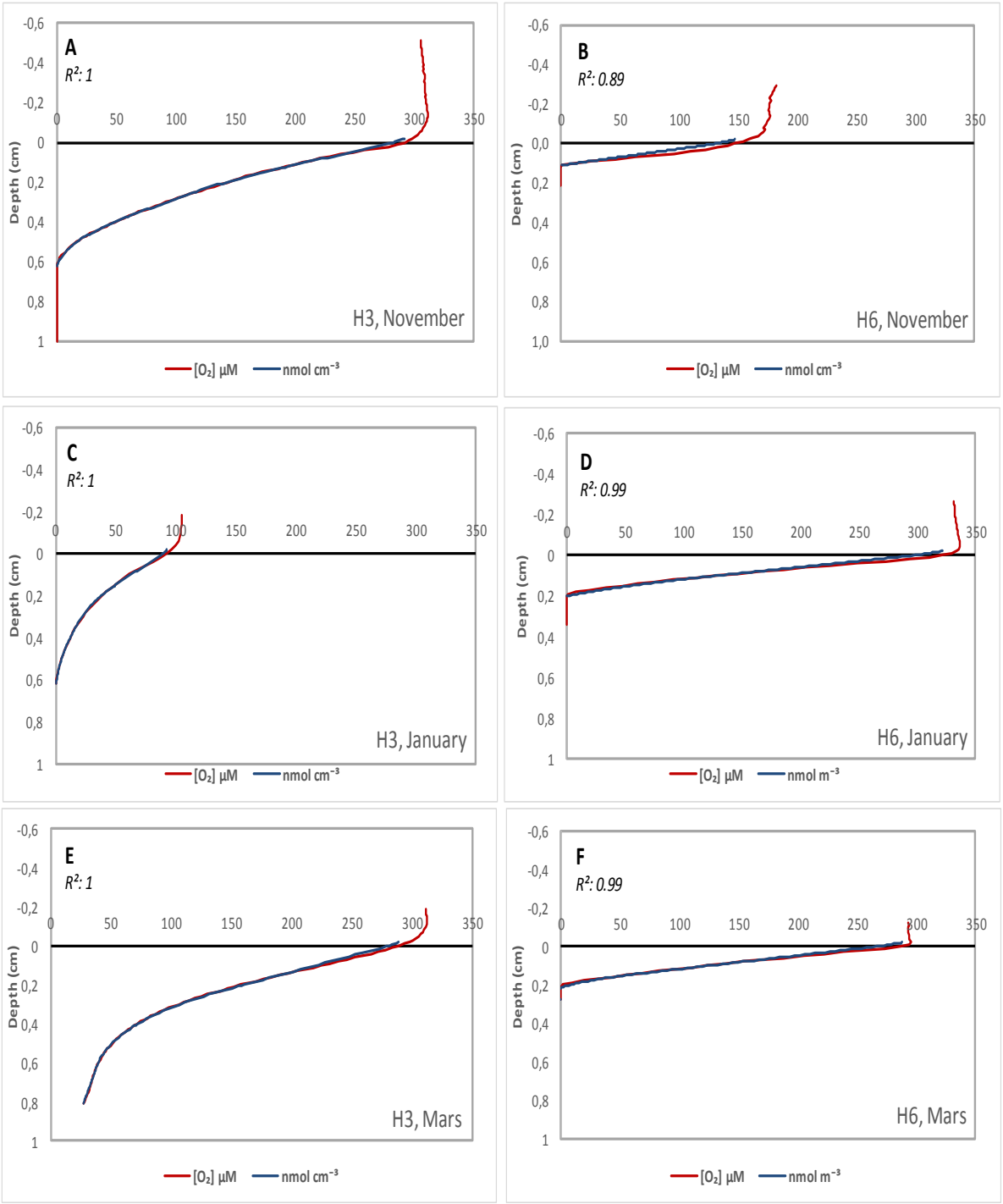

Figure 17. Calculated profiles from H3 (A, C, E) and H6 (B, D, F) with the sediment depth on the y-axis and the production rate (nmol $cm^{-3}d^{-1}$) on the lower x-axis and the [O_2] µM on the upper x-axis. The R^2 values are seen in the upper left corner for each diagram, which is a description of the quality of data. Red lines are the measured profiles from the microelectrodes and the blue line is the calculated profile from the program.

Table 2 illustrates the calculated consumption rates (mmol $m^{-2}d^{-1}$) of O_2 at different zones in the produced profile in figure 17.

At H3 in November, the profile was divided in four zones and one zone at H6. Both H3 and H6 had a consumption of O_2 at the surface (-6.4-, and -10.3 mmol $m^{-2}d^{-1}$ respectively). The consumption in the four zones at H3 were -1.7-, -2.3-, -0.3- and -3.5 mmol $m^{-2}d^{-1}$, whereas the consumption was zero at H6.

At H3 in January, the profile was divided in three zones and two zones at H6. Both H3 and H6 had a consumption of O_2 at the surface (-2.3-, and -14.8 mmol $m^{-2}d^{-1}$ respectively). The consumption in the three zones at H3 were -0.1-, -1.2-, -0.8- and, 0- and -7.3 mmol $m^{-2}d^{-1}$ at H6.

At H3 in March, the profile was divided in four zones and two zones at H6. Both H3 and H6 had a consumption of O_2 at the surface (-5.3-, and -13.2 mmol $m^{-2}d^{-1}$ respectively). The consumption in the four zones at H3 were 0-, -3.1-, -1.7- and 0 mmol $m^{-2}d^{-1}$ and, 0- and -17.2 mmol $m^{-2}d^{-1}$ at H6.

Table 2. Calculated consumption rates for each zone in the sediment and related O_2 fluxes. The number of zones have been determined by the program, which reduced the numbers of zones in the sediment through F-testing without reducing the quality of the fit. All fluxes are in the unit of mmol $m^{-2}d^{-1}$.

Calculated production and consumption rates in sediments at different zones and fluxes for O_2			
H3		**H6**	
November			
Calculated flux at top (mmol m^{-2} d^{-1}): -6.4		Calculated flux at top (mmol m^{-2} d^{-1}): -10.3	
Depth integration of production in each zone:		Depth integration of production in each zone:	
Zones	**Production**	**Zones**	**Production**
1	-1.7	1	0
2	-2.3		
3	-0.3		
4	-3.5		
January			
Calculated flux at top (mmol m^{-2} d^{-1})**:** -2.3		Calculated flux at top (mmol m^{-2} d^{-1}): -14.8	
Depth integration of production in each zone:		Depth integration of production in each zone:	
Zones	**Production**	**Zones**	**Production**
1	-0.1	1	0
2	-1.2	2	-7.3
3	-0.8		

March			
Calculated flux at top (mmol m^{-2} d^{-1}): -5.3		Calculated flux at top (mmol m^{-2} d^{-1}): -13.2	
Depth integration of production in each zone:		Depth integration of production in each zone:	
Zones	**Production**	**Zones**	**Production**
1	0.0	1	0
2	-3.1	2	-17.2
3	-1.7		
4	0.0		

5.4.3 The ratio between the calculated and the measured flux of O_2

Table 3 shows the comparison between the calculated- and the measured flux in mmol $m^{-2}d^{-1}$.The measured fluxes were derived from the core incubations. Bioturbation was not included in the program for the calculated flux, a potential difference could hence be caused by this parameter. Negative ratios between the calculated- and the measured flux, indicate a bigger measured flux.

The ratio between the calculated- and measured flux of O_2 in November was 2.7 and 4.3 for H3 and H6 respectively. The results from January were lacking for H3 but the ratio at H6 was 1.0. The ratio in March was negative for both H3 and H6, which had ratios of -10.5 and -2.9 respectively.

Table 3. The ratio between the calculated and measured flux (mmol $m^{-2}d^{-1}$). Negative ratios between the calculated- and the measured flux indicates a bigger measured flux.

The ratio between the calculated- and the measured flux			
Station	**Calculated flux (mmol m^{-2} d^{-1})**	**Measured flux (mmol m^{-2} d^{-1})**	**Ratio**
H3 November O_2	**-6.4**	**-3.0**	**2.7**
H6 November O_2	**-10.3**	**-2.4**	**4.3**
H3 January O_2	**-2.3**	**-**	**-**
H6 January O_2	**-14.8**	**-14.4**	**1.0**
H3 March O_2	**-5.3**	**-55.4**	**-10.5**
H6 March O_2	**-13.2**	**-38.1**	**-2.9**

5.5 N_2O concentrations from the outgoing sewage water at the STP in Himmerfjärden

Samples taken from the treated sewage water at the STP facility at Himmerfjärden. The samples were transported to Stockholm University for a later analysis on the gas chromatograph. The results can be seen in figure 18, with the N_2O concentration represented on the y-axis and the time for the

sampling on the x-axis. The first five sample opportunities were samples taken from a tank, containing water collected during a 24 h time period, whereas the last four sample opportunities were taken from water that directly enters Himmerfjärden. The highest emission occurred in March, which had a N_2O saturation of 275 481 % and the lowest in April (88 348 %).

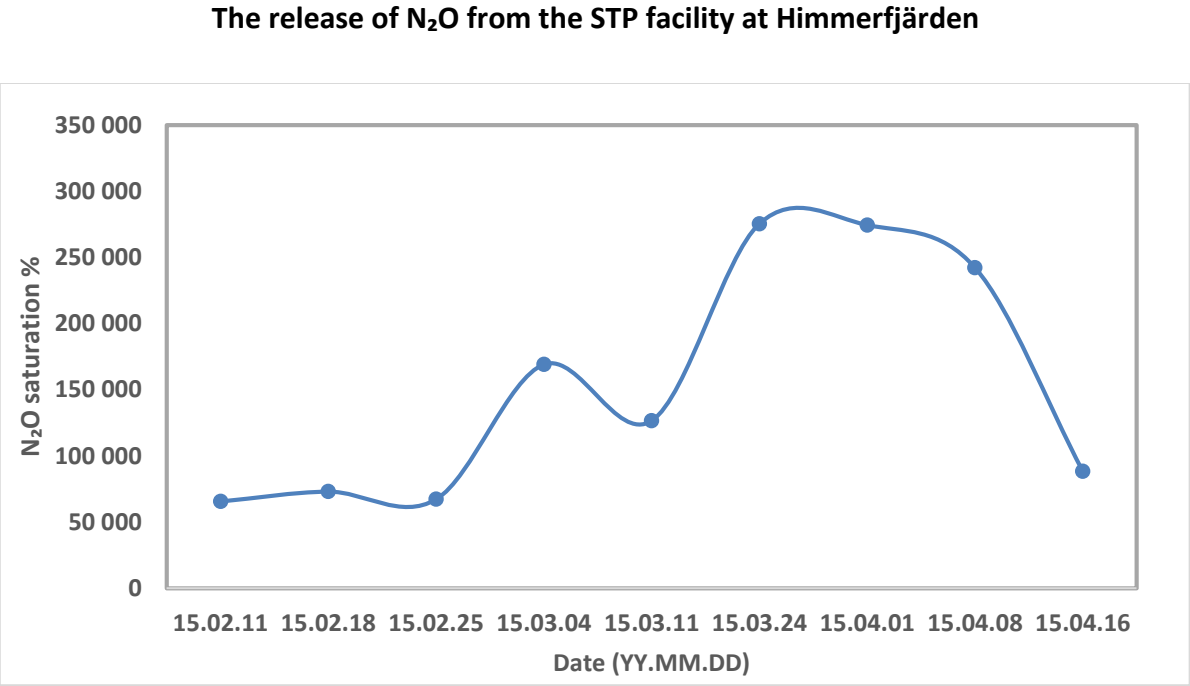

Figure 18. Samples taken from the outgoing sewage water at the STP facility at Himmerfjärden. The first five sample opportunities were samples taken from tank with water collected during a 24 h time period, whereas the last four sample opportunities were taken from water that directly entered Himmerfjärden.

5.6 Evaluation of the Elemental Analyzer-DeltaV Advantage mass spectrometer

During the analysis of the N_2O samples from the denitrification experiments, an extra peak with a mass of 46 interfered with the N_2O peak. To separate the two peaks, changing the helium flow or the temperature in the column are two possibilities for a better separation. This was not possible with this particular configuration of the mass spectrometer. Different injection amounts were tested but without a successful result. Another approach was to centrifuge the samples to get rid of the particles at the top (since the samples were stored upside down) and see if this changed the results, but it did not. The N_2O samples from the denitrification were not analyzed at all. Figure 19 shows the chromatograph of the extra peak with a mass of 46. The first peak in the lower window is the standard and the following two are samples but with different injection amounts (500- and 100 µl respectively). Both air- and water samples from the nitrification experiment was injected as well but did not look strange. Problems with the drift occurred as well after these samples and a new peak center had to be made. To get rid of a possible contamination inside the column, it was heated repeatedly. The detection limit of the mass spectrometer was tested as well. The mass spectrometer

only detected pure N_2O as standard, whereas a 1000 ppm standard could not be detected. Different amounts of the pure N_2O were not tested.

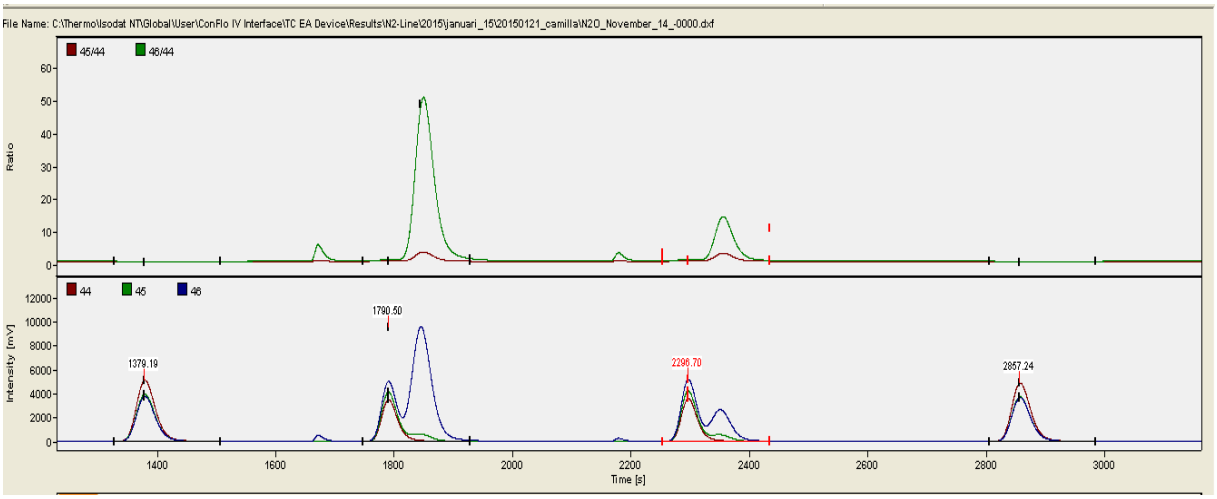

Figure 19. The first peak in the lower window is the standard and the following two are samples but with different injection amounts (500- and 100 µl respectively). The upper window represents the ration and the green line the mass of 46.

The problems continued with the analysis of the N_2 production, with an extra peak directly after the N_2 peak. The sample injection was changed from 500 µl to 100 µl to get a better separation. It was decided that the extra peak did not interfere with the N_2 peak and the analysis continued. A new column was bought as well but with the same result. The extra peak for N_2 can be seen in figure 20.

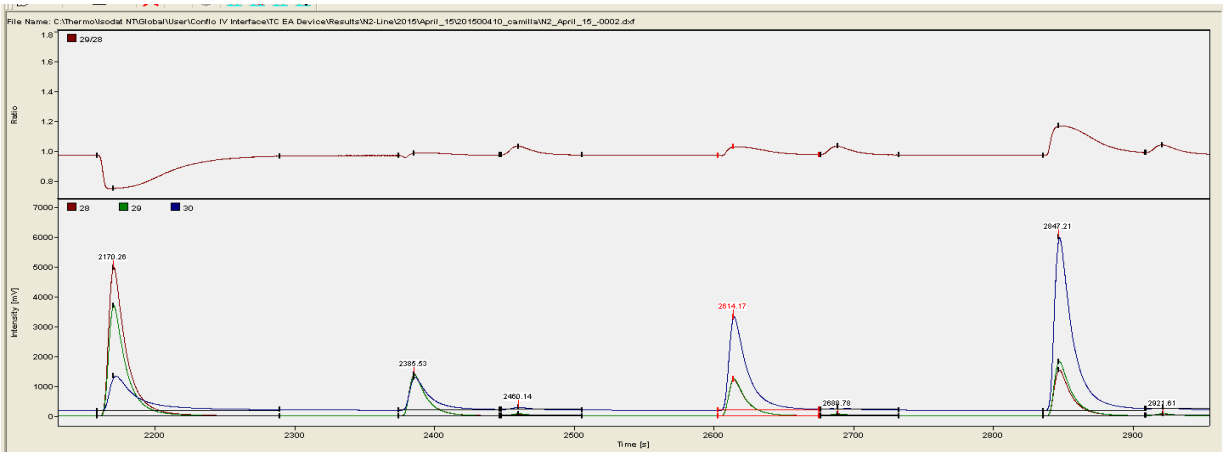

Figure 20. A chromatograph with the extra peak directly after the N_2 peak. The injection amount was changed from 500- to 100 µl to achieve a better separation.

5.7 Potential N_2O production through the nitrification process

5.7.1 $^{45\text{-}46}N$-N_2O production in the water column from $^{15}NH_4^+$ tracer experiments

10 minutes after the addition of the ^{15}N-NH_4^+ tracer, three samples and two blanks were killed with $ZnCl_2$, which represents time T_0. The procedure was repeated after 24- and 48 hours to see a potential production change over time. A Wilcoxon multi-comparison test was applied on the production of ^{45}N-N_2O and ^{46}N-N_2O (nM) over time for both H3 and H6, which showed no significant difference between

the spiked samples and their blanks ($p < 0.05$). The results from the statistics can be seen in appendices 10.2.2. The produced amount of N_2O (pmol) per hour can be seen in figure 20 and 21 for H3 and H6 respectively. Blue bars represent $^{45}N_2O$ production, red bars the blanks, the green bars the $^{46}N_2O$ production and the turquoise bars the blanks.

The results for H3 can be seen in figure 21. As mentioned before, there was no significant difference between spiked and blank samples. The K-values for the production in both sample and blank, can be seen in appendices 10.2.1.

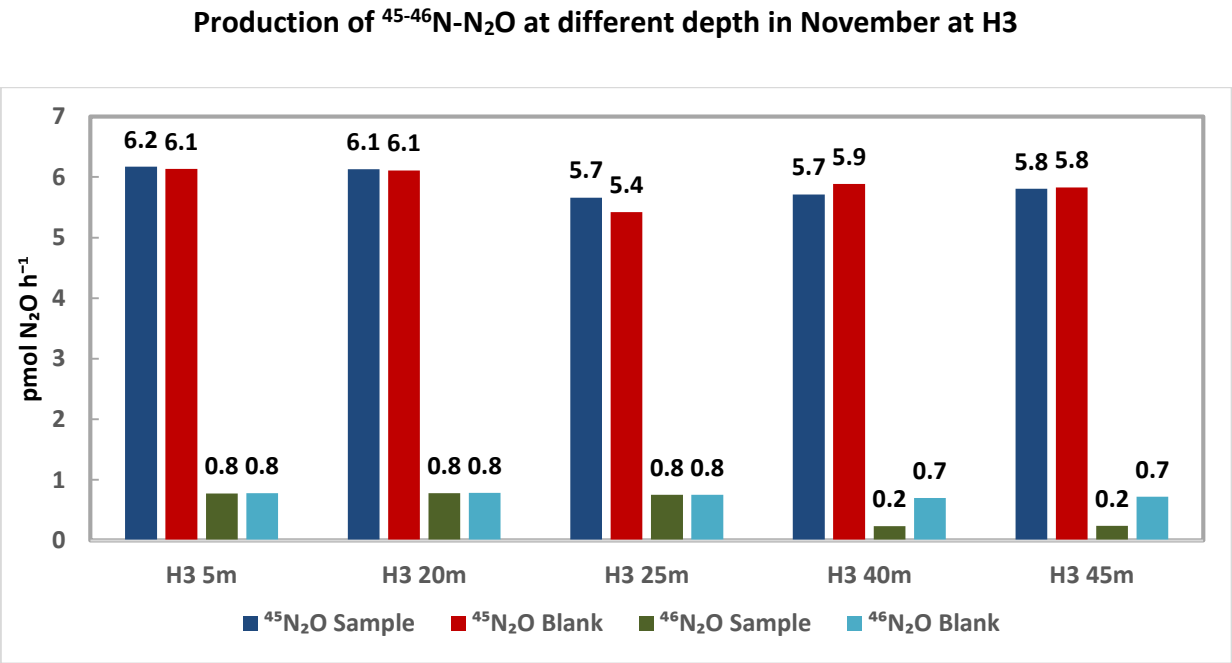

Figure 21. Production of the produced $^{45-46}N$-N_2O (nM) at different depths at H6 in November over a time frame of 48 hours. Blue bars represent $^{45}N_2O$ production, red bars the blanks, the green bars the $^{46}N_2O$ production and the turquoise bars the blanks. The multi-comparison Wilcoxon test showed that the production over time was statistical equal between blank and spiked samples.

The results from the addition of the ^{15}N-NH_4^+ tracer at H6 in November can be seen in figure 22. As mentioned before, there was no significant difference between spiked and blank samples. The results from the statistics can be seen in appendices 10.2.3 and the K-values in 10.2.1.

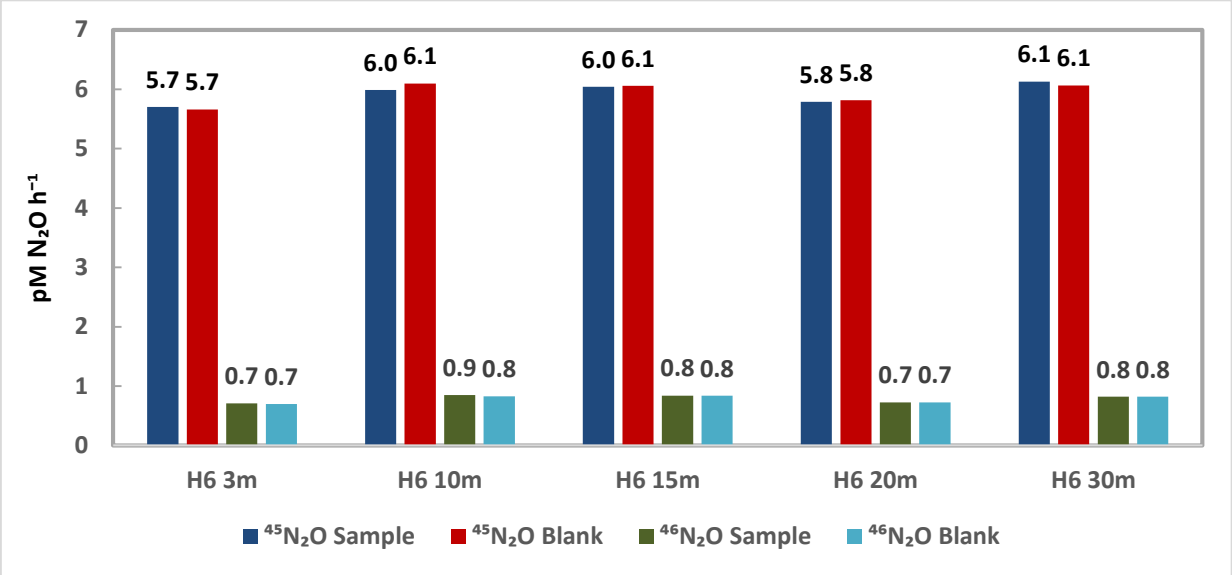

Figure 22. Production of the produced $^{45-46}N$-N_2O (nM) at different depths at H6 in November over a time frame of 48 hours. Blue bars represent $^{45}N_2O$ production, red bars the blanks, the green bars the $^{46}N_2O$ production and the turquoise bars the blanks. The multi-comparison Wilcoxon test showed that the production over time was statistical equal between blank and spiked samples.

5.8 Potential denitrification rates in the sediment

5.8.1 $^{29}N_2/^{30}N_2$ ratios during ^{15}N-NO_3^- tracer experiments for core incubation

As mentioned in section 2.3.2, one of the main assumptions, and hence a big limitation, is that the added $^{15}NO_3^-$ needs to be mixed uniformly with the natural abundance of $^{14}NO_3^-$. An imbalance between the nitrification and the influx of NO_3^- into different spots in the sediment, would lead to a higher production of $^{28}N_2$ and $^{30}N_2$ relative to $^{29}N_2$ (Nielsen, 1992). This means that the total denitrification activity could be underestimated, by how much is tested by applying different concentrations of the tracer. During high $^{15}NO_3^-$ concentrations, more of the tracer is trapped and measured directly as $^{29}N_2$. This decreases the likelihood of the possible miscalculation of the produced $^{28}N_2$ in comparison with experiments of low $^{15}NO_3^-$(Nielsen, 1992).

If the ratios between $^{29}N_2$ and $^{30}N_2$ is under two, they are considered uniformly mixed (Lohse, et al., 1996). The results can be seen in figure 23. Having this assumption in mind, the ratios for 25 µmol for H3 in November (fig. 23A), 50 µmol for H6 in November (fig. 23B), 50 µmol for H3 in January (fig. 23C), 25 µmol for H3 in March and 25 µmol for H6 in March, were considered to be not uniformly mixed.

Ratio between $^{29}N_2$ and $^{30}N_2$ during the $^{15}N\text{-}NO_3^-$ tracer experiment during core experiments

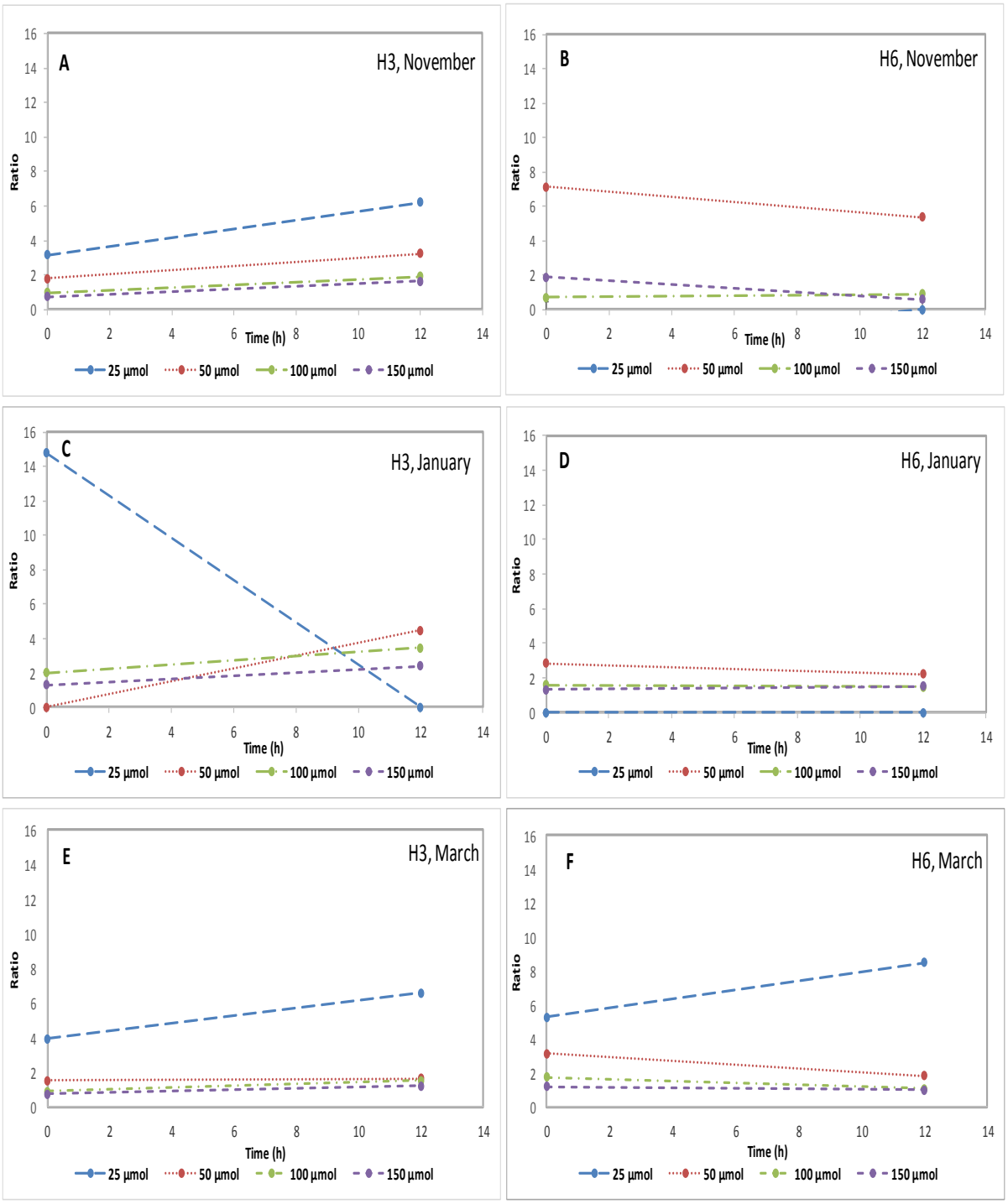

Figure 23. The ratio between $^{29}N_2$ and $^{30}N_2$ for different concentrations of $^{15}N\text{-}NO_3^-$ during core incubations. The X-axis represents the ratio and the y-axis the time in hours. Diagram A, C and E represents the results from H3 and diagram B, D and F the results from H6. 25 µmol for H3 in November (A), 50 µmol for H6 in November (B), 50 µmol for H3 in January (C), 25 µmol for H3 in March and 25 µmol for H6 in March were considered not uniformly mixed.

5.8.2 Verifying D_n independence of water column concentrations of $^{15}NO_3^-$, and a linear increase of D_w^{tot} with increasing $^{15}NO_3^-$ concentrations

After adding the $^{15}N\text{-}NO_3^-$ tracer in the water column with four different tracer concentrations (25-, 50-, 100-, and 150 µmol) for the 16 incubation cores, a pre-incubation time followed. The pre-incubation time was determined by the O_2 penetration depth from the microelectrode profiles. After the pre-incubation, the incubation started when the cores were closed with stoppers. Samples were taken after 12 hours, which ended the incubation.

To see whether the D_w^{tot} increased linearly with the $^{15}NO_3^-$ concentration, and if the coupled nitrification-denitrification process was independent of the $^{15}NO_3^-$ addition, both processes were compared as a function of water column $^{15}NO_3^-$ concentration. This is a control, to see whether assumption one and two are fulfilled (section 2.3.2), which determines if the results are valid or not. Results from H3 in January could not be displayed due to insufficient data points. In all the following figures (24 to 28), the blue data point's represents denitrification activity from D_w^{tot} and the red data points represents the activity from D_n. The denitrification rates are expressed in µmol $N_2\ m^{-2}h^{-1}$ (y-axis) and the NO_3^- in µmol (x-axis). The dotted lines represents the trendline and *n* reflects the number of replicates for each data point.

Figures 24 and 25 is the results from November and March at H3, which showed a D_n activity that was not independent of the $^{15}NO_3^-$ in the water column, and a D_w^{tot} that did not increase linearly over time. Hence, an even mix between the isotopes and no disturbance of the *in situ* denitrification rates could not be proven.

D_n independence of water column concentrations of $^{15}NO_3^-$, and a linear increase of D_w^{tot} with increasing $^{15}NO_3^-$ concentrations at H3 and H6

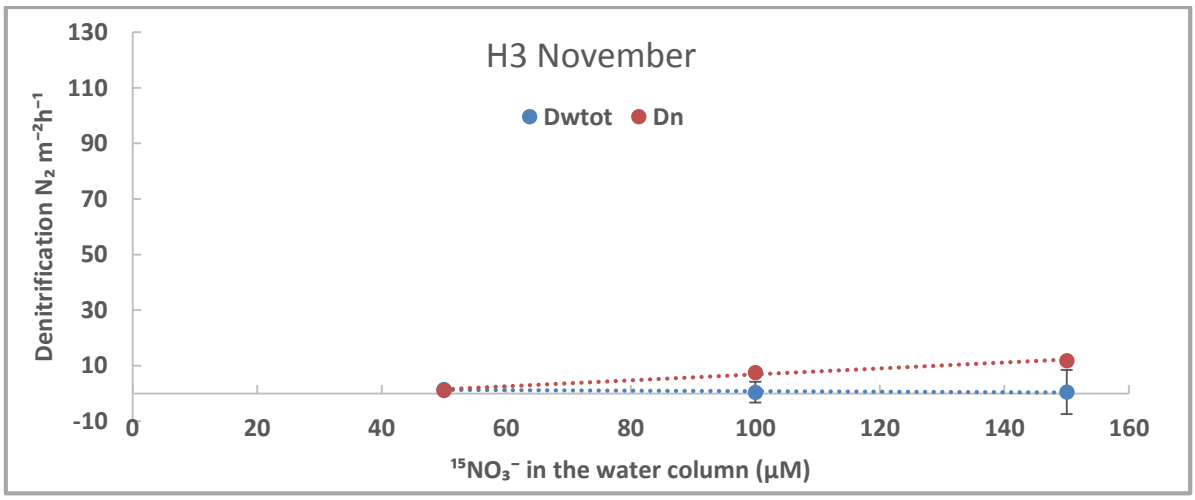

Figure 24. Denitrification of $^{15}NO_3^-$ (D_w^{tot}) and coupled nitrification-denitrification (D_n) as a function water column $^{15}NO_3^-$ concentration. Error bars for D_w^{tot} (n=2, 3, 2) and D_n (n=2, 1, 1) are SE.

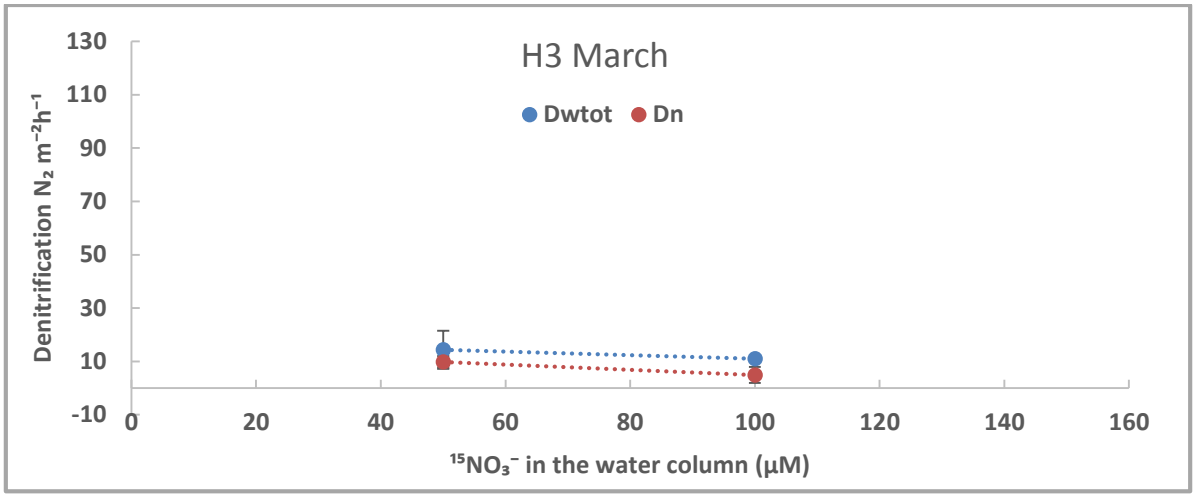

Figure 25. Denitrification of $^{15}NO_3^-$ (D_w^{tot}) and coupled nitrification-denitrification (D_n) as a function water column $^{15}NO_3^-$ concentration. Error bars for D_w^{tot} (n=2, 2) and D_n (n=2, 3) are SE.

Figures 26, 27 and 28 show the results from November, January and March at H6, which showed a D_n activity that was not independent of the $^{15}NO_3^-$ in the water column, and a D_w^{tot} that did not increase linearly over time. Hence, an even mix between the isotopes and no disturbance of the *in situ* denitrification rates could not be proven.

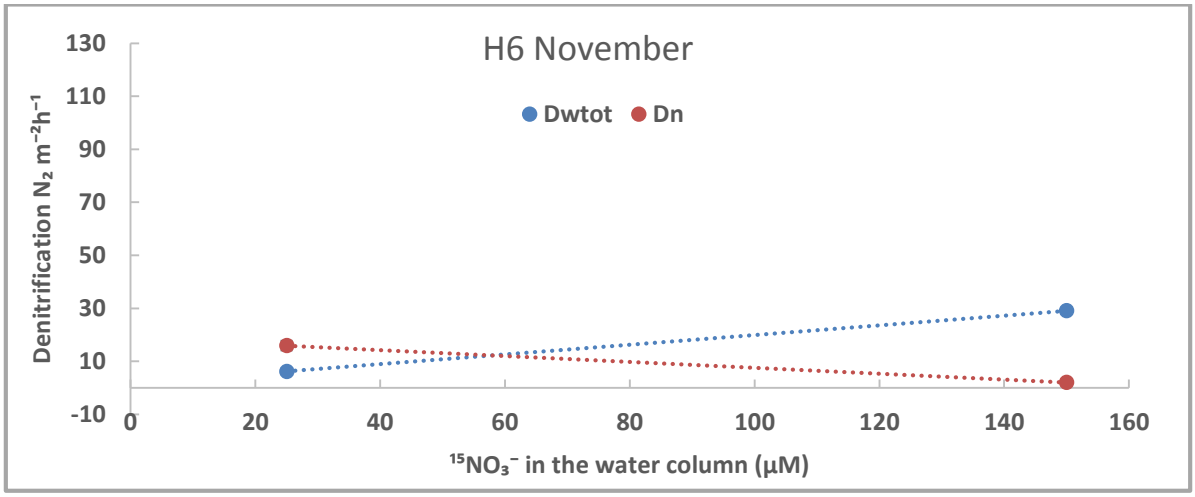

Figure 26. Denitrification of $^{15}NO_3^-$ (D_w^{tot}) and coupled nitrification-denitrification (D_n) as a function water column $^{15}NO_3^-$ concentration. Error bars for D_w^{tot} (n=2, 4) and D_n (n=2, 3) are SE.

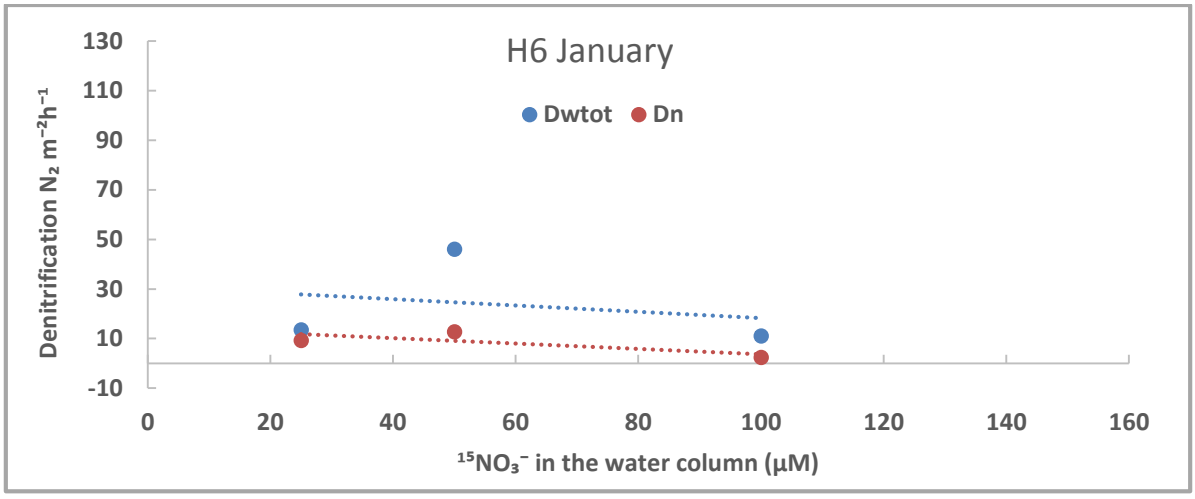

Figure 27. Denitrification of $^{15}NO_3^-$ (D_w^{tot}) and coupled nitrification-denitrification (D_n) as a function water column $^{15}NO_3^-$ concentration. Error bars for D_w^{tot} (n=1, 1, 2) and D_n (n=1, 1, 2) are SE.

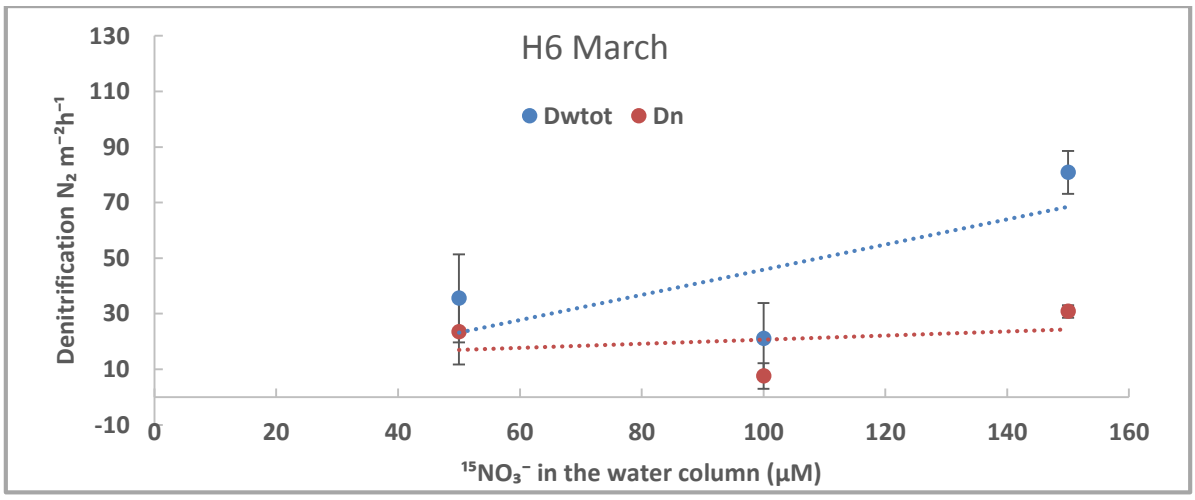

Figure 28. Denitrification of $^{15}NO_3^-$ (D_w^{tot}) and coupled nitrification-denitrification (D_n) as a function water column $^{15}NO_3^-$ concentration. Error bars for D_w^{tot} (n=4, 2, 2) and D_n (n=4, 2, 2) are SE.

The crucial assumptions that have to be fulfilled when the ^{15}N IPT is used for measuring the natural denitrification rates, were not fulfilled. This means that the reliability of the data, seriously has to be questioned and is hence not included in the results nor the discussion.

6 Discussion

6.1 N_2O-, temperature-, salinity-, O_2- and DIN profiles

6.1.1 Correlation between N_2O and temperature-, salinity-, O_2- and DIN profiles in the water column

The water column concentrations of N_2O were in most cases in equilibrium with the atmosphere at H3, and hence not a source of N_2O. Comparing the N_2O water profiles (fig. 6 and 7) and the results from the statistical analysis, a seasonal change cannot be seen at H3. The N_2O water profiles at H6 however, show a seasonal pattern with the highest concentration in October and March. At both time points the peaks are located directly under the chemocline, and one could suspect that these increased levels could point to a high *in situ* production of N_2O. If nitrification is the process producing these peaks of N_2O, a response in the form of a decrease of NH_4^+ and an increase of NO_3^- should have been detected (Rönner, 1982, Bange et al., 2006, Murray, et al., 2011), which not is seen. There is a peak of NO_3^-/NO_2^- in March at H6 but further down in the water column (fig. 7), but not as high as would have been expected if nitrification is the process alone to produce the elevated N_2O concentration. Since the chemocline in both October and March is somewhat weak, a strong chemocline blocking the transfer of the gas to the surface layer is not a likely explanation for the elevated N_2O values. To test the accuracy of the DIN data from the water column, the results were compared with the long term study performed by System Ecology at Stockholm University (www2.ecology.su.se/dbhfj/index.htm). The comparison made it clear that the DIN profiles in this work, correlates well with those measurements.

A correlation between DIN and N_2O cannot be seen for any of the profiles comparing figures 6 and 7 with figures 8 and 9. What can be said is that the profiles of DIN do not support a theory of nitrification as a big producer of N_2O. This needs to be further tested in future projects and maybe with the setup mentioned later in section 6.3.2.

6.2 Benthic DIN-, O_2- and N_2O fluxes and O_2 penetration depth

6.2.1 Benthic fluxes of DIN and sediment concentrations

The NH_4^+ flux ranged between 338.2- to 28.5- and 1788.2- to -0.7 µmol $m^{-2}d^{-1}$ at H3 and H6 respectively. The range of the NO_3^-/NO_2^- flux was between 180.5- to -123.9- and 1058.9- to -37.6 µmol $m^{-2}d^{-1}$ at H3 and H6 respectively (fig. 14). The range of the fluxes are similar to a previous study in the same area (Bonaglia, et al., 2014A). In the same study, it was found that stations closer to the opening to the Baltic Sea often had positive NO_3^- fluxes, whereas H6 had an influx of NO_3^- to the sediment and much higher NH_4^+ fluxes in comparison with the other stations.

The pattern of DIN fluxes did not change with season except in November at H6, and did not follow the same trends as Bonaglia, et al., 2014A, found in the same area 2012. Sometimes a

positive NH_4^+ flux corresponded with a negative NO_3^-/NO_2^- flux (November and March at H3), in some cases the fluxes of both NH_4^+-and NO_3^-/NO_2^- were positive (November and March at H6 and January at H3) or both negative (H6 in January). The high DIN flux in November at H6 was the one that stood out the most, which cannot be reflected by a higher DIN concentration in the sediments in comparison with the other seasons. $NH_4^+$and NO_3^-/NO_2^- had a positive flux in March at H6 as well, but with a four time lower DIN flux in comparison to November. This even with a NH_4^+ concentration four times higher in the sediment in March. Other studies has shown a positive correlation between O_2 uptake and NH_4^+ release (Jensen, et al., 1996), which is evident in March but not for the flux in November at H6. Mineralization of organic matter is parameter that affect the DIN fluxes. The sedimentation rate is expected to be high at H6 (Sedimentation rates at H5 were 0.98±0.26 in a study made by Thang, et al., 2012), which increases the release of NH_4^+, particularly during warmer months, due to mineralization of organic matter. It would explain the elevated NH_4^+ flux in November and March at H6. To be certain, profiles of the organic matter content should have been measured.

The peak of NO_3^-/NO_2^- in the upper two centimeters of the sediment at H3 in November and January, give indications of an active nitrification process. This in combination with the efflux of NH_4^+ and an influx of NO_3^-/NO_2^- points to an active denitrification as well. The pattern is not as clear at H6. A correlation between water concentrations of NO_3^- and sediment fluxes has been seen from other studies, where less NO_3^- in the water column leads to a higher efflux from the sediment (Bonaglia, et al., 2014A, Cabrita, et al., 2000, Murray, et al., 2015). This is often followed by a seasonal pattern with an efflux in the summer and an uptake during winter (Cabrita, et al., 2000, Murray, et al., 2015). This is not reflected in this study since H3 had the highest NO_3^-/NO_2^- concentration in the water column corresponded to an efflux of NO_3^- from the sediment in January, which is a contradiction to trends from earlier studies. The efflux of NO_3^- do not correspond with other studies, this could be due to relatively high concentrations in the sediment. A direct comparison with the study made by Bonaglia, et al., 2014A, is difficult to do since the sampling scheme is not the same. However, H6 could be compared in November and January, which showed a two times higher DIN concentration in the sediment in this study for both seasons.

There were some problems during the analysis of the DIN in the sediments, and in almost all cases they had to be re-analyzed due to too high concentrations and a re-dilution. This effects the concentrations, which are both O_2- and temperature sensitive. Another autoanalyzer system with a higher concentration spectra could have been more suitable in this case (ALPKEM, Flow Solution IV). Another reason for the irregular fluxes could be due to the high influence of the STP. Since the STP had a major shutdown, starting in the autumn 2013 until summer 2014, natural seasonal changes could be totally dominated by this external source. This means that these processes are not dependent on seasonal fluctuations, but rather the inputs from the STP. This is

more prominent at H6 than H3. The latest quarterly report from SYVAB showed a trend with increasing N release due to an increased incoming volume of sewage water. The number of inhabitants that the STP treats sewage water from have over the last couple of years increased from 280,000 (2012) to 315,000 (2015) and resulted in an increased influence on the surrounding environment.

6.2.2 O_2 uptake- and penetration depth

There was a distinct seasonal pattern in the O_2 uptake by the sediment. The fluxes ranged between 3.0- to 50.4- and 2.4- to 38.1 mmol $m^{-2}d^{-1}$ at H3 and H6 respectively, which were high in comparison with other studies in similar environments (Cabrita, et al., 2000, Bonaglia, et al, 2014A). The highest uptake rates occurred in March, where the rates were 17- respective 16 times higher than the lowest rates in November for H3 and H6 respectively. The consumption rates between the two stations were statistically equal in March though, which was unexpected since H6 normally has a higher consumption rate due to anoxia in the sediment, causing a steeper O_2 gradient between water and sediment´s. The variance was quite large at H3, which could explain the similar sediment O_2 uptake between the stations. A reasonable explanation for the high variance could be benthic activity, which enhances the sediment heterogeneity. The comparison between the measured- and the calculated flux from the program (table 3) showed that the measured flux is more than ten times higher than the calculated flux at H3 and three times higher at H6 in March. It became evident that the diffusion by itself cannot explain the O_2 uptake in the sediments. Since the O_2 penetration depth was deepest in March at H3 (fig. 17), benthic activity could be a good explanation. The time point for an increased activity also agrees well with other studies and was also visible in the sediment.

The pattern was a bit different at H6 since the penetration depth was unchanged from January to March, even if the measured flux was higher in March, hence it cannot can be explained by diffusion alone. Macrofauna could not be seen but it is not certain if meiofauna was present or not. Some studies also points to the importance of which kind of species that dominates at a particular site. High activity of meiofauna does not always increase the penetration depth since type of species is an additional factor (Bonaglia, et al., 2014B).

To be able to draw conclusions with higher accuracy of the effects on the benthic activity, complementary *in situ* investigations of which kind of communities that dominates at H3 and H6 needs to be made.

6.2.3 Benthic N_2O fluxes and microelectrode profiles

The highest efflux of N_2O occurred in October at H6, whereas the other seasons were statistically equal, even between the stations. The measured efflux between -0.1- to 2.1 µmol $m^{-2}d^{-1}$ falls within the range of other studies (Murray, et al., 2015, and references there in). This study did hence not

show a strong seasonal fluctuation of N_2O, at least not in autumn, winter or early spring time. Since the N_2O did not show a seasonal change, the elevated effluxes of DIN in November at H6 (fig.15), did neither correspond to higher N_2O fluxes, nor the change of the O_2 penetration depth though the seasons (fig. 17). Since information on the DIN concentrations in the sediment, DIN fluxes, O_2 penetration depths and O_2 uptakes in October are unavailable, none of these parameters can be correlated with the high sediment efflux of N_2O in October. What is known is that H6 had hypoxia (1.2 % O_2 saturation) in the bottom waters, and H3 its lowest O_2 levels (50 % saturation), the salinity was at the lowest for both stations and the temperature the highest at H3 (November for H6) in October. Anoxic waters often favors denitrification but not under too high H_2S concentrations, which was the case in both October and November at H6. The low O_2 penetration depth at H6 in November, the appearance (color, smell etc.) of the sediment and the high levels of H_2S in combination with the DIN flux, implies that denitrification and the coupled nitrification-denitrification is less dominant, but could still be active during this season. Instead, dissimilatory nitrate reduction of ammonia (DNRA) could be the dominant process in October at H6. Hypoxic conditions with high levels of H_2S , favors this chemolithoautothropic process in which H_2S is oxidized to couple the reduction of NO_3^- to NH_4^+ (Bonaglia, et al., 2014A). A previous study showed an activity increase of DNRA during summers, since the environments are typically hypoxic at that time (Bonaglia, et al., 2014A). This could also explain the high NH_4^+ efflux and the, in comparison to October, low efflux of N_2O at H6 in November.

The high N_2O flux in October was stimulated by higher temperatures, since the biological activity increases with temperature. If denitrification was the main producer through the seasons, the deeper O_2 penetration depth from November to March at H3, would result in a smaller possibility for the N_2O to escape to the water before it becomes consumed again by microbes. This could be an explanation for the lower N_2O effluxes in the season with a deeper O_2 penetration depth and higher O_2 uptake. Other aspects are the N_2O microprofiles in the sediment, where a maxima is seen at a depth of 1.7 millimeters at both stations. Comparing the microprofiles with the O_2 penetration depth, it becomes apparent that the N_2O maxima occurs within the oxic layer at H3 whereas it is directly under the oxic zone at H6. It supports the DIN profiles, in which nitrification is a more dominant process at H3 (hence causing a production of N_2O in the oxic zone) and denitrification as more dominant at H6 (hence causing a production of N_2O in the anoxic zone).

The high efflux of N_2O in October at H6 correlated negatively with O_2 levels in bottom waters together with the highest concentrations of N_2O in the water column, but without a bottom water maxima. If the sediment was the primary source, a bottom water maxima would have been expected. Instead, the maxima in the water column was further up, close to the chemocline. It was discovered that the emissions of N_2O from the STP were extremely high (fig. 18). The highest water

saturation values of N_2O reached 275 481 %, which is a factor of 2650 times higher than the atmospheric concentrations. The lower values in the beginning of the measurements could be explained by different sampling procedures. The N_2O concentration was more accurately measured during the last four samplings, since samples from outgoing sewage waters were killed directly and without contact with atmospheric O_2. It was already known that the STP strongly influenced the estuary with its release of DIN, however the huge amounts of emitted N_2O were unexpected. Since these are the first samples ever analyzed for N_2O at this particular STP, the emissions are not regulated. This implies that STP is the biggest source of N_2O in Himmerfjärden and outcompetes by far any other significant N_2O producer. This also could explain the maxima at H6 during October and March, which occurs at 20- and 10 m depth respectively since the STP releases the treated water at a depth of 25 m. The slightly different depth could be explained by water movements and the very high levels of N_2O in the water, which would stimulate a movement towards the surface and the air-water interface due to much lower concentrations in those environments. The emissions varied a lot as well, probably since it is dependent on the volume of incoming sewage water and the efficiency of the biological purification. Fluctuations in the emissions from the STP would definitely have a higher influence on the N_2O concentrations (mostly H6), than the seasonal parameters.

With the present knowledge of the extremely high emissions of N_2O from the STP, a regulation is definitely needed. But the work needs to continue with more continuous measurements, preferably throughout the year so the changes in the emissions can be well documented and correlated with changes in the Himmerfjärden estuary to further confirm the STP as the most dominant source.

6.3 Evaluation of the analytical results

6.3.1 Analysis of the ^{15}N-N_2O

During the analysis of the produced N_2O during the incubation experiment with $^{15}NH_4^+$, an extra peak disturbed mass 46 from the N_2O peak (fig. 19) and made it impossible to continue the analysis. The unusually high water background during these measurements was a big problem since water is very reactive and many different products can be produced. A solution for this could be to cut the transport line between the injection inlet and the mass spectrometer. The present setup is longer than necessary, which could decrease the water background and hence the source of error. Changing type of column could be another solution, but without knowing the properties of the product it would be both time- and money consuming.

Another question was the undetected peak of the 1000 ppm standard of N_2O. Rough estimates of the peak amplitude and the corresponding N_2O concentration in both standard and sample showed a correct standard concentration and an unusually high sample concentration. The

test of the CO_2 standard gas, showed a retention time that deviated from other studies. This makes it questionable whether N_2O is actually measured at all, or if the peak represents another molecule with the same characteristics. During the separation in the column, CO_2 should be the first molecule to enter the mass spectrometer with a two minutes separation from N_2O. The peak representing CO_2 was considerably smaller than the N_2O peak, which seems a bit strange since Himmerfjärden contain high levels of CO_2. This could mean that the N_2O peak in actuality is the CO_2 peak. The linearity should have been tested with different injections of the pure N_2O to increase the reliability of the instrument.

Whether N_2O is measured or not has remained unsolved and needs to be further investigated in future projects, even if the work in this thesis points to N_2O as undetectable.

6.3.2 Evaluation of the $^{15}NH_4^+$ incubation method

Even if it is proven that the method can detect N_2O, the $^{15}NH_4^+$ experiment showed no production of N_2O, which does not necessarily imply on an inactive nitrification, only that it does not produce N_2O. The setup was perhaps not favorable for this kind of experiment. When a tracer is added, the amount should only increase the ambient pool by no more than 10 % (Klotz, 2011). The 50 mM concentration that was used in this experiment, exceeded by far a 10 % increase of the ambient pool of NH_4^+. The size of the exetainer could also be of importance; small containers would mean a smaller overall pool of O_2 and NH_4^+ and an inhibitation of the process. The experiments made in November and January were performed in 12 ml exetainers and could be an explanation for the lack of results. Bigger bottles were used in March with lower amounts of the tracer. Controlling the O_2 levels would also increase the quality, either by doing continuous measurements (by e.g. optodes) of the O_2 over time, or bubble the bottles with N_2 to reach an anoxic environment and then adding a known amount of O_2. Controlling the parameters that control the process makes it easier to determine if it is active or not.

Time is another factor that influence the results. The first two experiments had a setup of samples taken every 24 hours. If the incubation time is too long, the environments starts to change and would not represent natural conditions at this time. During a 24 hour period, N_2O could be produced and then rapidly consumed if the environment favors this. Longer incubation times would also increase the chances of regeneration of NH_4^+ and hence dilute the labeled products (Klotz, 2011). The choice of incubation time was based on the knowledge that N_2O is often present in low concentrations and low production rates in natural environments. To be able to see any changes it was believed that a longer incubation time was needed. In the aftermath this seems a bit strange, since the dilution affect increases with time, and the high sensitivity of the mass spectrometer.

Since the samples were not analyzed until after the January sampling and it became evident that the results from November did not produce any N_2O, the setup was not changed until

the last sampling in March. Bigger bottles (250 ml), a lower tracer addition (2- and 10 µM), a bottle with 2 µM of tracer together with acetylene and a shorter incubation time was used (every 10 min the first 30 min and then every 30 minutes with a total incubation time of 2 hours). Acetylene was used since it inhibits the N_2O reductase in denitrification, it make certain that nitrification actual is the process producing N_2O. These samples and the ones from January have not been analyzed due to the uncertainties with the mass spectrometer. Still, without reliable results from the $^{15}N\text{-}NH_4^+$tracer experiment, it is difficult to completely rule out nitrification as a producer of N_2O.

6.3.3 Analysis of the $^{15}N\text{-}N_2$

During the analysis of N_2 produced during the incubation experiment of NO_3^-, an extra peak occurred after the peak of N_2 (fig. 20). The change of sample injection size improved the separation and it was observed that the extra peak would not add to the peak area of N_2. The extra peak has not been seen in similar studies with the same column. A water trap containing NaCl and ice was used for freeze water in the N_2-line during the analysis in this project, whereas other studies used a liquid nitrogen freezing trap. The difference between the traps are the temperatures, which were around -20°C for the NaCl ice trap and the liquid nitrogen freezing trap around -190°C. The latter temperature causes a separation between CO_2, N_2O and partly NO from the sample before entering the reduction oven (Holtappels, 2011). This means that all N_2O concentration in the samples was reduced to N_2 under these measurements, which would have caused an overestimation in the production of labelled N. The amount of N_2O produced during the experiment and the N transformation pathway to N_2O are additional parameters that affect the results. The change of trap also implies that NO was not separated from the sample, which if present, would result in an overestimation of the produced $^{30}N_2$.

6.3.4 Evaluation of the $^{15}NO_3^-$ tracer method

The crucial assumptions for the ^{15}N IPT were not satisfied in this experiment, which means that the measured denitrification rates cannot be discussed in this context since the estimates are not reliable. The major challenge with the IPT is to add an appropriate $^{15}NO_3^-$ concentration (Lohse, et al., 1996). A too low addition would change the assumed binomial distribution (see equation 27) of N_2, which would result in an underestimation of D_n since the rate of produced $^{28}N_2$ would be higher in comparison with produced $^{29}N_2$ and $^{30}N_2$ (Lohse, et al., 1996). A too high addition would influence the natural denitrification rates (Lohse, et al., 1996). Looking at figure 23, it could be argued that an addition of 25- and 50 µM concentrations of the tracer is too low since the ratio for those additions, in many cases, showed an uneven mix between the two isotope species. Other studies added 250 µM $^{15}NO_3^-$ during winters when the *in situ* concentration of NO_3^- was high (Rysgaard, et al., 1995, Lohse, et al., 1996, Jensen, et al., 1996). A concentration series with perhaps 100 µM as the lowest and 250 µM as the highest could be more appropriate since this estuary already contains high levels

of NO_3^-. To be even more certain of the *in situ* NO_3^- concentrations, measurements before the experiment could be an idea using a fast method, e.g. a spectrophotometric method.

The endpoint method used in this experiment sacrifices all cores at the same time. A specific rate for each core is obtained, which is an advantage in comparison to a time-series experiment. The time-series experiment express a single denitrification rate from several different cores, which could be different in quality due to sediment heterogeneity (Steingruber, et al., 2011). But a time-series gives indication of the production over time, which should increase linearly over time if the isotopes are uniformly mixed (Lohse, et al., 1996, Jensen, et al., 1996, Rysgaard, et al., 1995, Steingruber, et al., 2001). To improve the quality of the data, the endpoint experiment could be performed together with a linearity test in the water column in the same cores. The drawbacks would be the assumption of a close coupling between water column and the anoxic zone in the sediment, which would be incorrect to assume if the sediment has a thick oxic zone (Steingruber, et al., 2001).

The extra peak in the mass spectrometer could have contributed to the bad quality of the data. It was decided that it did not interfere with the N_2 peak, but in actuality was dependent on the size of the peak and has not been present in other studies with the same setup for the mass spectrometer. Another problem could have been the low addition of 100 µl $ZnCl_2$, since other studies added 250 µl $ZnCl_2$ (Rysgaard, et al., 1995, Jensen, et al., 1996, Lohse, et al., 1996). The microbial activity was perhaps not stopped and continuous reactions could have produced a product causing this extra peak.

The pre-incubation time could be another factor. The time needed to establish a stable gradient of NO_3^- was calculated after measuring the O_2 penetration depth on a core that was not treated in exactly the same way as the denitrification cores. Comparing the different microprofiles from the same core, it became also evident that the penetration depth slightly differed depending on location even if the core was small. The degree of disturbance was not equal between the cores, which of course changes the geochemical zoning in the sediment and hence the penetration depth. Combining these factors, it becomes apparent that is it not always easy to determine a correct pre-incubation time since it could be different for each core, which is essential for the quality of the results. More experience would shorten the time needed to do the microprofiles. The faster the measurements of the profiles after the sampling, the less chance of a changed environment and a more accurate measurements of the O_2 penetration depth can be made, hence a correct pre-incubation time. The degree of experience was definitely a factor for the results in this experiment.

Amount of added $^{15}NO_3^-$, using an endpoint method, an extra disturbing peak, type of freezing trap, amount of injected $ZnCl_2$, pre-incubation time and degree of experience are the main

factors that could explain the quality of the data. To distinguish what mattered the most or what was responsible would need additional experiments, where some of the factors mentioned above are changed.

7 Conclusion

The extremely high emission of N_2O from the STP completely rule out any other significant producer in the Himmerfjärden estuary. The high emissions during March and April from the STP and the location of the N_2O maxima in the water column at H6, strengthen the theory of the STP as the cause of the elevated N_2O concentrations, rather than by microbial processes such as nitrification or denitrification. N_2O concentrations did not change through the seasons at H3, and was not a source of N_2O into the atmosphere. This also points to the STP as a dominant parameter since H6 was closer and hence more affected. Continuous measurements are needed, preferably throughout the year so that changes in the emissions can be well documented and correlated with changes in the Himmerfjärden estuary to further confirm the STP as the most dominant source. The high sediment efflux of N_2O in October for both stations could be caused by higher temperatures, stimulated by a higher microbial activity. The NO_3^-/NO_2^- peaks in the upper two centimeters at H3 in November and January, points to an active nitrification process and the simultaneous influx of NO_3^-/NO_2^- to denitrification. The dominating processes at H6 are more difficult to point out and are irregular, probably due to a high influence of the STP. The amount of N_2O that is produced by natural processes in Himmerfjärden, can only be speculated in this study since the experimental design for the 15 IPT in this environment needs to be changed.

Whether the mass spectrometer can detect N_2O or not needs to be further investigated in future projects. With the present setup and the none detectible N_2O standards of 1000 ppm, and the relationship between peak area response and concentration between standard and sample, points to N_2O as undetectable in the mass spectrometer.

The reason for the unfulfilled assumptions in the $^{15}NO_3^-$ experiment, lies both in the analysis and in the experimental setup. Some suggestions for future changes in experimental setup could be to try another NO_3^- addition spectra, pre-incubation time or to do a combined endpoint- and time-series experiment for an enhanced quality of the data.

8 Acknowledgments

I would like to express my sincere appreciation to Volker Brüchert for all the guidance and supervision during this project and Stefano Bonaglia, Barbara Deutsch, Joanna Sawicka, Sandra Gdaniec and Sofie Sandelius, for their generous support during different stages, which made it possible to carry out this project. Many thanks to the very kind and generous staff at Askö, which made long, and cold days on the boat bearable. I would also like to acknowledge Christoffer Hemmingsson for all his generous support and guidance during the statistical analysis. A very special thanks to Jayne Rattray, Heike Siegmund and Malin Söderman for all help and long discussions during the analysis, which contained a lot of problems. Your guidance and knowledge was very essential for the results for this project. Last but not least I would like to thank Alan Wiech, my family and all friends for their never ending encouragements.

9 References

Aller, R. C., 1982, The effects of Macrobenthos on Chemical Properties of Marine Sediment and Overlying water, McCalt, P.L. and Tevesz, M.J.S., *Animal Sediment Relations*, Chapter 2

Bange, H.W., 2006, Nitrous oxide and methane in European coastal waters, *Estuarine, coastal and shelf science, 70, 361-374,* doi:10.1016/j.ecess.2006.05.042

Berg, P., 1998, Interpretation of measured concentration profiles in sediment pore water, *Limnol. Oceanogr. 47(7), 1998, 1500-151*

Bing-Jie, N., Ruscalleda, M., Pellicer-Nàcher, C., and Smets, B.F., 2011, Modeling Nitrous Oxide Production during Biological Nitrogen Removal via Nitrification and Denitrification: Extension to the General ASM model, *Environ. Sci. Tecnol., 45, 7768-7776, dx.doi.org/10.1021/es201489*

Bonaglia, S., Deutsch, B., Bartoli, M., Marchant, H.K., and Brüchert, V., 2014, Seasonal oxygen, nitrogen and phosphorous benthic cycling along an impacted Baltic Sea estuary: regulation and spatial patterns, *Biogeochemistry, 110:139-160, DOI: 10.1007/s10533-014-9953-6*

Bonaglia, S., Nascimento, F.J.A, Bartoli, M., Klawonn, I., and Brüchert, V., 2014, Meiofauna increases bacterial denitrification in marine sediments *Nat. Commun. 5:5133, doi: 10.1038/ncomms6133*

Cabrita, M.T., and Brotas, V., 2000, Seasonal variation in denitrification and dissolved nitrogen fluxes in intertidal sediments of the Tagus estuary, Portugal, *Mar. Ecol., Prog. Ser, Vol. 202:51-65*

Christensen, P.B., Nielsen, L.P., Sörensen, J., and Revsbech, N.P., 1990, Denitrification in nitrate-rich streams: Diurnal and seasonal variation related to benthic oxygen metabolism, *Limnol. Oceanogr. Vol 35(3):640-651*

Conover, W.J. and Imam, R.L., 1979, Reproduction Copy On Multiple-Comparison Procedures*,* University of California*, Informal Report, LA-7677-MS,* Los Alamos Scientific Laboratory, Post Office Box 1663, Los Alamos, New Mexico 87545

Department of Ecology, Environment and Plant Science, 2015, *Himmerfjärden: Eutrophication Study, http://www2.ecology.su.se/dbhfj/index.htm, (Derived 150703-150705)*

Devol, A.H., 2015, Denitrification, Anammox, and N_2 Production in Marine sediments, *Annu.Rev.Sci.2015. 7:403-23*

Holtappels, M., Lavik, G., Jensen and Kuypers, M.M, 2011, ^{15}N-Labeling Experiments to Dissect the Contributions of Heterotrophic Denitrification and Anammox to Nitrogen Removal in the OMZ Waters of the Ocean, *Methods in Enzymologi, Vol 486, Burlington: Academic Press, pp. 223-251*

Jensen, K.M., Jensen, M.H., Kristensen, E., 1996, Nitrification and denitrification in Wadden Sea sediments (Königshafen, Island of Sylt, Germany) as measured by nitrogen isotope pairing and isotope dilution, *Aqual.Microb.Ecol., Vol 11:181-191*

Klotz, G. M., 2011, Research on Nitrification and Related Processes, Part A, *Methods in Enzymology, Vol 486, Burlington: Academic press, pp.307-323*

Lohse, L., Kloosterhuis, T.H., Raaphorst, W., and Helder, W., 1996, Denitrification rates by the isotope pairing method and by the acetylene inhibition technique in continental shelf sediments of the Nort Sea, *Mar.Ecol.Prog.Ser, Vol 132:169-179*

Murray, R.H., Erler, D.V. and Eyre, B.D., 2015, Nitrous oxide fluxes in estuarine environments: response to global change, *Global Change Biology, doi:10.1111/gcb.12923*

Nielsen, L.P., 1992, Denitrification in sediment determined from nitrogen isotope pairing. *FEMS Microbiol. Ecol. 86 (4):357-362*

Olsson, C., 2013, “winter methane and nitrous oxide emissions from Himmerfjärden to the atmosphere”, (Bachelor´s theses, Stockholm University)

Ravishankara, A.R., Daniel, J.S. and Portmann, R.W., 2009, Nitrous Oxide (N_2O): The Dominant Ozone-Depleting Substance Emitted in the 21st Century, *Published Online August 27 2009, Science 2 October 2009:Vol. 326 no. 5949 pp. 123-125, DOI: 10.1126/science.1176985*

Rysgaard, S., Christensen, P.B., Nielsen, L.P., 1995, Seasonal variation in nitrification and denitrification in estuarine sediment colonized by benthic microalgae and bioturbating infauna, *Mar.ecol.Prog.ser. Vol 126:111-121*

Rönner, U. (1983), Distribution and consumption of nitrous oxide in the Baltic Sea, *Geochimica et Cosmochimica Act, 47,pp.2179 to 2188, 0016-7037/83/122179-10$03.00/0*

Schulz, H and Zabel, M., 2006, Marine geochemistry, second edition, Springer Berlin Heidelberg New York, Germany, ISBN-978-3-540-32143-9, pp.210-219, 223-228

Steingruber, S.M., Friedrich, J., Gächter, R. and Wehrli, B., 2001, Measurements of Denitrification in Sediments with the ^{15}N Isotope Pairing Technique, *Applied and Environmental Microbiology*, *Sept.2001, p. 3771-3778, doi: 10.1128/AEM.67.9.3771-3778.2001*

Sutka, R.L., Ostrom, N.E., Ostrom, P.H., Breznak, J.A., Gandhi, H., Pitt, A.J. and Li, F., 2006, Distinguishing Nitrous Oxide Production from Nitrification and Denitrification on the Basis of Isotopomer Abundances, *Applied and Environmental Microbiology, 72.1.638-644, doi:10.1128/AEM.72.1.638-644.2006*

Syvab, *Documents*, Syvab Himmerfjärdsverket, http://www.syvab.se/information/dokument/himmerfjardens-miljorapporter, (Derived 150705)

Thang., M.N., Brüchert, V., Formolo, M., Wegener, G., Ginters, L., Jorgensen, B.B., Ferdelman, T.G., 2012, The impact of Sediment and Carbon Fluxes on the Biogeochemistry of Methane and Sulfur in Baltic Sea Sediments (Himmerfjärden, Sweden), *Estauries and Costs, DOI 10.1007/s12237-012-9557-0*

Townsend-Small, A., M.G. Prokopenko and W.M. Berelson, 2014, Nitrous oxide cycling in the water column and sediment of the oxygen minimum zon, eastern subtropical North Pacific, Southern California, and Northern Mexico (23°N-34°), *J. Geophys.Res.Oceans, 119, 3158-3170,* doi: 10.1002/2013JC00580.

Walter, S., Breitenbach, U., Bange, H.W., Nausch, G. and Wallace, D.W.R., 2006, Distribution of N_2O in the Baltic Sea during transition from anoxic to oxic conditions, *Biogeoscience, 3, 557-570*

Yan, W., Libiao, Y., Yang, F., Wang, J. and Pei, M., 2012, Riverine N_2O concentratios, exports to estuary and emissions to atmosphere from the Changjiang River in response to increasing nitrogen loads, *Global Biogeochem. Cycles, 26,* GB4006, doi: 10.1029/2010GB00398

10 Appendices

10.1 Statistical analysis for N_2O in the water column

Since the data was normal distributed for the N_2O concentration in the water column, an ANOVA test was applied to determine groups with an equal mean. Since H_0 (H_0: $\mu_1=\mu_2...\mu_k$) was rejected an *All Pairs Tukey-Kramer test* was conducted to determine which means that were different. The results are illustrated in table 4, were connected circles and letters represents groups that are statistical equal. The results from the ANOVA test are visualized in figure 29.

An Anova test with the multi-comparison *All pairs Tukey-Kramer* method

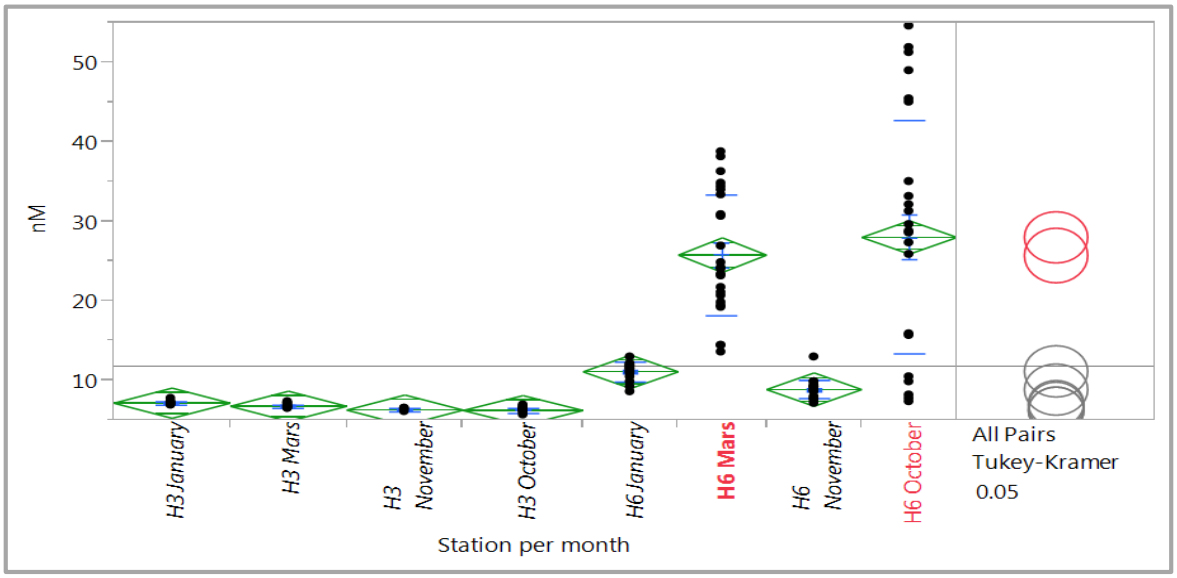

Figure 19. The statistical result for the N_2O concentration through the seasons. The green diamond represents mean and standard deviation. Connected circles show means that are statistical equal at a significance level of p<0.05.

Table 4. The result from the all pairs Tukey-Kramer test. Connected letters are groups with a statistical equal mean. P<0.05.

All pairs Tukey-Kramer test				
Station/month				**Mean**
H6 October	A			28.00
H6 March	A			25.77
H6 January		B		11.09
H6 November		B	C	8.85
H3 January		B	C	7.14
H3 March		B	C	6.74
H3 November			C	6.26
H3 October			C	6.21

10.2 Statistical Results for N_2O Production during Nitrification

10.2.1 K-values for the production of $^{45\text{-}46}$Production in both spiked- and blank samples

The production rates of $^{45\text{-}46}N_2O$ at H3 and H6 are shown in the form of K-values in table 5. Every depth is represented with both blank and spiked sample. The K-values to the left represent the $^{45}N_2O$ production and the column to the right the production of $^{46}N_2O$.

Table 5. *K-values for the production of $^{45\text{-}46}$Production in both spiked- and blank samples. The K-values to the left represent the $^{45}N_2O$ production and the column to the right the production of $^{46}N_2O$.*

K-values for the produced $^{45\text{-}46}N_2O$ over time					
Sample	Depth (m)	K-value	Station/sample	Depth (m)	K-value
H3					
H3 $^{45}N_2O$	5	-0.0014	H3 $^{45}N_2O$ Blank	5	0.0026
H3 $^{46}N_2O$	5	-0.0001	H3 $^{46}N_2O$ Blank	5	-0.0004
H3 $^{45}N_2O$	20	0.0030	H3 $^{45}N_2O$ Blank	20	-0.0003
H3 $^{46}N_2O$	20	-0.0004	H3 $^{46}N_2O$ Blank	20	-0.0003
H3 $^{45}N_2O$	25	-0.0223	H3 $^{45}N_2O$ Blank	25	0.0019
H3 $^{46}N_2O$	25	-0.0023	H3 $^{46}N_2O$ Blank	25	-0.0005
H3 $^{45}N_2O$	40	-0.0011	H3 $^{45}N_2O$ Blank	40	-0.0046
H3 $^{46}N_2O$	40	-0.0002	H3 $^{46}N_2O$ Blank	40	-0.0002
H3 $^{45}N_2O$	45	0.0013	H3 $^{45}N_2O$ Blank	45	-0.0002
H3 $^{46}N_2O$	45	0.0002	H3 $^{46}N_2O$ Blank	45	0.0000
H6					
H6 $^{45}N_2O$	3	-0.0044	H6 $^{45}N_2O$ Blank	3	-0.0008
H6 $^{46}N_2O$	3	-0.0005	H6 $^{46}N_2O$ Blank	3	-0.0001
H6 $^{45}N_2O$	10	0.0017	H6 $^{45}N_2O$ Blank	10	0.0023
H6 $^{46}N_2O$	10	0.0005	H6 $^{46}N_2O$ Blank	10	0.0023
H6 $^{45}N_2O$	15	-0.0003	H6 $^{45}N_2O$ Blank	15	0.0110
H6 $^{46}N_2O$	15	0.0001	H6 $^{46}N_2O$ Blank	15	0.0014
H6 $^{45}N_2O$	20	-0.0172	H6 $^{45}N_2O$ Blank	20	-0.0205
H6 $^{46}N_2O$	20	-0.0022	H6 $^{46}N_2O$ Blank	20	-0.0024
H6 $^{45}N_2O$	30	0.0071	H6 $^{45}N_2O$ Blank	30	0.0083
H6 $^{46}N_2O$	30	0.0012	H6 $^{46}N_2O$ Blank	30	0.0009

10.2.2 Statistical results for N_2O production at H3 in November

Figure 30 shows the distribution of K-values for the production of $^{45\text{-}46}N\text{-}N_2O$ at 5 m depth at H3. Levenes test rejected H_0 and the further analysis through a Kruskal-Wallis test can be seen in table 6. A p-value of 0.8614 means that H_0 cannot be rejected and thus that the mean between the Blanks and the spiked samples is not significant ($p<0.05$).

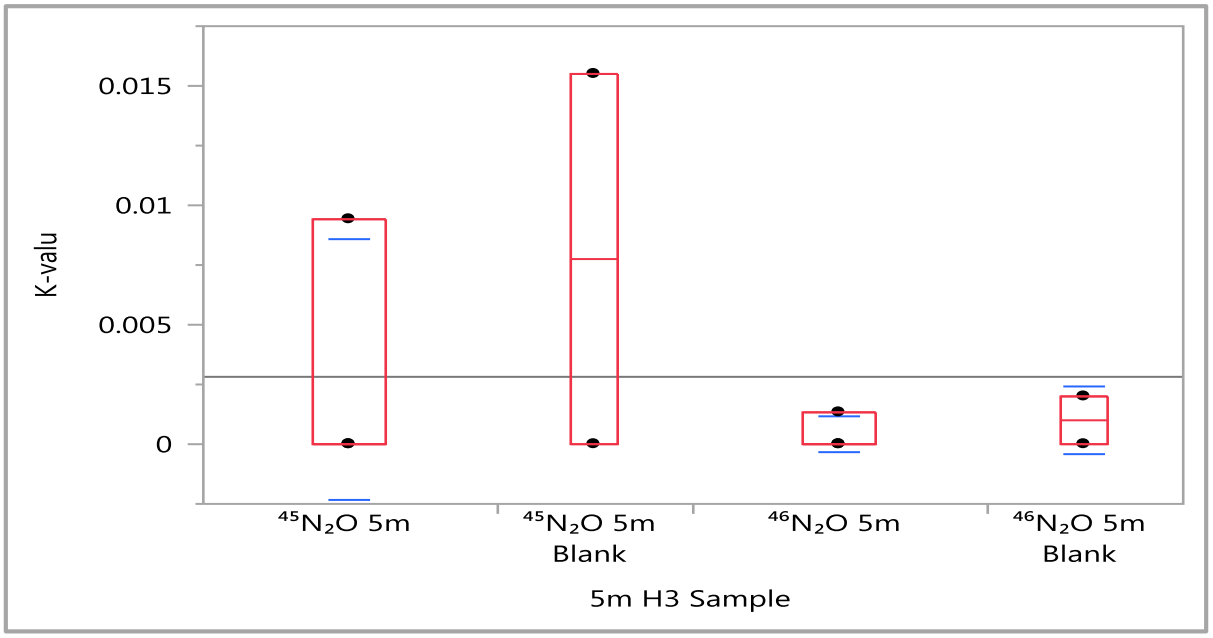

Figure 30. Distribution of K-values for the production of $^{45\text{-}46}N\text{-}N_2O$ at 5 m depth at H3.

Table 6. A Kruskal-Wallis test with a p-value of 0.8614, which means that H_0 cannot be rejected and thus that the mean between the blanks and the spiked samples is not significant ($p<0.05$).

Kruskal-Wallis test on Nitrification rates at 5 m					
Level	**Count**	**Score Sum**	**Expected Score**	**Score Mean**	**(Mean-Mean0)/Std0**
$^{45}N_2O$ 5m	3	16.000	16.500	5.33333	-0.000
$^{45}N_2O$ 5m Blank	2	13.500	11.000	6.75000	0.588
$^{46}N_2O$ 5m	3	14.000	16.500	4.66667	-0.514
$^{46}N_2O$ 5m Blank	2	11.500	11.000	5.75000	0.000
1-way Test, Chi-square Approximation					
Chi-square			**DF**		**Prob>ChiSq**
0.7500			3		**0.8614**

Figure 31 shows the distribution of K-values for the production of $^{45\text{-}46}N\text{-}N_2O$ at 20 m depth at H3. Levenes test rejected H_0 and the further analysis through a Kruskal-Wallis test can be seen in table 7. The p-value (0.2809) means that H_0 cannot be rejected and thus that the mean between the Blanks and the spiked samples is not significant ($p<0.05$).

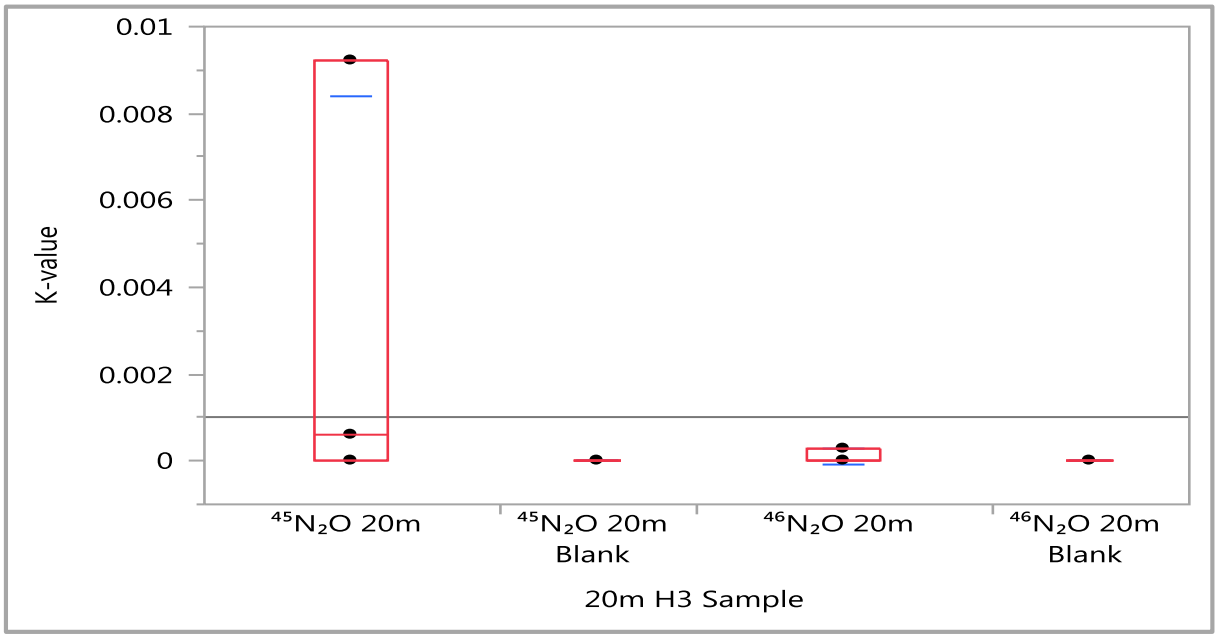

Figure 31. Distribution of K-values for the production of $^{45\text{-}46}N\text{-}N_2O$ at 20 m at H3.

Table 7. A Kruskal-Wallis test with a p-value of 0.2809, which means that H_0 cannot be rejected and thus that the mean between the Blanks and the spiked samples is not significant ($p<0.05$).

Kruskal-Wallis test on Nitrification rates at 20 m					
Level	**Count**	**Score Sum**	**Expected Score**	**Score Mean**	**(Mean-Mean0)/Std0**
$^{45}N_2O$ 20m	3	23.000	16.500	7.66667	1.683
$^{45}N_2O$ 20m Blank	2	8.000	11.000	4.00000	-0.803
$^{46}N_2O$ 20m	3	16.000	16.500	5.33333	-0.000
$^{46}N_2O$ 20m Blank	2	8.000	11.000	4.00000	-0.803
1-way Test, Chi-square Approximation					
Chi-square			**DF**		**Prob>ChiSq**
3.8257			3		**0.2809**

Figure 32 shows the distribution of K-values for the production of $^{45\text{-}46}N\text{-}N_2O$ at 25 m depth at H3. Levenes test rejected H_0 and the further analysis through a Kruskal-Wallis test can be seen in table 8. The p-value (0.5820) means that H_0 cannot be rejected and thus that the mean between the Blanks and the spiked samples is not significant (p<0.05).

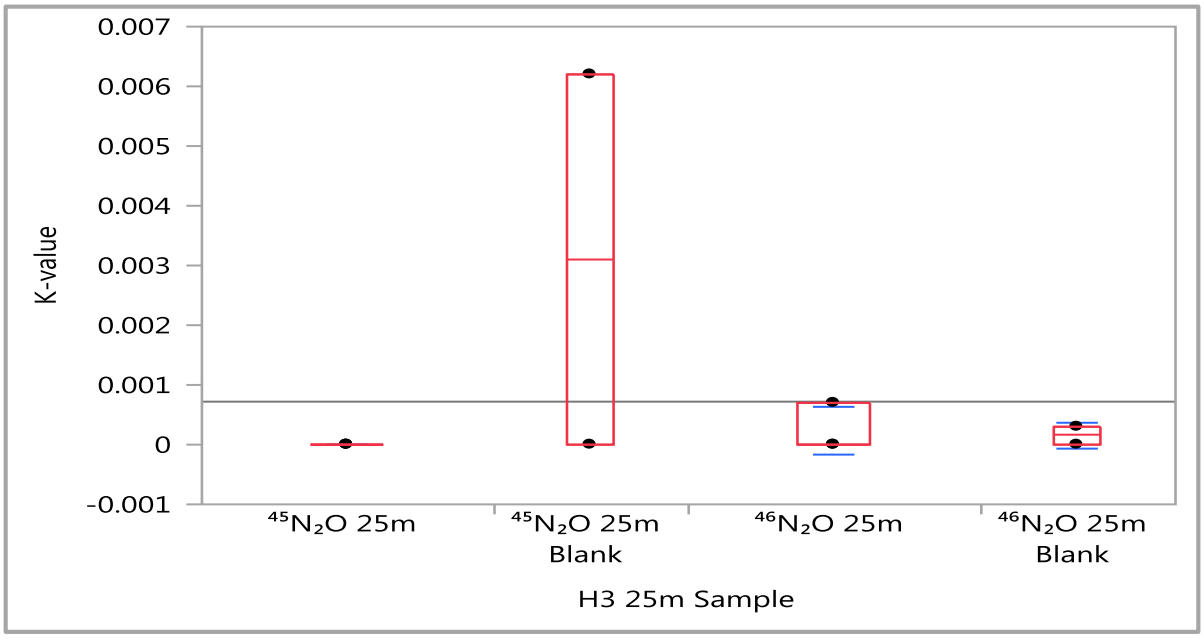

Figure 32. Distribution of K-values for the production of $^{45\text{-}46}N\text{-}N_2O$ at 25 m at H3.

Table 8. *A Kruskal-Wallis test with a p-value of 0.5820, which means that H_0 cannot be rejected and thus that the mean between the blanks and the spiked samples is not significant (p<0.05).*

Kruskal-Wallis test on Nitrification rates at 25 m at H3					
Level	**Count**	**Score Sum**	**Expected Score**	**Score Mean**	**(Mean-Mean0)/Std0**
$^{45}N_2O$ 25m	3	12.000	16.500	4.00000	-1.122
$^{45}N_2O$ 25m Blank	2	14.000	11.000	7.00000	0.803
$^{46}N_2O$ 25m	3	17.000	16.500	5.66667	0.000
$^{46}N_2O$ 25m Blank	2	12.000	11.000	6.00000	0.161
1-way Test, Chi-square Approximation					
Chi-square			**DF**		**Prob>ChiSq**
1.9541			3		**0.5820**

Figure 33 shows the distribution of K-values for the production of $^{45\text{-}46}N\text{-}N_2O$ at 40 m depth at H3. Levenes test rejected H_0 and the further analysis through a Kruskal-Wallis test can be seen in table 9. The p-value (0.9248) means that H_0 cannot be rejected and thus that the mean between the Blanks and the spiked samples is not significant ($p<0.05$).

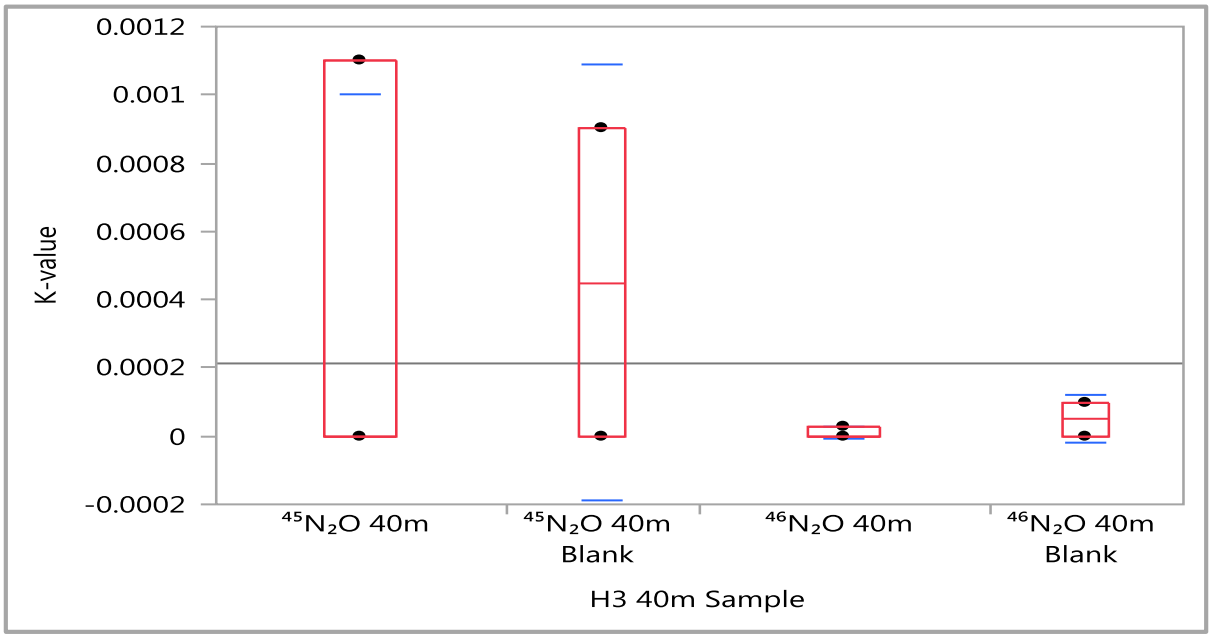

Figure 33. Distribution of K-values for the production of $^{45\text{-}46}N\text{-}N_2O$ at 40 m at H3.

Table 9. A Kruskal-Wallis test with a p-value of 0.9248, which means that H_0 cannot be rejected and thus that the mean between the Blanks and the spiked samples is not significant ($p<0.05$).

Kruskal-Wallis test on Nitrification rates at 40m					
Level	**Count**	**Score Sum**	**Expected Score**	**Score Mean**	**(Mean-Mean0)/Std0**
$^{45}N_2O$ 40m	3	17.000	16.500	5.66667	0.000
$^{45}N_2O$ 40m Blank	2	12.500	11.000	6.25000	0.294
$^{46}N_2O$ 40m	3	14.000	16.500	4.66667	-0.514
$^{46}N_2O$ 40m Blank	2	11.500	11.000	5.75000	0.000
1-way Test, Chi-square Approximation					
Chi-square			**DF**		**Prob>ChiSq**
0.4731			3		**0.9248**

Figure 34 shows the distribution of K-values for the production of $^{45\text{-}46}N\text{-}N_2O$ at 25 m depth at H3. Levenes test rejected H_0 and the further analysis through a Kruskal-Wallis test can be seen in table 10. The p-value (0.2549) means that H_0 cannot be rejected and thus that the mean between the Blanks and the spiked samples is not significant ($p<0.05$).

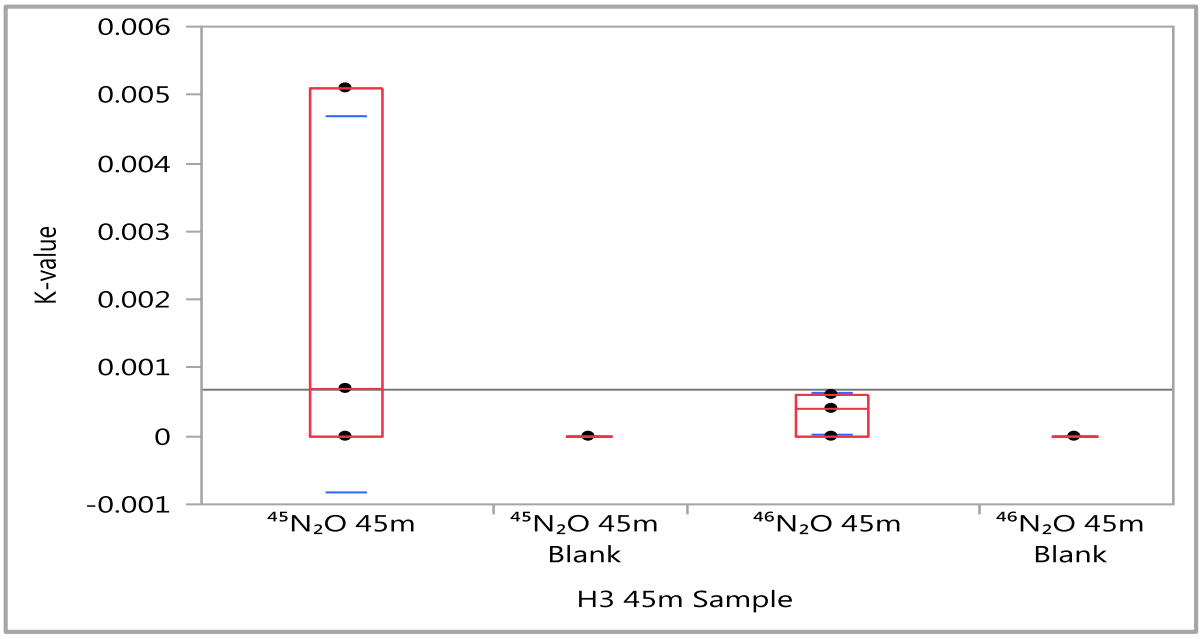

Figure 34. Distribution of K-values for the production of $^{45\text{-}46}N\text{-}N_2O$ at 25 m at H3.

Table 10. A Kruskal-Wallis test with a p-value of 0.2549, which means that H_0 cannot be rejected and thus that the mean between the Blanks and the spiked samples is not significant ($p<0.05$).

Kruskal-Wallis test on Nitrification rates at 45m					
Level	**Count**	**Score Sum**	**Expected Score**	**Score Mean**	**(Mean-Mean0)/Std0**
$^{45}N_2O$ 45m	3	22.500	16.500	7.50000	1.412
$^{45}N_2O$ 45m Blank	2	7.000	11.000	3.50000	-1.030
$^{46}N_2O$ 45m	3	18.500	16.500	6.16667	0.385
$^{46}N_2O$ 45m Blank	2	7.000	11.000	3.50000	-1.030
1-way Test, Chi-square Approximation					
Chi-square			**DF**		**Prob>ChiSq**
4.0615			3		**0.2549**

10.2.3 Statistical results for N_2O production at H6 in November

Figure 35 shows the distribution of K-values for the production of $^{45\text{-}46}N\text{-}N_2O$ at 3 m depth at H6. Levenes test rejected H_0 and the further analysis through a Kruskal-Wallis test can be seen in table 11. The p-value (0.8614) means that H_0 cannot be rejected and thus that the mean between the Blanks and the spiked samples is not significant ($p<0.05$).

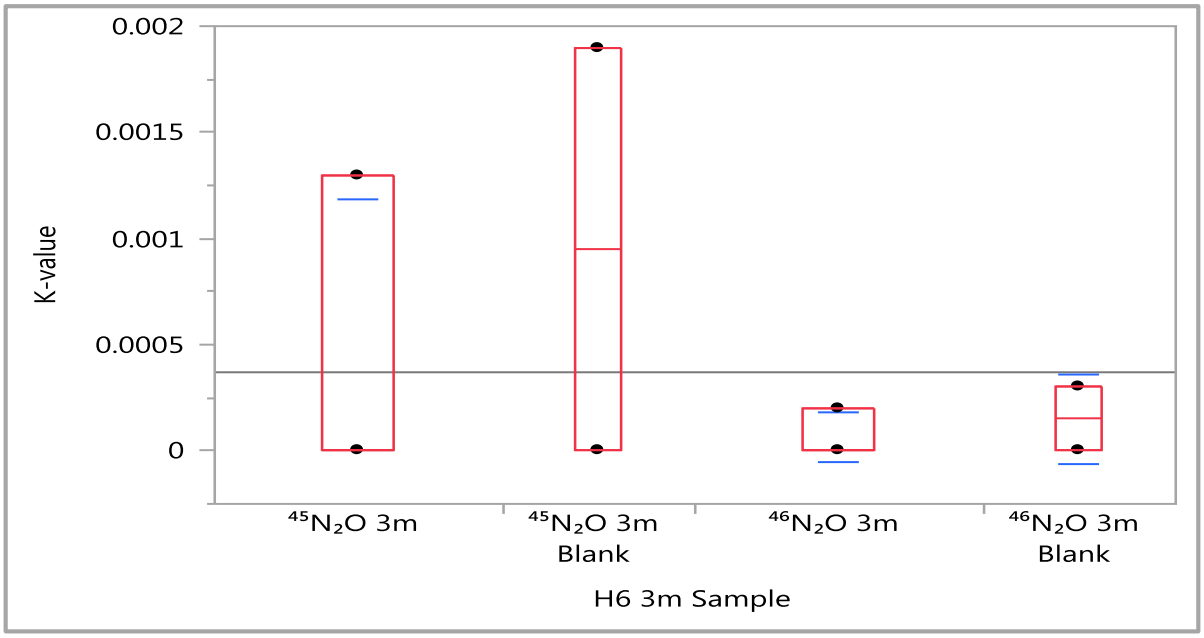

Figure 35. Distribution of K-values for the production of $^{45\text{-}46}N\text{-}N_2O$ at 3 m at H6.

Table 11. A Kruskal-Wallis test with a p-value of 0.8614, which means that H_0 cannot be rejected and thus that the mean between the Blanks and the spiked samples is not significant ($p<0.05$).

Kruskal-Wallis test on Nitrification rates at 3 m					
Level	**Count**	**Score Sum**	**Expected Score**	**Score Mean**	**(Mean-Mean0)/Std0**
$^{45}N_2O$ 3m	3	16.000	16.500	5.33333	-0.000
$^{45}N_2O$ 3m Blank	2	13.500	11.000	6.75000	0.588
$^{46}N_2O$ 3m	3	14.000	16.500	4.66667	-0.514
$^{46}N_2O$ 3m Blank	2	11.500	11.000	5.75000	0.000
1-way Test, Chi-square Approximation					
Chi-square			**DF**		**Prob>ChiSq**
0.7500			3		**0.8614**

Figure 36 shows the distribution of K-values for the production of $^{45\text{-}46}N\text{-}N_2O$ at 10 m depth at H6. Levenes test did not reject H_0 and the further analysis were conducted through an ANOVA test instead. Table 12 shows the result from the ANOVA test with a p-value of 0.3436, which means that H_0 cannot be rejected and thus that the mean between the Blanks and the spiked samples is not significant ($p<0.05$).

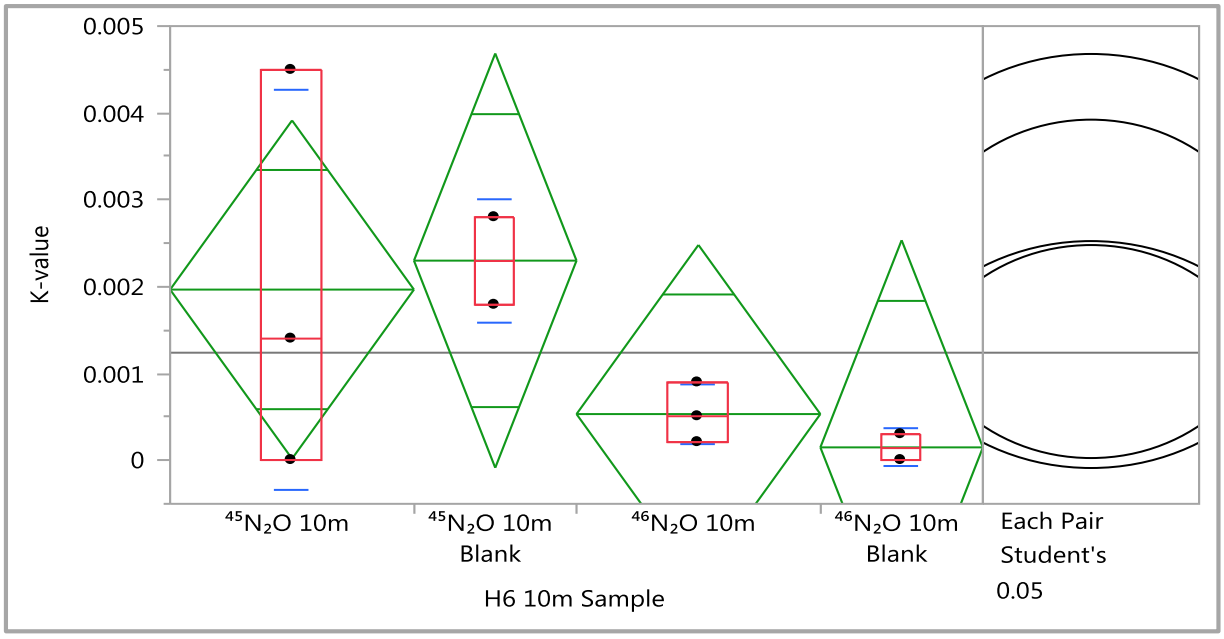

Figure 36. The distribution of the K-values for the production of $^{45\text{-}46}N\text{-}N_2O$ at 10 m at H6, together with an Each Pair Student´s t-test to confirm a similar variance between the groups. The green diamond represents mean and standard deviation. Connected circles show means that are statistical equal at a significance level of p<0.05.

Table 12. *An ANOVA test with a p-value of 0.3436, which means that H_0 cannot be rejected and thus that the mean between the Blanks and the spiked samples is not significant (p<0.05).*

ANOVA test on Nitrification rates at 10 m					
Source	**DF**	**Sum of Squares**	**Mean Square**	**F Ratio**	**Prob > F**
H6 10m Sample	3	0.00000771	2.5686e-6	1.3521	**0.3436**
Error	6	0.00001140	0.0000019		
C. Total	9	0.00001910			

Figure 37 shows the distribution of K-values for the production of $^{45\text{-}46}N\text{-}N_2O$ at 15 m at H6. Levenes test rejected H_0 and the further analysis through a Kruskal-Wallis test can be seen in table 13. The p-value (0.2293) means that H_0 cannot be rejected and thus that the mean between the Blanks and the spiked samples is not significant ($p<0.05$).

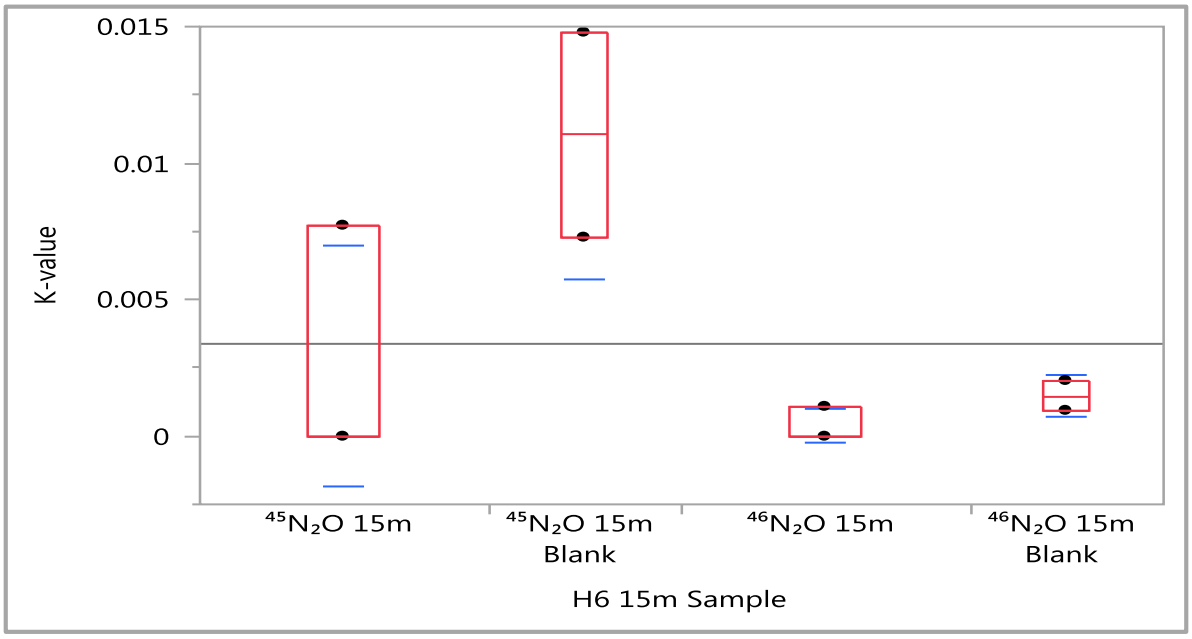

Figure 37. Distribution of K-values for the production of $^{45\text{-}46}N\text{-}N_2O$ at 15 m at H6.

Table 13. *A Kruskal-Wallis test can be seen in table 13. The p-value (0.2293) means that H_0 cannot be rejected and thus that the mean between the Blanks and the spiked samples is not significant ($p<0.05$).*

Kruskal-Wallis test on Nitrification rates at 15 m					
Level	**Count**	**Score Sum**	**Expected Score**	**Score Mean**	**(Mean-Mean0)/Std0**
$^{45}N_2O$ 15m	3	14.000	16.500	4.66667	-0.470
$^{45}N_2O$ 15m Blank	2	18.000	11.000	9.00000	1.751
$^{46}N_2O$ 15m	3	11.000	16.500	3.66667	-1.176
$^{46}N_2O$ 15m Blank	2	12.000	11.000	6.00000	0.135
1-way Test, Chi-square Approximation					
Chi-square			**DF**		**Prob>ChiSq**
4.3161			3		**0.2293**

Figure 38 shows the distribution of K-values for the production of $^{45\text{-}46}N\text{-}N_2O$ at 20 m at H6. Levenes test did not reject H_0 and the further analysis were conducted through an ANOVA test instead. Table 14 shows the result from the ANOVA test, with a p-value of 0.2515. This means that H_0 cannot be rejected and thus that the mean between the blanks and the spiked samples is not significant ($p<0.05$).

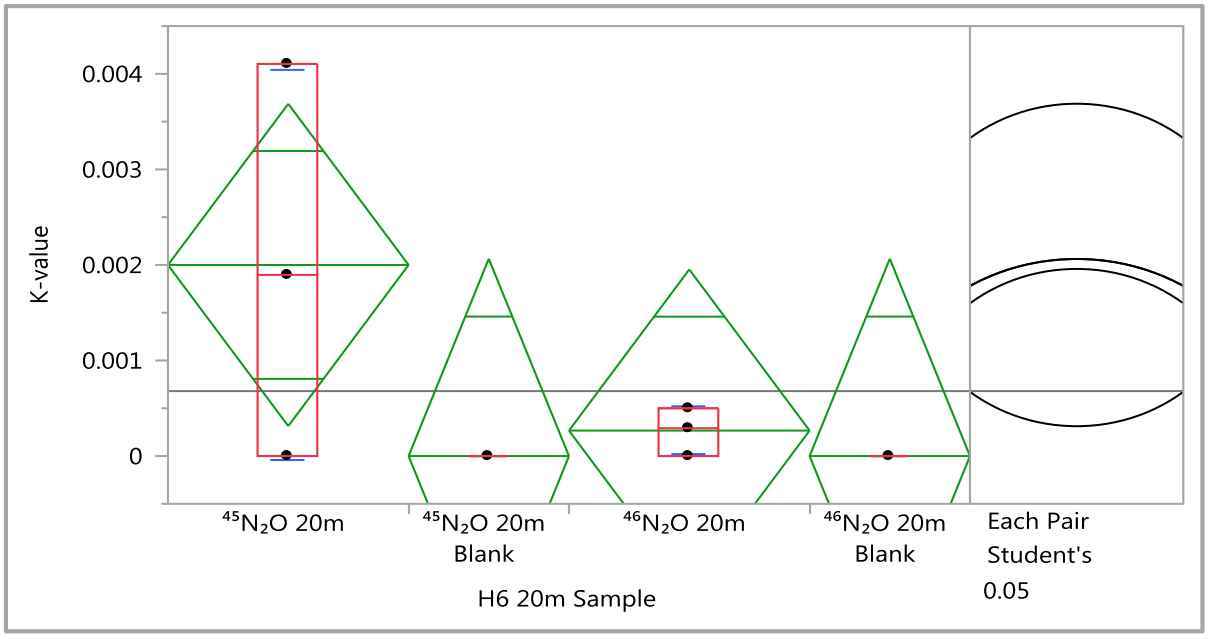

Figure 38. The distribution of the K-values for the production of $^{45\text{-}46}N\text{-}N_2O$ at 20 m at H6, together with an Each Pair Student´s t-test to confirm a similar variance between the groups. The green diamond represents mean and standard deviation. Connected circles show means that are statistical equal at a significance level of p<0.05.

Table 14. An ANOVA test, with a p-value of 0.2515. This means that H_0 cannot be rejected and thus that the mean between the blanks and the spiked samples is not significant ($p<0.05$).

ANOVA test on Nitrification rates at 20 m					
Source	**DF**	**Sum of Squares**	**Mean Square**	**F Ratio**	**Prob > F**
H6 20m Sample	3	0.00000759	2.5298e-6	1.7760	**0.2515**
Error	6	0.00000855	1.4244e-6		
C. Total	9	0.00001614			

Figure 39 shows the distribution of the K-values for the production of $^{45\text{-}46}N\text{-}N_2O$ at 15 m depth at H6. Levenes test rejected H_0 and the further analysis through a Kruskal-Wallis test can be seen in table 15. The p-value (0.3455) means that H_0 cannot be rejected and thus that the mean between the blanks and the spiked samples is not significant ($p<0.05$).

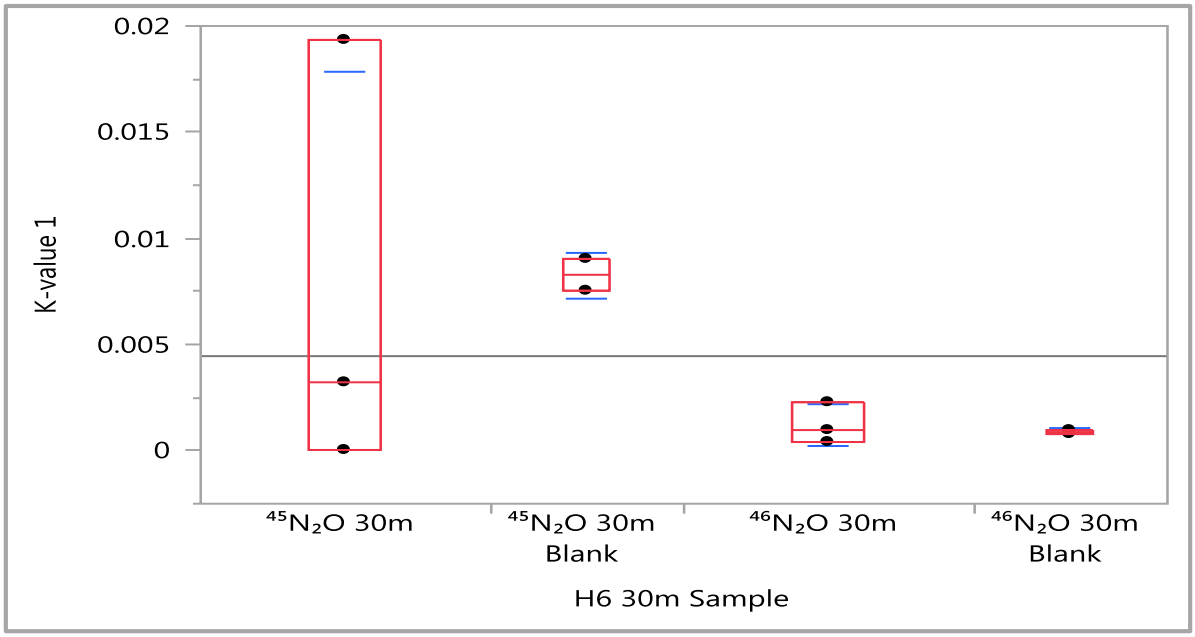

Figure 39. Distribution of K-values for the production of $^{45\text{-}46}N\text{-}N_2O$ at a depth of 15 m at H6.

Table 15. *A Kruskal-Wallis test with a p-value of 0.3455, which means that H_0 cannot be rejected and thus that the mean between the blanks and the spiked samples is not significant ($p<0.05$).*

Kruskal-Wallis test on Nitrification rates at a depth of 30m at H6					
Level	**Count**	**Score Sum**	**Expected Score**	**Score Mean**	**(Mean-Mean0)/Std0**
$^{45}N_2O$ 30m	3	18.000	16.500	6.00000	0.229
$^{45}N_2O$ 30m Blank	2	17.000	11.000	8.50000	1.441
$^{46}N_2O$ 30m	3	12.500	16.500	4.16667	-0.800
$^{46}N_2O$ 30m Blank	2	7.500	11.000	3.75000	-0.786
1-way Test, Chi-square Approximation					
Chi-square			**DF**		**Prob>ChiSq**
3.3155			3		**0.3455**